Connectivity Analysis of Brain Function in Children with Foetal Alcohol Spectrum Disorder and Control Children during Number Processing

by

Robyn Herron

(Student Number: HRRROB008)

SUBMITTED TO THE UNIVERSITY OF CAPE TOWN

In partial fulfilment of the requirements for the degree

MSc (Med) in Biomedical Engineering

Faculty of Health Sciences

UNIVERSITY OF CAPE TOWN

Date of submission: March 2008

Supervisor: Assoc. Prof. E.M. Meintjes

Department of Human Biology

University of Cape Town

DECLARATION

I, ROBYN HERRON, hereby declare that the work on which this dissertation is based is my original work (except where acknowledgements indicate otherwise) and that neither the whole work nor any part of it has been, is being, or is to be submitted for another degree in this or any other university.

I empower the university to reproduce for the purpose of research either the whole or any portion of the contents in any manner whatsoever.

Signature: . Signed by candidate

Date: 30/5/2008

Acknowledgements

I would like to gratefully acknowledge the great help, including financial, given to me by:

Ernesta Meintjes, University of Cape Town

Baxter Rogers, Vanderbilt University

Sandra Jacobson, Wayne State University

Joseph Jacobson, Wayne State University

Eric Murphy, Wayne State University

Vaibhav Diwadkar, Wayne State University

Christopher Molteno, Univeristy of Cape Town

Frances Robertson, University of Cape Town

University of Cape Town Postgraduate Funding Office

Abstract

Maternal drinking during pregnancy is a significant problem in the Western Cape, South Africa, with an accompanying high incidence of children diagnosed with foetal alcohol spectrum disorder (FASD). Little is known about the neural correlates governing the disorder that manifest as behavioural abnormalities and cognitive impairments, particularly in arithmetic calculation, repeatedly reported in affected children.

The effect of prenatal alcohol exposure on number processing in children was investigated in a functional magnetic resonance imaging (fMRI) study (Meintjes et al., 2007). The results indicate significant differences in activation between alcohol-exposed and non-exposed control children during Exact Addition and Proximity Judgement tasks. This raised the question of whether the groups of children differ in functional connectivity during the number processing tasks.

Therefore, the objective of this study was to analyse connectivity between functionally specialised brain areas in the previously collected fMRI data. The fMRI data of 14 controls and 7 alcohol-exposed children for Exact Addition and 15 controls and 9 alcohol-exposed children for Proximity Judgement was available for analysis. A primary aim was to determine normal functional connectivity in control children during number processing and a secondary aim, to investigate any differences in functional connectivity in children with FASD.

Regions of interest chosen for functional connectivity analysis were extracted from fMRI activation maps based on their relevance in the number processing literature and importance in the findings of Meintjes and colleagues (2007).

Model-based and exploratory functional connectivity mapping techniques were studied and implemented on the fMRI data. The Inter-region Correlation and Seed-voxel Connectivity methods were based on simple correlation and linear regression theory. Inter-region Correlation tested pair-wise correlation between the average time series of regions of interest, while Seed-voxel Connectivity compared the average time series of a seed region of interest with the time series of every voxel in the brain, yielding a statistical parametric map illustrating areas showing significant functional connectivity to the seed region. Psychophysiological Interaction (PPI) analysis was used to determine which areas of the brain showed significant functional integration in the number processing context. Granger causality mapping was also investigated.

The pattern of fronto-parietal functional connectivity seen in the control children's data during both Exact Addition and Proximity Judgement tasks seems to agree with that expected

during number processing (e.g. Chochon et al., 1999; Stanescu-Cosson et al., 2000). A lack of predicted fronto-parietal connectivity to the dorsolateral prefrontal cortex may be explained by similar findings in working memory tasks where children do not seem to activate a network of parietal and dorsolateral prefrontal cortex areas to the same degree as adults (Scherf et al., 2006).

The alcohol-exposed children showed less extensive functional connectivity, particularly fronto-parietal, when compared to that seen in the control children. This may explain some of the functional activation differences reported by Meintjes et al. (2007), but the lack of statistical power to detect significant group differences yielded the observation inconclusive and further studies with more alcohol-exposed subjects are suggested.

Table of Contents

List of Figures

List of Tables

Glossary

***a priori* model:** a model based on previous knowledge

Acalculia: the inability to perform simple mathematical calculation

Agenesis: absence or failure of formation

Alcohol-related neurodevelopmental disorder (ARND): the diagnosis of children with a history of maternal drinking during pregnancy, who exhibit cognitive or behavioural deficits but lack the facial abnormalities required for the diagnosis of FAS

Autoregressive model: the estimation of the current value of a time series from a linear sum of past values

BOLD imaging: a functional magnetic resonance imaging technique that exploits T2* tissue contrast (which results from changes in blood oxygenation following changes in neural activity)

Deoxyhaemoglobin: haemoglobin not combined with oxygen, i.e. reduced

Diamagnetism: the magnetic property of a substance with an even number of protons and neutrons that causes it to be weakly repelled from a magnetic field

Dyscalculia: the difficulty in performing simple mathematical problems

Echo planar imaging: rapid switching of the linear field gradients following a single RF pulse, corresponding to a raster-like scanning trajectory in k-space

Effective connectivity: 'the influence one neuronal system exerts over another' (Friston et al., 1993a)

Electroencephalography (EEG): measurement and registration of brain electric potentials recorded from electrodes attached to the scalp (Stedman, 2000)

Fisher z-transformation: the normalisation of the distribution of a correlation coefficient

Flip angle: the angle through which the net magnetisation vector is tipped relative to the direction of the static magnetic field following radiofrequency pulse excitation

fMRI Preprocessing: analyses performed on the original fMRI data to remove confounding effects (e.g. motion and low frequency noise) and improve the signal-to-noise ratio to prepare the data for further analysis

Foetal alcohol spectrum disorder (FASD): a range of defects caused by prenatal exposure to alcohol, including cognitive and behavioural deficits

Foetal alcohol syndrome (FAS): the most extreme form of foetal alcohol spectrum disorder, diagnosed by a characteristic facial dysmorphology (short palpebral fissures, thin upper lip, indistinct philtrum), small head circumference and growth retardation.

Functional connectivity: 'the observed temporal correlations between spatially remote neurophysiological events' (Friston et al., 1993b)

Functional integration: interactions between specialised brain regions

Functional magnetic resonance imaging (fMRI): measurement and localisation of MRI signal changes over time

Functional segregation: specialisation of functions within different brain regions

Gradient echo (GRE): reversal of the direction of a linear field gradient to rephase the magnetic dipole moments (which lose phase coherence over time) before signal acquisition

Granger causality mapping (GCM): a functional and effective connectivity technique that maps the functional relationships in time between a seed region and the rest of the brain, characterising instantaneous and causal effects

Granger causality: the use of temporal precedence information in time series to determine a direction of causality between them

Gyromagnetic ratio: a unique constant for each type of atom, which quantifies the relationship between the Larmor precession frequency and strength of the applied magnetic field (e.g. $\gamma = 42.575$ MHz/T for 1H).

Haemoglobin: a protein located in red blood cells that has a high affinity for oxygen

Hypoplasia: reduced formation

Inter-region correlation: correlation analysis between the average time series of two regions of interest

Inversion time (TI): time following inversion of the spins with a 180° inversion pulse

***k*-space:** two-dimensional Fourier Transform or spatial frequency space

Larmor frequency: the frequency of precession of a magnetic dipole moment placed in an external magnetic field

Magnetic resonance imaging (MRI): the application of nuclear magnetic resonance to radiological imaging, creating high resolution anatomical images

Magnetoencephalography (MEG): the measurement and recording of the magnetic field of the brain (Stedman, 2000)

Microcephaly: abnormal smallness of the head

Morphometric: pertaining to the measurement of shape or form

Nuclear magnetic resonance: a resonance interaction of nuclei that have a magnetic dipole moment placed in an applied magnetic field

Oxyhaemoglobin: haemoglobin combined with oxygen

Paramagnetism: the magnetic property of a substance with an uneven number of protons and neutrons that causes it to be attracted to a magnetic field

Partial foetal alcohol syndrome (PFAS): a less extreme form of FASD than full FAS, diagnosed when there is confirmed exposure to alcohol before birth, the presence of two of the three principal facial anomalies associated with FAS and at least one additional deficit: small head circumference, growth retardation or cognitive and / or behavioural impairment.

Perfusion: flow of blood per unit volume of tissue

Positron emission tomography (PET): the creation of tomographic images revealing certain biochemical properties of tissue by computer analysis of positrons emitted when radioactively tagged substances are incorporated into the tissue (Stedman, 2000)

Psychophysiological Interaction: a change in the functional contribution of one brain area to another in response to a change in experimental context

Radio-frequency: the $10^4 - 10^{11}$ Hz range of frequencies in the electromagnetic spectrum

Repetition time (TR): the time between radio-frequency excitation pulses

Seed-voxel connectivity: an exploratory functional connectivity mapping technique that compares the average time series of a single region of interest to the time series of every voxel in the brain

Single photon emission computed tomography (SPECT): tomographic imaging of metabolic and physiologic functions in tissues, the image being formed by computer synthesis of photons of a single energy emitted by radionuclides administered in suitable form to the patient (Stedman, 2000)

Teratogen: an agent that causes abnormal prenatal development

Time to echo (TE): the time between the radio-frequency excitation pulse and echo

Tomography: the creation of an image in a certain plane

Volumetric: pertaining to the measurement of volume

List of Abbreviations

ADC	Analogue-to-Digital converter
AG	Angular gyrus
AR	Autoregressive
ARND	Alcohol-related neurodevelopmental disorder
BOLD	Blood oxygenation level-dependent
CSF	Cerebro-spinal fluid
DCM	Dynamic causal modelling
DLPFC	Dorsolateral prefrontal cortex
EEG	Electroencephalography
EMF	Electromotive force
EPI	Echo planar imaging
FAS	Foetal Alcohol Syndrome
FASD	Foetal Alcohol Spectrum Disorder
fcMRI	Functional connectivity mapped with MRI
FID	Free induction decay
fMRI	Functional Magnetic Resonance Imaging
FWHM	Full width at half maximum
GCM	Granger Causality mapping
GLM	General linear model
GRE	Gradient echo
HIPS	Horizontal segment of the intraparietal sulcus
LPFC	Lateral prefrontal cortex
MAR	Multivariate autoregressive
MEG	Magnetoencephalography
MNI	Montreal Neurological Institute
MR	Magnetic resonance

MRI	Magnetic Resonance Imaging
NMR	Nuclear magnetic resonance
PCS	Precentral sulcus
PET	Positron Emission Tomography
PFAS	Partial Foetal Alcohol Syndrome
PFC	Prefrontal cortex
pMFC	Posterior medial frontal cortex
PPI	Psychophysiological Interaction
PSPL	Posterior superior parietal lobule
ReML	Restricted maximum likelihood
RF	Radio-frequency
ROI	Region of interest
SEM	Structural equation modelling
SPECT	Single Photon Emission Computed Tomography
SPM	(1) statistical parametric map
	(2) Statistical Parametric Mapping (software package)
TE	Time to echo
TI	Inversion time
TR	Repetition time
VIP	Ventral intraparietal area in the monkey cortex
VPR	Variable parameter regression

List of Symbols

$\boldsymbol{\mu}$	magnetic dipole moment
$\boldsymbol{B_0}$	static magnetic field applied for magnetic resonance imaging
H	potential energy associated with $\boldsymbol{\mu}$ in the presence of $\boldsymbol{B_0}$
ω_L	Larmor frequency measured in rad/s
f_L	Larmor frequency measured in Hz
γ	gyromagnetic ratio
T	tesla
$\boldsymbol{M}$	net magnetisation vector
$\boldsymbol{M_0}$	net magnetisation vector at equilibrium
M_{xy}	transverse magnetisation component
M_z	longitudinal magnetisation component
$\boldsymbol{B_{RF}}$	radio-frequency pulse
$\boldsymbol{B_1}$	radio-frequency pulse
α	flip angle
Φ	time-varying magnetic flux
ε	electromotive force
T_1	spin-lattice relaxation time constant
T_2	spin-spin relaxation time constant
T_2^*	rate of decay of transverse magnetisation governed by magnetic field inhomogeneity effects
G_z	slice encoding linear field gradient
G_x	frequency encoding linear field gradient
G_y	phase encoding linear field gradient
$s_r(t)$	received MR time signal (i.e. in a stationary reference frame)
$s(t)$	demodulated baseband MR signal (i.e. in a rotating reference frame)
k	spatial-frequency, including k_x, k_y (and k_z) components

r	sample Pearson product moment correlation coefficient
z	standardised sample correlation coefficient
β	parameter estimate in regression analysis
$F_{x,y}$	measure of linear dependence between time series x and y in GCM
$F_{x\to y}$	measure of directed influence from time series x to y in GCM
$F_{y\to x}$	measure of directed influence from time series y to x in GCM
$F_{x.y}$	measure of instantaneous causality between time series x and y in GCM

1 Introduction

1.1 Background

Alcohol is a teratogen; capable of causing abnormal foetal development. Foetal alcohol spectrum disorder (FASD) describes a continuum of defects caused by prenatal exposure to alcohol and can lead to cognitive and behavioural deficits in children (Stratton et al., 1996; Mattson and Riley, 1996).

Hoyme and colleagues (2005) describe specific criteria for diagnosing different degrees of FASD. Foetal alcohol syndrome (FAS), the most extreme form of FASD, is diagnosed by a characteristic facial dysmorphology (short palpebral fissures, thin upper lip, indistinct philtrum), as seen in Fig.(1.1), small head circumference and growth retardation. Partial FAS (PFAS) is diagnosed when there is confirmed exposure to alcohol before birth, the presence of two of the three principal facial anomalies associated with FAS and at least one additional deficit: small head circumference, growth retardation or cognitive and / or behavioural impairment. Alcohol-related neurodevelopmental disorder (ARND) is the term applied to children with a history of maternal drinking during pregnancy, who exhibit cognitive or behavioural deficits but lack the facial abnormalities required for the diagnosis of FAS (Stratton et al., 1996).

Figure 1.1: Short palpebral fissures, a thin upper lip and an indistinct philtrum are characteristic facial features of FAS

FASD is difficult to diagnose in infancy and childhood because a history regarding prenatal alcohol exposure may be lacking, the distinctive facial dysmorphology need not be exhibited and abnormal behaviour could be confused with other disorders (Jacobson et al., 2008). Deficits in number processing and executive function are among the most consistently reported problems (e.g. Streissguth et al., 1991; 1994; Kopera-Frye et al., 1996). Poorer language, memory, and motor function are also frequently seen (Mattson and Riley, 1998).

In the Cape Coloured community in Cape Town, South Africa, there is an unusually high incidence of alcohol abuse and dependence in women of child-bearing age, very heavy alcohol consumption during pregnancy (Croxford and Viljoen, 1999) and consequently one of the highest incidences of FAS in the world. The incidence has been estimated to be 18 to 141 times greater than in the United States (May et al., 2000). This population is therefore ideally suited to research of FASD.

This study forms part of a larger initiative designed to advance our understanding of the neural substrates that mediate FASD, ultimately hoping to contribute to improved diagnosis and treatment of the disorder.

1.2 Literature review

1.2.1 Foetal Alcohol Spectrum Disorder

Prenatal exposure to alcohol was originally thought to cause non-specific and diffuse brain damage (Clarren, 1986; Mattson and Riley, 1996) because of the numerous cognitive and behavioural deficits seen in children with FASD (Mattson and Riley, 1998). Children with full FAS are generally mentally retarded (IQ < 70) but the range of intellectual disability varies widely (Streissguth et al., 1990; 1991; Mattson et al., 1997). It has been found that the IQ of children with ARND depends on the mother's age as well as alcohol consumption during pregnancy (Jacobson et al., 1994; 2004). Deficits in executive functions and arithmetic, in particular, appear to be characteristic of the disorder (Streissguth et al., 1989; 1991; 1994; Kopera-Frye et al., 1996; Burden et al., 2005a; Howell et al., 2006). However, number reading and writing ability remains intact (Kopera-Frye et al., 1996) and the arithmetic deficit

has been shown to be independent of IQ (Goldschmidt et al., 1996; Carmichael Olson et al., 1998). Other difficulties experienced by children with FASD include deficits in verbal learning (Streissguth et al., 1989; Mattson et al., 1996; Coles et al., 1997; Kaemingk et al., 2003), attention and working memory (Kodituwakku et al., 1995; Coles et al., 1997; 2002; Burden et al., 2005b; Rasmussen, 2005), cognitive processing speed and response time (Streissguth et al., 1990; Jacobson et al., 1993; 1994; Coles et al., 2002; Burden et al., 2005a), visual-spatial reasoning (Carmichael Olson et al., 1998), motor control (Roebuck et al., 1998a; 1998b) and eyeblink conditioning (Jacobson et al., 2008).

Experimental studies with laboratory animals, autopsy reports and sophisticated neuroimaging investigations have determined that alcohol has a particular teratogenic effect, affecting specific regions of the brain differentially. Neuroanatomical effects associated with FASD were initially identified from post-mortem results and include microcephaly, partial or complete agenesis of the corpus callosum, abnormalities of the cerebellum and brain stem and failure of certain cells to migrate during embryonic development (Jones and Smith, 1973; Clarren, 1977; Clarren and Smith, 1978; Mattson, 2000).

Structural magnetic resonance imaging (MRI), volumetric and morphometric analyses of children with FASD extended previous observations to include disproportionate hypoplasia of the parietal lobe, basal ganglia (especially the caudate nucleus) and cerebellum (Archibald et al., 2001). Mildly reduced perfusion of the left hemisphere, particularly the parietooccipital region, has been demonstrated using single photon emission computed tomography (SPECT) and suggests impairment of the arithmetic and logical-grammatical functions in that region (Riikonen et al., 1999).

Whole-brain surface based image analyses have allowed researchers to extract new, specific and detailed information about the effects of prenatal exposure to alcohol on the brain (Riley et al., 2004). Results show anterior and inferior displacement of the posterior regions of the corpus callosum, which connects the temporal and parietal lobes (Sowell et al., 2001a). Reduction in the size of the ventral aspects of the frontal cortex and narrowing of the inferior parietal and perisylvian regions together with increased grey matter densities have been found (Sowell et al., 2002a). A voxel-based morphometry analysis shows a disproportionate increase in grey matter compared to white matter in the left hemisphere perisylvian cortices of the temporal and parietal lobes (Sowell et al., 2001b). Similarly, the cortical surface grey matter asymmetry typically found in the posterior inferior temporal lobes was shown to be

altered in the brains of children with FASD (Sowell et al., 2002b). The anterior and posterior inferior cerebellar vermal regions were found to be reduced in size and displaced (O'Hare et al., 2005). Significant excesses in cortical thickness have been reported in the bilateral temporal, bilateral inferior parietal and right frontal cortical regions (Sowell et al., 2008).

It is the functional significance of any structural abnormalities that may lead to an understanding of the cognitive and behavioural deficits seen in children with FASD. Previous functional magnetic resonance imaging (fMRI) studies in children with FASD reported reductions in superior parietal and frontal cortical activity during a spatial working memory task (Malisza et al., 2005) and reduced activity in left medial and posterior temporal cortices together with increased activity in right dorsal frontal cortex in a verbal learning study (Sowell et al., 2007). The apparent vulnerability of the parietal lobe to prenatal alcohol exposure (Sowell et al., 2001b; Mattson, 2000) has been investigated by Meintjes et al. (2007) using two number processing tasks.

1.2.2 Number Processing

Acalculia and dyscalculia are the absence of and difficulty with performance of arithmetic calculation, respectively. Traditionally, lesion studies were the only means of determining function (or lack thereof) in the brain. Dissociable types of dyscalculia were discovered when different types of number processing tasks were administered to patients with differently located brain lesions and selective deficits were recorded (Dehaene and Cohen, 1997; Dehaene, 1997; Chochon et al., 1999). For example, one of the symptoms of Gerstmann's syndrome, which involves a lesion of the left inferior parietal lobule, is a lack of quantitative numerical knowledge but with preserved knowledge of digit naming and rote learned arithmetic facts (Gerstmann, 1940; Dehaene et al., 1992). This finding suggested the importance of the inferior parietal cortex in number processing, but lesion size made it difficult to infer a precise spatial location for this functional deficit (Chochon et al., 1999).

Neuroimaging advances allowed the non-invasive study of brain function on a large scale (providing enough data for sound group statistical analyses, unlike previous lesion study results (Chochon et al., 1999)). A fronto-parietal network involving the bilateral inferior parietal cortex, prefrontal cortices (PFC) and anterior cingulate gyrus was consistently reported to be active during number processing tasks (e.g. Chochon et al., 1999; Stanescu-

Cosson et al., 2000), involved in both magnitude representation and non-arithmetic task execution and error monitoring (Menon et al., 2000).

A triple-code model for number processing was proposed by Dehaene in 1992, based on data from lesion studies, animal studies and clinical testing with infants, normal and gifted adults. Neuroimaging findings allowed Dehaene and colleagues to update the model in 2003. The model assumes that number processing is organised neurally as a quantity system, the activation of which is dependent on the magnitude and distance between the numbers being manipulated, a verbal system for word representation of numbers and a visual system for internal visualisation of Arabic numerals and maintenance of visuo-spatial attention.

Further studies revealed likely candidate brain areas responsible for the above functions. Chochon and colleagues (1999) demonstrated that bilateral intraparietal activation was present in a number comparison task (slightly greater on the right than the left) and was greater during a subtraction task (involving manipulation of quantities) than a multiplication task (reliant on rote learned facts accessible in verbal memory). Stanescu-Cosson and colleagues (2000) found that there was greater bilateral intraparietal activation during approximation than calculation and that the activation increased in proportion with number magnitude. Concurrently, it was found that the angular gyrus was active bilaterally during exact calculation with small numbers (i.e. simple addition and multiplication), when the intraparietal region showed little or no activation (Stanescu-Cosson et al., 2000). Menon and colleagues (2000) discovered that with increasing arithmetic complexity (i.e. increasing the number of operands), the bilateral activation of angular gyrus and adjoining intraparietal sulcus increased. Simon and colleagues (2002) showed that the depth of the horizontal segment of the intraparietal sulcus was activated solely during calculation and not during other tasks, while the left angular gyrus was activated during both calculation and language processing tasks but not during visuo-spatial tasks. It was found that activation of the posterior superior parietal lobule was not specific to the calculation task, occurring during spatial, attentional, eye and finger movement tasks too (Simon et al., 2002).

Dehaene and colleagues (2003) identified three areas within the parietal lobe that appear to play distinct roles in number processing: the bilateral anterior section of the horizontal segment of the intraparietal sulcus (HIPS), the bilateral posterior superior parietal lobule (PSPL) and the left angular gyrus (AG), which appear to be important for quantity representation, spatial attention and verbal processing of number, respectively.

Supporting evidence for the proposed model includes the fact that the bilateral anterior HIPS is activated when a quantitative representation of number is required, whether or not explicit magnitude processing follows (Eger et al., 2003). Also, the activation of the anterior HIPS is independent of the modality and notation used to present the numbers (e.g. Arabic numerals or sequences of words) (Dehaene and Cohen, 1995; Naccache and Dehaene, 2001; Pinel et al., 2001). The bilateral PSPL is activated during number counting (Piazza et al., 2003) and a variety of visuo-spatial tasks, including attention orienting and mental rotation (Dehaene et al., 2003). Dehaene and colleagues (2003) proposed that the PSPL is responsible for number-based attention, especially required during number comparison (Pinel et al., 2001) and approximation tasks (Dehaene et al., 1999) when it is necessary to attend to specific quantities on a quasi-spatial 'mental number line'. The left AG, associated with the adjacent perisylvian language system, is activated in proportion to the verbal processing requirements of a number processing task (Stanescu-Cosson et al., 2000), particularly for multiplication, which is heavily dependent on rote verbally encoded number facts (Dehaene et al., 2003). It is also activated in other types of language mediated processes, for example reading and phoneme detection (Simon et al., 2002; Dehaene et al., 2003).

A fronto-parietal circuit is activated in the brains of number-competent macaque monkeys during simple number processing tasks, which appears to be homologous to the number processing network identified in humans (Simon et al., 2002). Single-cell electrophysiological studies of activity in the ventral intraparietal (VIP) area of the macaque monkey brain provide additional support for the existence of a brain region specialised for semantic representation of quantity in man. The region is believed to be homologous to the anterior HIPS (Nieder and Miller, 2003; Dehaene et al., 2004). Research in timing and delay of neuronal firing in macaque monkeys has shown that neurons fire in response to specific numerosities and that numerical information is first computed in the parietal cortex before being transmitted to the lateral prefrontal cortex (Nieder et al., 2002; Nieder and Miller, 2003; Dehaene et al., 2004).

The frontal activations seen to accompany parietal activations during number processing tasks in man appear to have an important supportive function, witnessed when, for example, lesions to the prefrontal cortex result in a form of acalculia (Menon et al., 2000; Delazer et al., 2004). By increasing task difficulty (by changing the rate of task presentation), Menon and colleagues (2000) found that inferior frontal activation was affected by the time pressure

imposed rather than by the complexity of the calculations being computed. The left precentral sulcus (PCS) is activated in a region that overlaps the premotor strip at the coordinates of finger representation (Zago et al., 2001). It has been suggested that this activation may be related to the importance of finger counting in the acquisition of numerical knowledge. The posterior medial frontal cortex (pMFC), which includes the dorsal anterior cingulate, is also activated in number processing. This region has been shown to be involved in continuous monitoring of performance (response decision and execution, response errors and conflicts) (Ridderinkhof et al., 2004). Any adjustments required following error detection by the pMFC appear to be implemented by the lateral prefrontal cortex (LPFC) (Ridderinkhof et al., 2004). Badre and Wagner (2004) have shown that the middle areas of the dorsolateral prefrontal cortex (DLPFC) are activated when selection between conflicting responses is required, particularly with reference to the requirements of the task. Ridderinkhof and colleagues (2004) suggest strong functional connections between the pMFC and PFC due to their frequently observed concomitant and interdependent activity.

The two core number processing abilities of the brain are magnitude comparison (e.g. number comparison – "which number is larger?", proximity judgement – "which of two numbers is closer to a third number?") and exact calculation (e.g. addition, subtraction, multiplication) (Dehaene and Cohen, 1997; Menon et al., 2000; Feigenson et al., 2004). By implementing two number processing tasks, Exact Addition and Proximity Judgement, in a functional neuroimaging study, Meintjes and colleagues (2007) determined that normal control children activate an expected fronto-parietal network (e.g. Stanescu-Cosson et al., 2000), while activations in children with FASD differ significantly from those observed in healthy controls. In both number processing tasks, the fronto-parietal network activated in the control group consists of the left posterior HIPS, bilateral precuneus, bilateral DLPFC, bilateral pMFC, left PCS and bilateral anterior insula, differing only in the activation of the anterior HIPS, which is right lateralised during Proximity Judgement and left lateralised during Exact Addition. Children with FASD show significantly less activation of the left posterior HIPS during both tasks. In addition, during Proximity Judgement, FAS / PFAS children show significantly less activity compared to controls in the right anterior HIPS, pMFC and left PCS but significantly greater activation of bilateral AG, precuneus and posterior cingulate. During Exact Addition, the children with FASD show increased activation of areas not typically linked to number processing, such as the bilateral cuneus / calcarine sulcus, anterior cerebellum, and thalamus.

This project aims to investigate the integrity of the neural pathways during number processing in normal children compared to children with FASD.

1.2.3 Connectivity

Lesion studies and experiments on non-human mammals (e.g. Lawler and Cowey, 1987) led to the belief that the brain is compartmentalised into areas specialised for performing a particular task (Büchel and Friston, 2000). As techniques for examining the workings of the brain were developed (e.g. intracranial electrode recordings, nontomographic xenon-133 inhalation (Prohovnik et al., 1980) and electroencephalography (EEG)), the theory of functional integration has emerged (Horwitz, 2003). The discovery of non-invasive neuroimaging techniques (e.g. positron emission tomography (PET) and fMRI) has allowed the measurement of functional activity throughout the volume of the brain (Horwitz, 2003).

The concepts of functional and effective connectivity were introduced (Aertsen & Preissl, 1991) and formalised (Friston et al., 1993a; 1993b) to quantify the strength of interactions between specialised brain regions. *Functional connectivity* is defined as 'the observed temporal correlations between spatially remote neurophysiological events' (Friston et al., 1993b). In fMRI, simultaneous variations in blood oxygenation level-dependent (BOLD) signal indicate synchronous changes in cerebral blood flow and therefore, the existence of functional connections at the neuronal level (Cordes et al., 2000). The interdependence of functionally related brain regions can be determined by calculating the degree of correlation between regional fMRI time series (Cordes et al., 2000). Functional connectivity is simply a statement about the observed correlations in activity without making any direct inferences about mediation among the correlations (Friston et al., 1993a).

Effective connectivity is defined as 'the influence one neuronal system exerts over another' (Friston et al., 1993a). It is dynamic; quantifying activity- and time-dependent changes in function across the brain (Friston, 1998). Effective connectivity measurements rely on the ability to resolve a delay in activation between regions (measured in milliseconds at the neuronal level), indicating causality of function (Roebroeck et al., 2005). Therefore, the practical implementation of effective connectivity differs from that of functional connectivity, which relies only on instantaneous correlations (Büchel and Friston, 2000). Many methods of extracting effective connectivity information from neurophysiological data are model-based

(e.g. structural equation modelling and dynamic causal modelling) and, therefore, the results depend on the anatomical accuracy, computational complexity and ability to interpret the model (Friston et al., 1993b; Büchel and Friston, 1997; Marrelec et al., 2006). Some methods (e.g. Granger causality mapping) are data-driven and exploratory in nature, useful in the initial stages of investigation if little is known from the literature about the functional network being studied (Roebroeck et al., 2005).

In order to compare connectivity results between experiments and across different signal acquisition modes (e.g. EEG, PET, fMRI), a thorough understanding of the biological basis of the signal is essential (Horwitz, 2003). The different types of data differ in temporal and spatial resolution and require different preprocessing and computational algorithms for the analysis of interregional dependencies. The results are only as valid as the model chosen, time series preparation, statistical assessment and neural substrate assumed (Caclin and Fonlupt, 2006; Horwitz, 2003).

Correlation is a simple method for measuring functional connectivity, originally used in the analysis of electrophysiological data from multiunit electrode recordings, which can be applied to neuroimaging data (Büchel and Friston, 2000). The amount of correlation between two average fMRI time series quantifies the functional relationship between two regions of interest (ROIs). Similarly, calculating the cross correlation between the average fMRI time series of an ROI and the fMRI time series of every other voxel in the brain, yields a map of areas functionally connected to the ROI (Arfanakis et al., 2000).

Resting functional connectivity mapped with MRI (fcMRI) measures functional connectivity across the brain during rest (Cordes et al., 2000). Maps showing synchronous changes in signal intensity in the resting state can identify areas that are functionally connected, and which tend to activate together during the performance of a particular task. Although the technique has been found to be feasible, bulk motion and low frequency aliasing can present a problem (Cordes et al., 2000).

Pure correlation analysis may incorrectly show functional connections where there are, in fact, common inputs (Büchel and Friston, 2000). Therefore, partial correlation analysis has been proposed to measure direct correlation between regions, once the effects of common influences have been removed (Marrelec et al., 2006).

Simple linear regression between time series of interest yields information about the functional connectivity between regions. For example, if the activity (i.e., haemodynamic changes in the BOLD signal) of one region is regressed on the activity of a second region, the regression coefficients reflect the variability in the first region that can be explained in terms of the variability in the second region (Friston et al., 1997).

A vector of regression coefficients from multiple linear regression analyses estimates the effective contributions to an ROI from regions across the brain (Büchel and Friston, 2000). Areas of the brain that have similar patterns of activation during the progress of the experiment are considered to be functionally connected. Even though a linear model is used to estimate a non-linear physiological phenomenon, it has been shown that multiple linear regression sufficiently explains brain function in response to 'simple and well-organised' experiments (Büchel and Friston, 2000).

However, the many inputs to an ROI do interact with one another. They are not linearly separable and independent as assumed by linear models (Friston, 1998). Therefore, the linear model has been extended to include modulatory effects between regions. Vectors of 'driving' and 'modulatory' regression coefficients are interpreted as measures of connection strength for the proposed paths between brain regions (Büchel and Friston, 2000). The method is sufficient for calculating effective connectivity to a single region at a time, but more complicated models are necessary when more ROIs are introduced. However, each contribution is incorrectly assumed to be constant over the range of activation for the duration of the experiment (Büchel and Friston, 2000).

Variable parameter regression (VPR) recognises that connectivity is not constant over the whole range of activation for the duration of the experiment and that there will be differences between times of 'activation' and 'non-activation' (Büchel and Friston, 2000).

Psychophysiological Interaction (PPI) analysis, first proposed by Friston and colleagues (1997), is a means of quantifying functional integration within the brain. A change in the functional contribution of one brain area to another ('physiological') in response to a change in experimental context ('psychological') is termed a PPI (Friston et al., 1997). The technique has been used for connectivity analyses of both fMRI and PET neuroimaging data. A limiting

factor of the PPI technique is that it is based on instantaneous regression equations and does not exploit the temporal information contained in the time series data. This restricts the analysis to functional connectivity as nothing can be concluded about the causality relating the detected influences (Roebroeck et al., 2005).

More regions of interest and non-linear modulatory effects have been included in structural equation modelling (SEM) (Büchel and Friston, 2000; Gonzalez-Lima and McIntosh, 1995). Developed in the fields of economics, psychology and social sciences (Büchel and Friston, 1997), SEM is a technique designed to quantify path connectivity between pre-selected regions of interest. Applied in the field of neuroimaging, SEM tests the goodness of fit of an anatomical model with assumed directed connections (Ramnani et al., 2004) to the observed covariance structure. The covariance structure describes the degree of relatedness between regions (Büchel and Friston, 1997) and the free parameters in the model quantify the connection strengths. Although the technique is linear, non-linear modulations can be inferred by comparing models with and without a modulatory influence or by including non-linear variables in the model (Büchel and Friston, 1997). Disadvantages of the method include a limit to the number of regions that can be modelled due to computational expense, and the absence of temporal modelling (Ramnani et al., 2004).

Historically applied to EEG and magnetoencephalography (MEG) data (Ramnani et al., 2004), multivariate autoregressive (MAR) models use the temporal structure of a network of voxel-based fMRI time series to infer information about interregional dependencies (Harrison et al., 2003). The current values of many (i.e. multivariate) time series are estimated from a linear sum of past values (i.e. an autoregressive process) and therefore effective connectivity to one region in the network is estimated from the historical influence of all other regions. Depending on the requirements of the experiment, the MAR model may contain every region connected to every other region, or, like SEM, have fewer connections based on anatomical and / or functional connectivity information (Harrison et al., 2003).

Granger causality mapping (GCM) is an application of MAR in the context of Granger causality (Granger, 1969; Geweke, 1982). Temporal and spatial information inherent in fMRI time series data is exploited. GCM maps the functional relationships in time between a seed region and the rest of the brain and does not rely on *a priori* model. The connectivity maps characterise both instantaneous effects between coactivated brain regions (i.e. functional connectivity) and causal effects (i.e. effective connectivity) acting over time (Goebel et al.,

2003). Directed, non-instantaneous effects occur if activity changes in one region effect changes in a second region at a later point in time.

Unlike previous models, dynamic causal modelling (DCM) was developed especially for the analysis of functional imaging data (Ramnani et al., 2004) and distinguishes between neurodynamics (where non-linear and dynamic changes occur) and haemodynamics (where changes are observed) (Friston et al., 2003). A neuronal model of interacting cortical regions is subjected to experimentally designed driving and modulatory inputs, the effects of which are distributed throughout the system. Any changes in neuronal activity are convolved with the local haemodynamic response to cause the measured fMRI time series response (Buxton, 2002; Friston et al., 2003). The difference between the observed and measured data is minimised using a non-iterative, non-linear fitting process. The resultant neurodynamic parameters are interpreted as measures of effective connectivity, quantifying interregional- and self-connections (Friston et al., 2003). DCM analysis relies on the design of multifactorial experiments (i.e. combining two or more factors within a task, for example, visual and auditory stimuli) with enduring modulatory inputs (e.g. attention or non-attention to the auditory cues while watching the visual stimulus) to produce useful effective connectivity results (Friston et al., 1997; 2003).

It is possible for functional connectivity to be negative, indicating an inverse relationship between signals in different brain regions. Regions that activate during goal-directed cognitive tasks, like working memory, have been found to exhibit negative connectivity with regions that de-activate during the same tasks (Raichle et al., 2001; 2007). These regions have been referred to as the 'default mode network' believed to be responsible for 'intrinsic functional activity' and the constantly high energy demands of the brain unexplained by transient evoked activity during task performance (Raichle et al., 2007).

Das et al. (2005) suggest that 'breakdowns in the interactions between brain regions may be related to the affect-related symptoms' and therefore, knowledge about 'normal' connectivity in the brain and where the children with FASD differ may help in understanding the disorder better. Previously-collected fMRI data was used for connectivity analysis. This limited the types of analyses possible, and, for example, effective connectivity analyses, which require a particular experimental design, could not be implemented. The functional connectivity techniques of correlation and linear regression, however, allow the extraction of simple yet meaningful information about functional integration between brain regions.

2 Theory

2.1 Magnetic Resonance Imaging Theory

2.1.1 The MRI Signal, Spatial Encoding and Image Formation

Discovered in 1946 by two physics research groups led by E. Purcell and F. Bloch, nuclear magnetic resonance (NMR) applied to radiological imaging forms the basis of magnetic resonance imaging (MRI) (Bushberg et al., 2002). As the name suggests, NMR involves the placement of appropriate nuclei in a strong magnetic field to witness a resonance phenomenon. The word 'nuclear' has been omitted from the name 'MRI' to avoid confusion with another medical imaging technique, nuclear medicine, which involves ionising radiation.

Nuclei that have an uneven number of nucleons (i.e. protons and neutrons) have net angular momentum and an associated magnetic dipole moment $\boldsymbol{\mu}$ that causes them to align with and precess about an applied magnetic field. Biologically relevant examples of such nuclei include hydrogen-1, carbon-13 and phosphorous-31. The hydrogen nucleus, or 'proton', is most often imaged with MRI due to its abundance of 63% in tissue water and natural abundance of 99.985%.

Randomly oriented protons that are placed in an external magnetic field, $\boldsymbol{B_0}$, (typically of magnitude 1.5 T or 3 T in medical applications) interact with the field according to the nuclear Zeeman relationship

$$H = -\boldsymbol{\mu} \cdot \boldsymbol{B_0}, \tag{2.1}$$

where H is the potential energy associated with a magnetic dipole moment $\boldsymbol{\mu}$ in the presence of $\boldsymbol{B_0}$.

The equation describing the motion of a magnetic dipole moment $\boldsymbol{\mu}$ placed in a field $\boldsymbol{B_0}$ is

$$\frac{d\boldsymbol{\mu}}{dt} = \boldsymbol{\mu} \times \gamma \boldsymbol{B}_0 . \tag{2.2}$$

The field exerts a torque of $\boldsymbol{\mu} \times \boldsymbol{B}_0$ on the magnetic dipole moment which causes $\boldsymbol{\mu}$ to precess about the direction of $\boldsymbol{B}_0$ (assumed to be the longitudinal, z-direction) at the Larmor frequency given by

$$\omega_L = \gamma B_0 \text{ rad/s} \tag{2.3}$$

or

$$f_L = \frac{\gamma}{2\pi} B_0 \text{ Hz}, \tag{2.4}$$

which is proportional to the strength of the local magnetic field. γ is the gyromagnetic ratio and is a unique constant for each type of atom (e.g. $\gamma = 42.575$ MHz/T for ^{1}H). Therefore, in a magnetic field of 1.5 T, the resonance frequency of ^{1}H is calculated to be 63.86 MHz. Once equilibrium has been established, summation of the millions of precessing magnetic dipole moments in the sample results in a weak net magnetisation vector, $\boldsymbol{M}_0$, parallel to the applied field $\boldsymbol{B}_0$ (Buxton, 2002), as illustrated in Fig.(2.1a).

A time-dependent radio-frequency (RF) pulse, $\boldsymbol{B}_{RF}$, of the form

$$\boldsymbol{B}_{RF} = 2\boldsymbol{B}_1 \cos(\omega t), \tag{2.5}$$

transmitted perpendicular to the direction of the main magnetic field $\boldsymbol{B}_0$ and oscillating at the Larmor precession frequency ω_L, will 'excite' the magnetisation. The protons in the sample absorb energy (a resonance effect that would not occur at any other frequency) and once the RF pulse has been turned off, release that energy in order to return to an equilibrium state. The macroscopic effect is that the net magnetisation vector $\boldsymbol{M}$ is tipped into the transverse plane through some angle, resulting in a transverse magnetisation component, M_{xy}, that

precesses about the longitudinal axis at the Larmor frequency once $\boldsymbol{B_{RF}}$ has been turned off, as illustrated in Fig.(2.1b).

The flip angle α is determined by the duration of the RF pulse. A 90-degree pulse is defined as the time for which $\boldsymbol{B_1}$ must be applied to tip the magnetisation vector $\boldsymbol{M}$ through 90° (i.e. entirely into the transverse plane) and is given by

$$t_{\frac{\pi}{2}} = \frac{\pi}{2\gamma B_1}. \tag{2.6}$$

Similarly a 180-degree pulse rotates $\boldsymbol{M}$ through 180° until it is anti-parallel to the external magnetic field and there is no transverse magnetisation component, M_{xy}. The time required for this inversion is given by

$$t_{\pi} = \frac{\pi}{\gamma B_1}. \tag{2.7}$$

According to Faraday's law of induction

$$\varepsilon = \frac{-\partial \Phi}{\partial t}, \tag{2.8}$$

rotation of the transverse magnetisation vector, M_{xy}, causes a time-varying magnetic flux, Φ, that induces a proportional electromotive force (EMF), ε, in a transversely aligned receiver coil. This EMF is the MRI signal and is called a free induction decay (FID). It includes contributions from all precessing transverse magnetisation in the sample (Buxton, 2002).

Once the RF pulse has been switched off, the magnetisation vector will realign with the main magnetic field, as illustrated in Fig.(2.1c). The rate of regrowth of the longitudinal magnetisation component M_z is governed by the spin-lattice relaxation time constant T_1 that depends on the interaction of the spins with the lattice. T_1 is defined as the time taken for the

longitudinal magnetisation to relax to 63% of its maximum value M_0. Protons in different chemical environments, such as grey matter and cerebro-spinal fluid (CSF), have different T_1 rate constants that are exploited to produce image contrast (Matthews, 2001).

The FID is an exponentially decaying signal due to the dephasing of the precessing magnetic dipole moments (Buxton, 2002). At a microscopic level, the individual protons experience different local magnetic fields and therefore each magnetic dipole moment precesses at a slightly different rate, causing a loss of phase coherence over time. At a macroscopic level this manifests as a time dependent reduction in the transverse magnetisation component M_{xy} that is quantified by the spin-spin relaxation time constant T_2. T_2 is defined as the time taken for 63% of the MRI signal to decay due to dephasing. Relatively fixed protons (e.g. in biological macromolecules) have short T_2 time constants due to fast dephasing of spins, whereas relatively mobile protons (e.g. in water) have longer T_2 time constants as individual spins experience an average local magnetic field and lose phase coherence slowly (Bushberg et al., 2002).

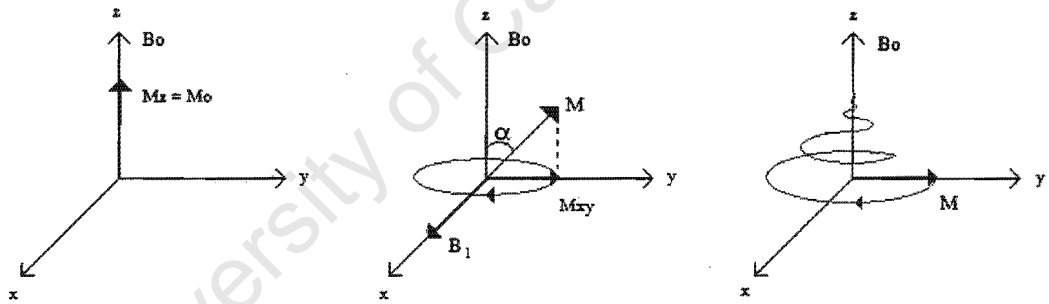

Figure 2.1: Diagram illustrating (a) the alignment of the net magnetisation vector $\boldsymbol{M}$ with the magnetic field $\boldsymbol{B_0}$ at equilibrium, (b) the effect of an RF pulse $\boldsymbol{B_1}$ at the Larmor frequency on the magnetisation vector $\boldsymbol{M}$ and creation of the transverse magnetisation component M_{xy} in a stationary reference frame and (c) the combined effects of longitudinal magnetisation M_z regrowth (T_1) and transverse magnetisation M_{xy} decay (T_2) on the relaxation of magnetisation vector $\boldsymbol{M}$, drawn in a stationary reference frame.

Spatial encoding, performed before and during signal acquisition, is used to differentiate the contributions to the signal from different regions in the sample in order to produce an image. As seen in Eq.(2.3), the frequency of precession of each proton is proportional to the local

magnetic field that it experiences. Three mutually orthogonal linear field gradients, G_x, G_y and G_z (illustrated in Fig.(2.2)), superimposed on the main field $\boldsymbol{B_0}$ at different times during the pulse sequence, are used to produce small variations in the local magnetic field experienced by protons at different positions. This will affect their precessional frequencies and can be used to locate them.

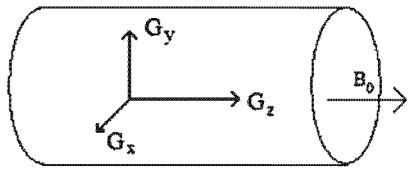

Figure 2.2: Diagram illustrating the mutually orthogonal directions of the linear field gradients G_x, G_y and G_z with reference to the bore of the magnet and direction of the static magnetic field B_0

The slice encoding gradient, G_z, is applied perpendicular to the imaging plane during the RF pulse. For example, if G_z is applied in the longitudinal z-direction, it causes the resonance frequencies of the spins to vary linearly with z-position (Bushberg et al., 2002). Application of a sinc-like RF pulse in the time domain transforms into a rectangular-like pulse in the frequency domain, therefore selectively exciting only those protons for which the resonance condition is fulfilled. The strength and frequency bandwidth of the RF pulse are chosen according to the z-position and thickness of the slice of interest. The resonance condition is only satisfied for a small band of frequencies and therefore a small band of tissue protons is excited.

By applying linear field gradients G_x and G_y in the x- and y-directions, respectively, exact Cartesian coordinates for the position of a certain signal contribution may be established. The frequency encoding gradient, G_x, is applied to encode cross sectional frequency during signal acquisition. G_x causes the frequency to vary as a function of position along the x-axis. The phase encoding gradient, G_y, is applied after slice selection but before signal acquisition, for a certain length of time to encode a particular phase distribution of the spins along the y-axis. The higher the frequency, the more phase is acquired by the spins. The excitation-relaxation cycle, repeated for n different phase encoding gradients for an image with matrix size $m \times n$, where $n \leq m$, achieves spatial encoding in the phase encoding direction.

The received MRI time signal $s_r(t)$ (i.e. from a stationary reference frame) contains contributions from all precessing transverse magnetisation in the volume of interest (Buxton, 2002), expressed as

$$s_r(t) = \int_{vol} M(\mathbf{r}, t) dV \,. \tag{2.9}$$

The demodulated baseband signal $s(t)$ (i.e. from a reference rotating at the Larmor frequency ω_L) can be written

$$s(t) = s_r(t) e^{+i\omega_L t}, \tag{2.10}$$

$$s(t) = \int_x \int_y m(x, y) e^{-i2\pi[k_x(t)x + k_y(t)y]} dx dy, \tag{2.11}$$

and

$$s(t) = F_{2D}\{m(x, y)\}\Big|_{\substack{k_x(t) = \frac{\gamma}{2\pi}\int_0^t G_x(\tau)d\tau \\ k_y(t) = \frac{\gamma}{2\pi}\int_0^t G_y(\tau)d\tau}}, \tag{2.12}$$

where k_x and k_y are spatial-frequency variables and time integrals of the gradient waveforms G_x and G_y, respectively. From Eq.(2.12) it can be seen that, at any given time, the MRI signal, $s(t)$, is the two-dimensional Fourier Transform of $m(x, y)$ at some spatial-frequency, k. Therefore, it is possible to locate the magnetisation contribution at (x, y) using a two-dimensional inverse Fourier transformation of the MRI signal to create an MRI image. Two-dimensional Fourier Transform space is referred to as k-space. It contains the raw, digitised MRI signal data. Each row contains the magnitude and phase information for a single value of the phase encoding gradient, G_y. Therefore, for every repetition of the pulse sequence with a different value of G_y (corresponding to a different value of k_y), another row of frequency encoded data is entered into k-space until enough data has been collected for the desired resolution to be achieved once the image has been reconstructed. An example of k-space data and its associated image is illustrated in Fig.(2.3). Because k is defined as the time integral of

the gradient waveform G, the order in which k-space is filled is determined by the order of gradient switching in the pulse sequence. The k-space grid is two-dimensional (i.e. $k_x \times k_y$) unless phase encoding is performed in the slice select, z-direction as well, resulting in a three-dimensional ($k_x \times k_y \times k_z$) grid and corresponding image.

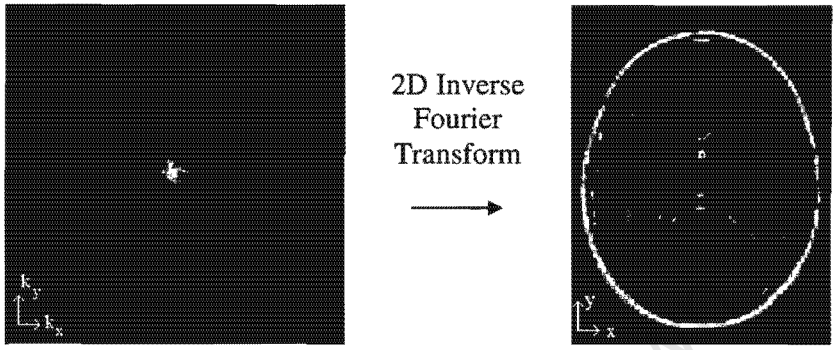

(a) (b)

Figure 2.3: Diagram illustrating an example of (a) a k-space grid and (b) the corresponding magnetic resonance image

2.1.2 Functional MRI

Unlike structural MR imaging, functional magnetic resonance imaging (fMRI) is dynamic, capturing how the MRI signal changes over time in response to some task. Brain function results from electrochemical transfer of information among neurons. Nerve impulses are propagated along nerve fibres electrically, and between neurons, chemically, by means of neurotransmitters at synapses. Neuronal activity requires energy, which, according to Gjedde (2001), is mostly used at synapses and is provided by oxidative metabolism of glucose. An increased oxygen demand is supplied and surpassed by increased cerebral blood flow, resulting in an increased concentration of oxyhaemoglobin in local venous blood.

The magnitude of the MR signal depends on the local magnetic environment of the nuclear spins. External field inhomogeneities cause rapid dephasing of spins (quantified by the relaxation time constant T_2^*) and therefore, a decrease in signal.

The haemoglobin in red blood cells is an intrinsic MRI contrast agent. Deoxyhaemoglobin is paramagnetic, causing the applied magnetic field to be attracted and the magnetic flux lines to increase. The field distortions around blood vessels containing a high proportion of deoxyhaemoglobin cause faster decay of transverse magnetisation in surrounding tissue (due to reduced T_2*) and therefore, reduced signal (Buxton, 2002).

However, the increased concentration of oxyhaemoglobin in local venous blood after increased neural activity, causes the proportion of deoxyhaemoglobin to be reduced. Oxyhaemoglobin is diamagnetic, reducing magnetic field distortions and resulting in a higher MR signal from surrounding tissue with increased T_2*.

In summary, neural activity indirectly determines the oxygenation state of haemoglobin in local blood vessels, which in turn determines the magnetic environment of that blood and the MR signal from surrounding tissue (Ogawa et al., 1993). The fMRI technique that exploits the T_2* tissue contrast that results from changes in blood oxygenation is called blood oxygenation level-dependent (BOLD) imaging.

The BOLD fMRI signal is related to neural events through the haemodynamics. The haemodynamic response to neural activity is a delayed, temporally and spatially smoothed version of the stimulus. Neural activity occurs at a temporal resolution of milliseconds but the haemodynamic response generally lasts 12 to 18 s. Therefore, it is impossible to capture the functioning of single neurons using fMRI but, according to Matthews (2001), single neurons work together as functional aggregates, which are large enough to be imaged.

The changes in BOLD fMRI signal associated with neural activity are of the order 0.5 – 3% at 1.5 T. As the main field is increased, the signal to noise ratio increases (5 – 15% at 4 T) but the occurrence of magnetic susceptibility artefacts and physiological noise also increase. The relatively low values of the signal to noise and contrast to noise ratios are improved by repetition of stimuli, which reduces the amount of variance in the results (Matthews, 2001).

Unlike conventional high resolution structural MR imaging, where, at most, a few rows of *k*-space are acquired for every excitatory RF pulse, functional MR imaging requires fast acquisition to reduce motion artefacts and increase temporal resolution (Ogawa et al., 1993).

Fast acquisition is achieved by filling multiple rows of *k*-space for every RF pulse. The most common *k*-space geometry used for fMRI at 1.5 T is single shot, gradient echo (GRE), echo planar imaging (EPI) (Buxton, 2002), where the entire *k*-space grid is filled with every RF pulse.

Examples of the EPI pulse sequence and corresponding *k*-space grid are illustrated in Fig.(2.4). EPI involves rapid switching of the linear gradients following a single RF pulse. The gradient switching corresponds to a raster-like scanning trajectory in *k*-space, resulting in enough data being collected after a single excitation to produce a low spatial resolution but high temporal resolution image. Gradient echoes provide signal rephasing. The time available for image acquisition is limited by the persistence of the signal due to T_2* attenuation. Decay in the signal corresponds to reduced *k*-space values, typically at the higher frequencies, and therefore spatial blurring of the image (Buxton, 2002). EPI acquisition is limited to the order of T_2*, approximately 100 ms.

fMRI data is four-dimensional; three spatial dimensions (x, y, z) and time. The time series of a single voxel (volumetric element) is the average signal of all the precessing spins in a small volume of space centred at an (x, y) coordinate in a particular slice (z) (Büchel and Friston, 2000; Buxton, 2002).

An fMRI experiment involves the design and implementation of a psychophysical experiment. An imaging protocol of alternating blocks of stimulus and control task is presented to a subject lying still in the MR scanner. fMRI data is acquired using an EPI pulse sequence, for the duration of the experiment (Buxton, 2002; Matthews, 2001). The number of images acquired per slice is determined by the length of functional experiment and desired temporal resolution. The number of slices imaged is particular to the MR scanner and depends on the instrumentation size restrictions and the repetition time (TR). Specialised software is used to preprocess the data and overlay the functional images on a high resolution three-dimensional structural image acquired during the same scanning session.

The collected fMRI data is statistically analysed slice by slice, voxel by voxel, to determine whether there are significant correlations between the individual signals and the haemodynamically convolved stimulus. The general linear model (GLM) is used to model the data as a linear combination of task contributions and random noise. Univariate tests are

performed at every voxel and least squares analysis is used to calculate parameter estimates that provide the best fit to the data (Friston et al., 1995). Voxels that show significant correlation with the stimulus imply significant activation of the part of the brain represented by the voxel during the stimulus relative to the control task. The information is mapped onto a high resolution structural MR image of the brain. Such a statistical parametric map (SPM) illustrates where in the brain information is processed (Friston et al., 1997). Group comparisons may be performed once individual data has been warped into a common brain space (e.g. the Montreal Neurological Institute (MNI) average brain and the Talairach atlas (Talairach and Tornoux, 1988)) or a customised template for the group of interest (Matthews, 2001).

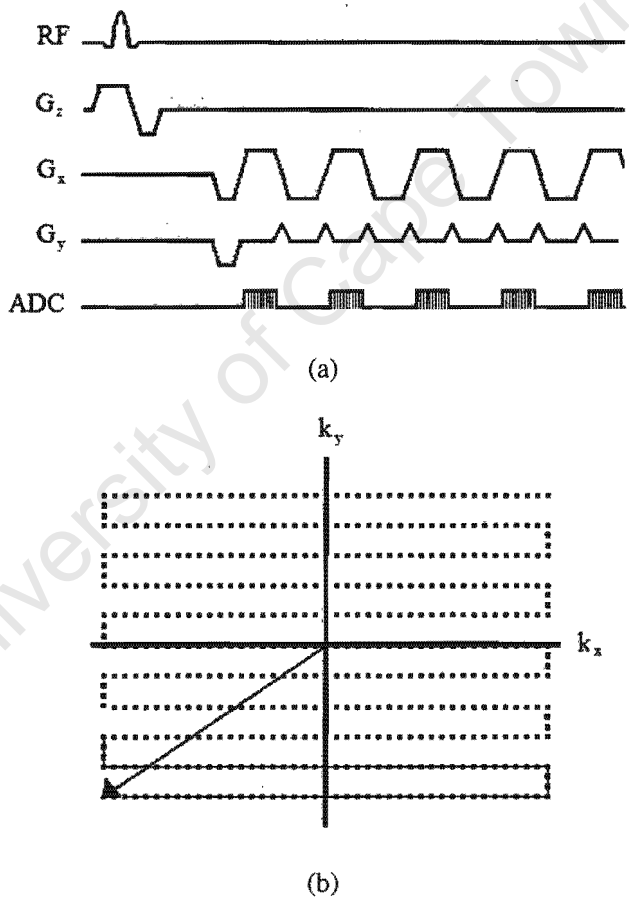

Figure 2.4: Diagram illustrating the correspondence between (a) the EPI pulse sequence and (b) its *k*-space trajectory

2.2 Connectivity Theory

2.2.1 Inter-region Correlation

The functional connectivity between anatomically distinct regions of interest may be assessed by measuring simultaneous occurrences of activity in response to some stimulus using correlation analysis.

Correlation is a method of quantifying the strength of a linear relationship between two variables (Van Belle et al., 2004). The variables x and y are standardised to u and v, respectively,

$$u_i = \frac{x_i - \bar{x}}{s_x} \tag{2.13}$$

$$v_i = \frac{y_i - \bar{y}}{s_y} \tag{2.14}$$

to remove the effects of units and constant offsets by subtracting the mean and dividing by the standard deviation, where

$$s_x^2 = \sum \frac{(x_i - \bar{x})^2}{n-1} \text{ and } s_y^2 = \sum \frac{(y_i - \bar{y})^2}{n-1}. \tag{2.15}$$

The sample Pearson product moment correlation coefficient r,

$$r = \frac{\sum (x_i - \bar{x})(y_i - \bar{y})}{\sqrt{\sum (x_i - \bar{x})^2 (y_i - \bar{y})^2}} = \frac{1}{n-1} \sum u_i v_i , \tag{2.16}$$

is based on the fact that adding the products of the standardised variables yields a net positive result if the variables vary together (and are therefore positively correlated); a net negative result if one of the variables increases while the other decreases and vice versa (and are therefore negatively correlated); and a result near zero if the variables are not related linearly (Van Belle et al., 2004).

The sample correlation coefficient r, however, does not have a normal distribution. Applying the Fisher z-transformation

$$z = \frac{\sqrt{n-3}}{2} \ln\left(\frac{1+r}{1-r}\right) = \sqrt{n-3} \arctan h(r) \tag{2.17}$$

changes the distribution to a normal distribution with zero mean and unit variance (Van Belle et al., 2004). Due to the standardisation, it is possible to compare z-correlation values from different analyses.

An example showing a positive correlation association is illustrated in Fig.(2.5). The scatter plot of the signal of time series two versus that of time series one for every point in time shows the correlation between variables. Using least squares, a straight line is fitted through the data points of the scatter plot in Fig.(2.5(b)). The slope of the straight line quantifies the relationship between the variables and its significance may be interpreted in the same way as the significance of the correlation coefficient (Van Belle et al., 2004).

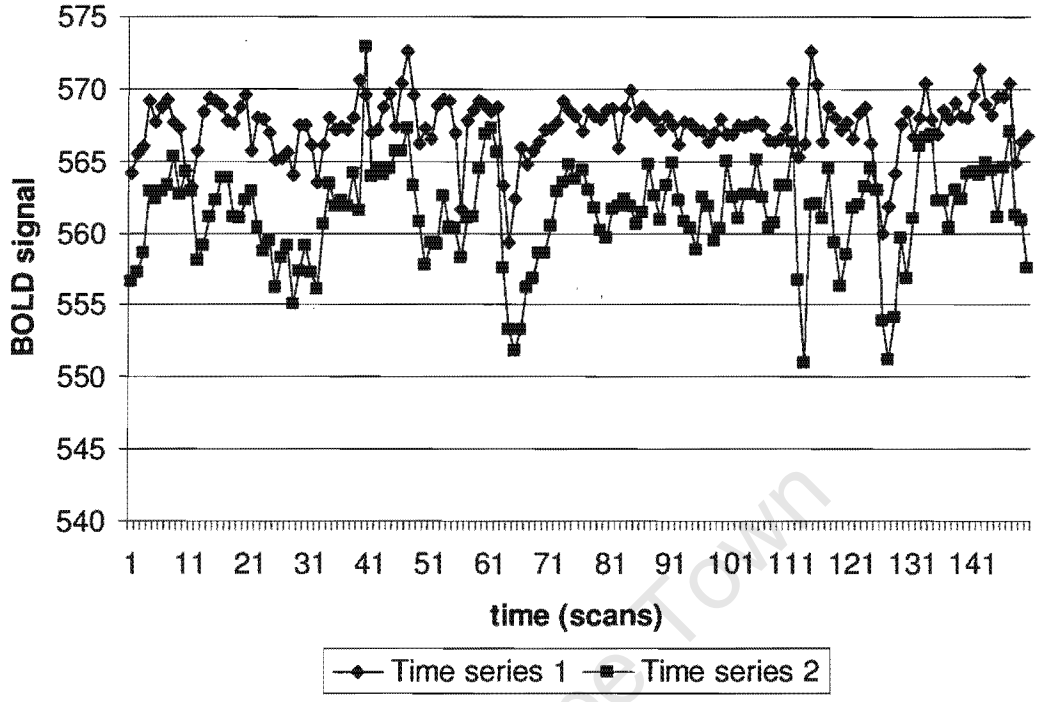

(a)

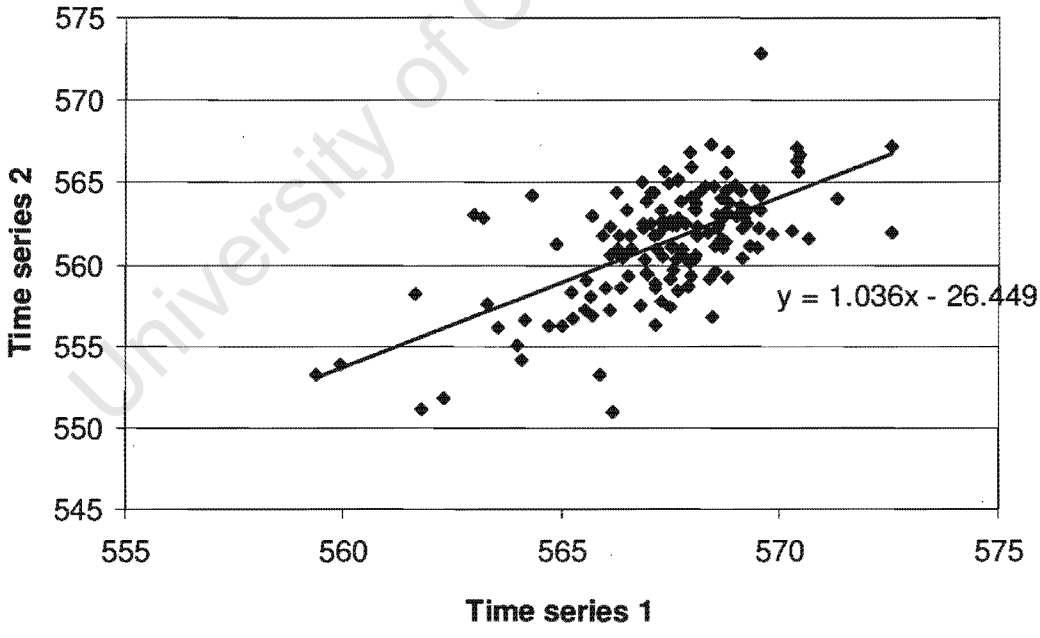

(b)

Figure 2.5: (a) Comparison of two superimposed time series and (b) a scatter plot showing the correlation and least squares regression between the two time series

The normalised correlation coefficient (z-score) and slope of the best fit line both quantify the relationship between the time series being compared. However, selecting which measure is most appropriate for a particular analysis seems to depend on the amount of error associated with the measurements of the time series being compared. Errors of measurement cause attenuation of correlation between variables (Van Belle et al., 2004). It appears that the noise sensitive z-score is most useful when comparing quantities with similar amounts of measurement error while the slope value is most appropriate when comparing quantities with different noise characteristics, i.e. where one time series (e.g. X) has less error than the other (e.g. Y) in the linear regression Y = bX. This is because the slope estimate assumes zero noise in the independent variable X and, as such, is a more appropriate measure when using an averaged quantity that, by definition, will have less noise than a single measurement.

Inter-region Correlation involves correlation analysis of the average within-task time series of two activation clusters of interest. Since these two averages will have approximately the same amount of noise associated with them, it is appropriate to use the z-score. The method is most useful when a hypothesis of *a priori* model is available for testing.

If information about functional connections to a particular region of interest is not available or a model cannot be fully specified, an exploratory technique is necessary for determining general connectivity to a region of interest.

2.2.2 Seed-voxel Connectivity

Seed-voxel Connectivity is an exploratory mapping technique that is used in determining functional connectivity to a seed region of interest. The average time series of a single region of interest is compared to the time series of every voxel in the brain. Because the time series of an ROI has been averaged over many voxels, it will have less noise associated with it than the time series of a single voxel. Therefore, the best fit line's slope value that, unlike the z-score, is less affected by the noise at each voxel, is used to quantify the relationship between the time series of an ROI and that of a single voxel.

Simple linear regression between two time series $\boldsymbol{x}_i$ and $\boldsymbol{x}_k$ is quantified by

$$x_i = x_k \beta_{ik} + G.\beta_G + e_i, \tag{2.18}$$

where the principle of least squares is used to ensure that the difference between the observed (x_i) and predicted ($\hat{x}_i$) values is minimised, i.e.

$$Min\left(\sum_{i=1}^{n}(x_i - \hat{x}_i)^2\right). \tag{2.19}$$

The regression slope β_{ik} (parameter estimate) describes the contribution of activity x_k at region k (explanatory variable) to activity x_i at region i (response variable). Confounding effects such as global signal and motion are included in the matrix G. The random error term e_i is assumed to be normally distributed (Friston et al., 1997; Van Belle et al., 2004).

Because only two time series, x_i and x_k, are present, a test of the null hypothesis $\beta_{ik} = 0$ to determine whether the regression is significant is equivalent to a test to determine whether the correlation between x_i and x_k is significant, and therefore amounts to a test for significant functional connectivity between regions i and k (Friston et al., 1997, Van Belle et al., 2004).

Two theoretically equivalent approaches can be used to create a Seed-voxel Connectivity map. By calculating the best fit line between the within-task time series of every voxel in the brain compared to the average within-task time series of the seed region, the slope values can be displayed on a statistical parametric map (SPM) at a particular significance threshold. Alternatively, by entering the activity x_k at region k as an explanatory variable in the general linear model and computing its contribution to the activity x_i for every voxel in the brain (i.e. multiple i's), the significance of this regression can be tested and displayed as an SPM (Friston et al., 1997).

2.2.3 Psychophysiological Interactions

Psychophysiological Interaction (PPI) analysis is a generalisation of Seed-voxel Connectivity, quantifying functional integration within the brain specifically in terms of the experimental context (Friston et al., 1997).

PPI analysis determines which areas of the brain significantly covary in activity with the region of interest during a particular cognitive task (Friston et al., 1993b; Boksman et al., 2005). Unlike simple linear regression between the time series of two regions of interest, PPIs are interpreted specifically in terms of the experimental paradigm (Das et al., 2005).

If all brain regions are included in the statistical model, together with other assumptions, the changing neuronal contributions can be interpreted in terms of effective connectivity. When fewer regions are included in the model for computational simplicity, the influence is interpreted in terms of contributions between regions, rather than effective connectivity (Friston et al., 1997).

PPIs differ from both psychological and physiological interactions. Psychological interactions only involve experimental factors in explaining localised changes in brain activity. The analysis is used to determine which areas of the brain significantly covary in activity with the interaction between different experimental conditions. For example, an experiment involving attention and non-attention (g_a) to varying presentation rates of auditory stimuli (g_r) is illustrated in the psychological interaction regression equation

$$x_i = g_r \times g_a \cdot \beta_i + [g_r g_a G] \cdot \beta_G + e_i, \tag{2.20}$$

where g_r and g_a are vectors and the interaction $(g_r \times g_a)$ is an element by element product of g_r and g_a. The main effects (g_r and g_a), the interaction term $(g_r \times g_a)$, and matrix of confounds, G, are explanatory variables in Eq.(2.20) and e_i is an error term. The regression coefficient β_i quantifies the contribution of the psychological interaction $(g_r \times g_a)$ to the activity x_i at region i.

Similarly, physiological interactions only involve the interactions between neurophysiological measurements from certain brain regions and their influence on the activity in another brain region (Friston et al., 1997). As an example, the activities x_a and x_b

at regions a and b, respectively, can be shown to contribute to the activity at region i using the physiological interaction regression equation

$$\boldsymbol{x}_i = \boldsymbol{x}_a \times \boldsymbol{x}_b \cdot \beta_i + [\boldsymbol{x}_a \boldsymbol{x}_b \boldsymbol{G}] \cdot \boldsymbol{\beta}_G + \boldsymbol{e}_i, \tag{2.21}$$

where $\boldsymbol{x}_a$ and $\boldsymbol{x}_b$ are vectors of MRI signal at regions a and b, respectively, for every time point and the interaction ($\boldsymbol{x}_a \times \boldsymbol{x}_b$) is an element by element product of $\boldsymbol{x}_a$ and $\boldsymbol{x}_b$. The main effects ($\boldsymbol{x}_a$ and $\boldsymbol{x}_b$), the interaction term ($\boldsymbol{x}_a \times \boldsymbol{x}_b$), and matrix of confounds, $\boldsymbol{G}$, are explanatory variables in Eq.(2.21) and $\boldsymbol{e}_i$ is an error term. The regression coefficient β_i quantifies the contribution of the physiological interaction ($\boldsymbol{x}_a \times \boldsymbol{x}_b$) to the activity $\boldsymbol{x}_i$ at region i.

However, PPIs incorporate an interaction between both psychological and physiological variables in predicting neurophysiological activity elsewhere in the brain. Regions that significantly covary with the psychophysiological interaction are considered to be functionally connected to the seed region for the purpose of performing the experimental task (Friston et al., 1993b; Boksman et al., 2005).

The signal $\boldsymbol{x}_i$ at region i is estimated from the interaction between the physiological activity $\boldsymbol{x}_k$ in seed region k and the experimental parameter $\boldsymbol{g}_p$ using the linear regression equation

$$\boldsymbol{x}_i = \boldsymbol{x}_k \times \boldsymbol{g}_p \cdot \beta_i + [\boldsymbol{x}_k \boldsymbol{g}_p \boldsymbol{G}] \cdot \boldsymbol{\beta}_G + \boldsymbol{e}_i, \tag{2.22}$$

where both $\boldsymbol{x}_k$ and $\boldsymbol{g}_p$ are vectors and the $\boldsymbol{x}_k \times \boldsymbol{g}_p$ interaction term is an element by element product of $\boldsymbol{x}_k$ and $\boldsymbol{g}_p$. The main effects ($\boldsymbol{x}_k$ and $\boldsymbol{g}_p$) are removed from the interaction term and grouped with the matrix of confounds, $\boldsymbol{G}$ (including effects of motion, global activity and low frequency interference), to ensure orthogonality between effects. The main effects ($\boldsymbol{x}_k$ and $\boldsymbol{g}_p$), the interaction term ($\boldsymbol{x}_k \times \boldsymbol{g}_p$), and $\boldsymbol{G}$, are explanatory variables in Eq.(2.22) and $\boldsymbol{e}_i$ is an error term. The regression coefficient β_i quantifies the contribution of the psychophysiological interaction to the activity $\boldsymbol{x}_i$ at region i.

An example of such a PPI in the number processing data could be choosing the activity at the left anterior HIPS and the time course of the Exact Addition task as explanatory variables in

Eq.(2.22). Calculating the interaction term and performing the linear regression for every voxel i in the brain, yields a vector of regression coefficients (β_i's) that would indicate which areas of the brain significantly covary with the activity in the left anterior HIPS in the context of the Exact Addition task.

If the predicted value of x_i, using Eq.(2.22), is significantly similar to the actual activity at region i, it is concluded that region i is functionally connected to region k in the particular experimental context (Friston et al., 1997).

Alternatively, PPIs can be understood simply in terms of regression analysis. Regression of the activity at region i on the activity at seed region k is quantified by a slope value and interpreted as the influence the seed region k exerts on region i. If changing the experimental context, such as changing difficulty in a parametric design, changes the slope value (and therefore the contribution of k on i), a psychophysiological interaction has occurred (Friston et al., 1997).

PPIs are illustrated using statistical parametric maps. Brain areas that have positively covarying activity with the seed region activity during the task but not during the baseline condition (or during different difficulties of a parametric design) are shown and indicate significant task specific contribution from the seed region (Boksman et al., 2005).

Although PPI analysis can be implemented using any experimental design, it is ideal to use factorial imaging designs where the psychological and physiological variables as well as the psychophysiological interaction between them are orthogonal by design and therefore will not interfere in the regression analysis. However, according to Friston et al. (1997), as long as care is taken to remove the main effects from the design matrix before the final regression analysis is performed, unwanted correlation and incorrect conclusions can be avoided.

A limiting factor of the PPI technique is that it is based on instantaneous regression equations and does not take the temporal structure of the time series into consideration. This limits the connectivity analysis to functional connectivity as nothing can be concluded about the causality relating the detected influences (Roebroeck et al., 2005).

2.2.4 Granger Causality Mapping

Granger causality mapping (GCM), originally proposed by Clive Granger (1969) for temporally structured economic analyses, is used to extract functional and effective connectivity information from fMRI data and does not rely on *a priori* model. It is used to explore functional relationships in time between a seed region and the rest of the brain. The connectivity maps characterise both instantaneous effects between coactivated brain regions (i.e. functional connectivity) and causal effects (i.e. effective connectivity) acting over time (Goebel et al., 2003). Directed, non-instantaneous effects occur if activity changes in one region effect changes in a second region at a later point in time. Temporal and spatial information inherent in fMRI time series data is exploited using a combination of vector autoregressive (AR) modelling and Granger causality to generate the connectivity maps.

Various linear univariate and bivariate autoregressive models of the time series of interest are calculated. The current value of a time series $\boldsymbol{x}$ (or $\boldsymbol{y}$) can be predicted from a regression of its own past (denoted by the subscript 1), given by

$$\boldsymbol{x}_t = \sum_{s=1}^{p} \boldsymbol{E}_{1s}\boldsymbol{x}_{t-s} + \boldsymbol{u}_{1t} \qquad \text{var}(\boldsymbol{u}_{1t}) = \boldsymbol{\Sigma}_1 \tag{2.23}$$

$$\boldsymbol{y}_t = \sum_{s=1}^{p} \boldsymbol{G}_{1s}\boldsymbol{y}_{t-s} + \boldsymbol{v}_{1t} \qquad \text{var}(\boldsymbol{v}_{1t}) = \boldsymbol{T}_1 \tag{2.24}$$

or its own past values and the past values of another time series $\boldsymbol{y}$ (or $\boldsymbol{x}$) (denoted by the subscript 2),

$$\boldsymbol{x}_t = \sum_{s=1}^{p} \boldsymbol{E}_{2s}\boldsymbol{x}_{t-s} + \sum_{s=1}^{p} \boldsymbol{F}_{2s}\boldsymbol{y}_{t-s} + \boldsymbol{u}_{2t} \qquad \text{var}(\boldsymbol{u}_{2t}) = \boldsymbol{\Sigma}_2 \tag{2.25}$$

$$\boldsymbol{y}_t = \sum_{s=1}^{p} \boldsymbol{G}_{2s}\boldsymbol{y}_{t-s} + \sum_{s=1}^{p} \boldsymbol{H}_{2s}\boldsymbol{x}_{t-s} + \boldsymbol{v}_{2t} \qquad \text{var}(\boldsymbol{v}_{2t}) = \boldsymbol{T}_2 . \tag{2.26}$$

Eq.(2.25) and (2.26) can be written as

$$\begin{bmatrix} \boldsymbol{x}_t \\ \boldsymbol{y}_t \end{bmatrix} = \sum_{s=1}^{p} \begin{bmatrix} \boldsymbol{E}_{2s} & \boldsymbol{F}_{2s} \\ \boldsymbol{H}_{2s} & \boldsymbol{G}_{2s} \end{bmatrix} \begin{bmatrix} \boldsymbol{x}_{t-s} \\ \boldsymbol{y}_{t-s} \end{bmatrix} + \begin{bmatrix} \boldsymbol{u}_{2t} \\ \boldsymbol{v}_{2t} \end{bmatrix} \qquad \text{var} \begin{bmatrix} \boldsymbol{u}_{2t} \\ \boldsymbol{v}_{2t} \end{bmatrix} = \boldsymbol{Y} = \begin{bmatrix} \boldsymbol{\Sigma}_2 & \boldsymbol{C} \\ \boldsymbol{C}' & \boldsymbol{T}_2 \end{bmatrix}, \quad (2.27)$$

where $\boldsymbol{C} = \text{cov}(\boldsymbol{u}_{2t}, \boldsymbol{v}_{2t})$ and $\boldsymbol{x}$ and $\boldsymbol{y}$ are the fMRI time series of two different regions or voxels.

The autoregressive coefficients $\boldsymbol{E}$, $\boldsymbol{F}$, $\boldsymbol{G}$ and $\boldsymbol{H}$ regress the current value of $\boldsymbol{x}$ or $\boldsymbol{y}$ onto a number of past values determined by the order p. Roebroeck and colleagues (2005) used the Schwartz Criterion order selection method to minimise error variance and computational complexity in the model. The terms $\boldsymbol{u}$ and $\boldsymbol{v}$ are measures of residual noise in the estimates not explained by the model. They have corresponding measures of error variance, namely the cross covariance matrices $\boldsymbol{\Sigma}$, $\boldsymbol{T}$ and $\boldsymbol{Y}$. It is possible to assess whether time series are dependent on one another by using these AR models. An improvement in the prediction (such as may result from inclusion of the values of another time series) results in less noise and therefore a reduction in the error variance (Goebel et al., 2003).

Granger (1969) recognised that cause always precedes effect and that temporal precedence information in the time series of interest can be exploited to determine the direction of causality. He proposed the use of AR models to predict the current value of a time series $\boldsymbol{x}$, both including (Eq.(2.25)) and not including (Eq.(2.23)) past values of another time series $\boldsymbol{y}$. If the prediction of time series $\boldsymbol{x}$ is improved (i.e. the error variance is reduced) when past values of time series $\boldsymbol{y}$ are included in the model, then the time series $\boldsymbol{y}$ is said to *Granger cause* the time series $\boldsymbol{x}$ (Roebroeck et al., 2005) and the time series are said to be effectively connected.

Extending Eq.(2.25) and (2.26) by including the current value of the other time series $\boldsymbol{y}$ (or $\boldsymbol{x}$) in the prediction of $\boldsymbol{x}$ (or $\boldsymbol{y}$) (denoted by the subscript 3) yields

$$\boldsymbol{x}_t = \sum_{s=1}^{p} \boldsymbol{E}_{3s}\boldsymbol{x}_{t-s} + \sum_{s=0}^{p} \boldsymbol{F}_{3s}\boldsymbol{y}_{t-s} + \boldsymbol{u}_{3t} \qquad \text{var}(\boldsymbol{u}_{3t}) = \boldsymbol{\Sigma}_3 \tag{2.28}$$

$$\boldsymbol{y}_t = \sum_{s=1}^{p} \boldsymbol{G}_{3s}\boldsymbol{y}_{t-s} + \sum_{s=0}^{p} \boldsymbol{H}_{3s}\boldsymbol{x}_{t-s} + \boldsymbol{v}_{3t} \qquad \text{var}(\boldsymbol{v}_{3t}) = \boldsymbol{T}_3 . \tag{2.29}$$

Granger (1969) coined the term *instantaneous causality* for the case where, for example, the current value of time series $\boldsymbol{y}$, together with the past values of time series $\boldsymbol{x}$ and $\boldsymbol{y}$ (Eq.(2.28)), improves the prediction of the current value of time series $\boldsymbol{x}$. This directionless influence between time series equates to simple correlation and therefore quantifies functional connectivity (Goebel et al., 2003).

Including all the information (i.e. past, present and future) of the other time series $\boldsymbol{y}$ (or $\boldsymbol{x}$) in the regression (denoted by the subscript 4) yields

$$\boldsymbol{x}_t = \sum_{s=1}^{p} \boldsymbol{E}_{4s}\boldsymbol{x}_{t-s} + \sum_{s=-\infty}^{p} \boldsymbol{F}_{4s}\boldsymbol{y}_{t-s} + \boldsymbol{u}_{4t} \qquad \text{var}(\boldsymbol{u}_{4t}) = \boldsymbol{\Sigma}_4 \tag{2.30}$$

$$\boldsymbol{y}_t = \sum_{s=1}^{p} \boldsymbol{G}_{4s}\boldsymbol{y}_{t-s} + \sum_{s=-\infty}^{p} \boldsymbol{H}_{4s}\boldsymbol{x}_{t-s} + \boldsymbol{v}_{4t} \qquad \text{var}(\boldsymbol{v}_{4t}) = \boldsymbol{T}_4 . \tag{2.31}$$

Geweke (1982) implemented Granger causality in the context of AR modelling. He created measures of dependence and feedback between the time series, defined in terms of the AR error variance. The measure of linear dependence between time series $\boldsymbol{x}$ and $\boldsymbol{y}$ ($F_{x,y}$) is given by

$$F_{x,y} = F_{x\to y} + F_{y\to x} + F_{x.y}, \tag{2.32}$$

where $F_{x\to y}$ is the influence from $\boldsymbol{x}$ to $\boldsymbol{y}$, $F_{y\to x}$ is the influence from $\boldsymbol{y}$ to $\boldsymbol{x}$ and $F_{x.y}$ includes any instantaneous correlation between the two time series.

The directed influence from y to x is quantified by the logarithm of the error variance ratio $|\Sigma_1|/|\Sigma_2|$, given by

$$F_{y\to x} = \ln\left(\frac{|\Sigma_1|}{|\Sigma_2|}\right), \tag{2.33}$$

in which Σ_1 is the error variance associated with the linear regression of x on its own past (Eq.(2.23)) and Σ_2 is the error variance associated with the linear projection of x on the past of both x and y (Eq.(2.25)). Introducing past values of y into the bivariate prediction of the current value of x can only reduce or maintain the error variance seen in the univariate prediction, so that $|\Sigma_1| \geq |\Sigma_2|$. Therefore, the ratio $|\Sigma_1|/|\Sigma_2|$ will always be greater than 1 and its logarithm ($(F_{y\to x})$ in Eq.(2.33)) will always be positive.

A similar explanation holds for the directed influence from x to y, $F_{x\to y}$, given by the expression

$$F_{x\to y} = \ln\left(\frac{|T_1|}{|T_2|}\right). \tag{2.34}$$

It has been shown by Geweke (1982) that the directed influence terms $F_{y\to x}$ and $F_{x\to y}$ can be written as

$$F_{y\to x} = \ln\left(\frac{|\Sigma_1|}{|\Sigma_2|}\right) = \ln\left(\frac{|T_3|}{|T_4|}\right) \tag{2.35}$$

and

$$F_{x\to y} = \ln\left(\frac{|T_1|}{|T_2|}\right) = \ln\left(\frac{|\Sigma_3|}{|\Sigma_4|}\right), \tag{2.36}$$

respectively, which relate the future values of a time series to its current value.

The instantaneous term $F_{x,y}$ quantifies the *instantaneous causality* referred to by Granger (1969) and is given by

$$F_{x,y} = \ln\left(\frac{|\Sigma_2||T_2|}{|Y|}\right) = \ln\left(\frac{\Sigma_2}{\Sigma_3}\right) = \ln\left(\frac{T_2}{T_3}\right). \tag{2.37}$$

For example, a reduction in error variance Σ_3 compared to Σ_2 implies that the current value of y improved the prediction of the current value of x compared to that obtained using only the past values of x and y (Goebel et al., 2003).

Using Eq.(2.33), (2.34) and (2.37) in Eq.(2.32) yields

$$F_{x,y} = \ln\left(\frac{|\Sigma_1||T_1|}{|Y|}\right), \tag{2.38}$$

which can be simplified to

$$F_{x,y} = \ln\left(\frac{\Sigma_1}{\Sigma_4}\right) = \ln\left(\frac{T_1}{T_4}\right) \tag{2.39}$$

using the results of Eq.(2.35) and (2.36). Using x as an example, it is seen from Eq.(2.39) that linear dependence $F_{x,y}$ involves the improvement in the prediction of the current value of x associated with its own past values (Eq.(2.23)) by including past, present and future values of y (Eq.(2.30)).

Two time series are linearly independent ($F_{x,y} = 0$) if and only if incorporating past, present and future values of the other time series does not improve the prediction of the current value

of the time series of interest, i.e. $\Sigma_1 = \Sigma_2 = \Sigma_3 = \Sigma_4$, $T_1 = T_2 = T_3 = T_4$ and $C = 0$ (Geweke, 1982).

By only assessing functional and effective connectivity between two regions at a time (i.e. comparing the time series of the seed region of interest and that of every voxel in the brain in a pairwise manner), GCM ignores any influence other regions may have on the interaction (Kaminski et al., 2001). This problem of common input can be minimised by foregoing the mapping aspect and extending the AR models to include multiple regions of interest. Influence measures between time series can be calculated that are conditional on the other regions in the model. Kaminski et al., 2001, propose the use of the directed transfer function (DTF) to evaluate the directional influences between any pair of time series, in the context of a multivariate neurobiological data set (e.g. EEG). It has been shown that the results generated in this way can be interpreted in terms of Granger causality.

A limitation of GCM is that it is 'based on the existence of time lags' at the haemodynamic level (Abler et al., 2006). Unless the time lags present at the neuronal processing level survive the temporal smoothing imposed by the haemodynamic response and subsequent sampling during BOLD measurement, the method will not be useful in determining causality. The detection capacity for directed influence is reduced if the sampling interval (TR, measured in seconds) differs greatly from the influence delay at the neuronal level (measured in milliseconds).

Therefore, if the experiment is not set up with the measurement of effective connectivity in mind, and the neural delays are not long enough to be translated into measurable haemodynamic delays, Granger causality fails to extract any directed influence between brain regions responsible for completing the task.

3 Methods

3.1 Participants

fMRI data for two number processing tasks had been collected in a previous study (Meintjes et al., 2007) and was available for analysis. A total of 15 right-handed, 8- to 12-year-old children diagnosed with FAS / PFAS and 17 right-handed, non-exposed, age- and gender-matched controls were assessed between May 2005 and October 2006. The children were all from the Cape Coloured community in Cape Town, South Africa, which has a very high incidence of alcohol abuse and prenatal alcohol exposure.

3.2 Neuroimaging Assessment

3.2.1 MRI Protocol

Data was collected using a 1.5 T Magnetom Symphony whole body MRI scanner (Siemens Medical Systems, Erlangen, Germany) equipped with a head volume coil. High-resolution structural MR images were acquired in the sagittal plane using a three-dimensional inversion recovery gradient echo sequence (72 slices, TR = 1900 ms, TE = 3.93 ms, TI = 1100 ms, slice thickness 2 mm and 250 × 250 mm field of view [resolution 1.4 × 1.0 × 2 mm]). fMRI functional volumes were acquired with a T_2*-weighted gradient echo, echo planar imaging sequence (154 volumes, 20 interleaved slices, TR = 2000 ms, TE = 50 ms, volume thickness 5 mm, inter slice gap 1 mm and 230 × 230 mm field of view [resolution 3.6 × 3.6 × 5 mm]), which is sensitive to blood oxygenation level-dependent contrast.

3.2.2 fMRI Experimental Tasks

Two number processing fMRI tasks, Exact Addition and Proximity Judgement ("which of two numbers is closest to a third number?"), were performed by each child (Jacobson et al., 2006; Meintjes et al., 2007). Before scanning, each child practised the tasks in a mock

scanner, in order to get used to the loud noises and close space of the MRI scanner, thereby reducing anxiety and facilitating timeous completion of the MRI scans.

The experimental tasks were programmed using E-Prime software (Psychology Software Tools, Inc., Pittsburgh, USA) and the visual stimuli presented using a data projector and rear projection screen mounted at the foot of the patient bed. The child's response was registered using a Lumitouch response system (Photon Control Inc., Burnaby, Canada), which was held in the right hand and pressed with the index and middle fingers. The child could talk to the examiner using an intercom built into the scanner and could stop the scan in an emergency by squeezing a ball held in his / her left hand.

It has been shown that a self-paced block design produces the same results during a number comparison task as a fixed presentation rate design (Rogers et al., 2007). Therefore, a self-paced design was chosen to accommodate the large range of mathematical abilities among the children in the sample. Each child completed as many problems as possible at his / her own pace during each 40 s block. A fixation square is displayed for 500 ms at the start of each active block and for 500 ms between problems.

In the Exact Addition task, two numbers are displayed one above the other for 1 s, after which two possible solutions appear horizontally below the two numbers (Fig.(3.1a)). The display remains on the screen until the child makes a selection or the 40 s for the block expires. Sums are selected randomly from a list in which the solution is never greater than 12 and from which tied problems (2 + 2) and sums involving unity have been excluded (Jacobson et al., 2006; Meintjes et al., 2007).

The child is instructed to add the top two numbers together and select the correct answer from the two choices displayed below by pressing the button on the same side as the correct number. In the control block, the child is shown one non-numeric symbol, followed by two non-numeric symbols displayed horizontally below the first symbol, one of which is identical to the first symbol displayed. The child is instructed to press the button on the same side as the identical symbol.

In the Proximity Judgement task, a single number is displayed for 1s, followed by two numbers displayed horizontally below it (Fig.(3.1b)), from which the child selects the one numerically closer to the initial number. Problems are selected randomly from a list of 1- and 2-digit numbers. The control block for this task follows the same format but with non-numeric symbols. A symbol is displayed for 1 s, followed by two possible symbols displayed horizontally below the first symbol. The child selects the one that is identical to the initial one by pressing the button on the side of that symbol (Jacobson et al., 2006; Meintjes et al., 2007).

The visual and response requirements of the number processing tasks are repeated in the control tasks. Paired 40 s blocks of active task and control task are followed by 20 s rest periods during which the child is instructed to stare at a fixation square displayed on the screen. The blocks are repeated three times and the total length of each experimental task is 5 min.

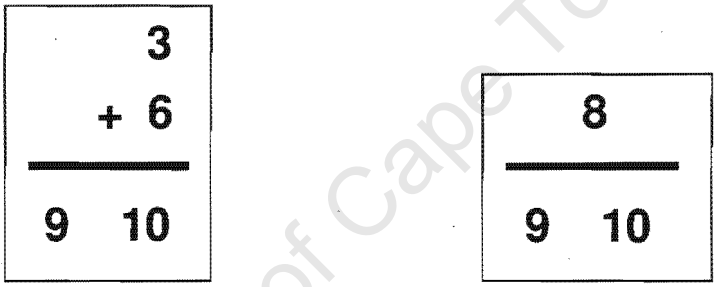

Figure 3.1: Examples of stimulus presentation for the (a) Exact Addition task and (b) Proximity Judgement tasks

3.2.3 Image Preprocessing

The button-press responses to the number processing tasks were recorded on a computer and analysed. Criteria leading to the exclusion of the subject's data included: inconsistent task completion rates between active blocks within a task, markedly faster responses compared with practice sessions in the mock scanner, repeatedly pressing the same button, alternately pressing each of the two buttons or an overall task accuracy of less than 66%. The data for one child with FAS was excluded because she could not consistently identify numbers correctly (Jacobson et al., 2006; Meintjes et al., 2007).

fMRI data analyses were performed using Brain Voyager QX (Brain Innovation, version 1.8, Maastricht, The Netherlands) and SPM5 (Statistical Parametric Mapping, 2005, Functional Imaging Laboratory, The Wellcome Department of Imaging Neuroscience, Institute of Neurology, University College London, United Kingdom). The first four dummy volumes of each run were excluded from the analyses to avoid any transient effects at the start of each experiment, leaving 150 volumes to be preprocessed. Slice scan time correction was performed on the data in Brain Voyager QX using sinc interpolation to correct for the continuous acquisition of image slices within a volume throughout the repetition time (Roebroeck et al., 2005). The functional volumes were spatially realigned with rigid-body transformations (i.e. trilinear estimation and interpolation) to the first volume (acquired in the middle of the imaging session due to Siemens' interleaved acquisition). The correction removes small head motion artefacts from the image (Boksman et al., 2005). Data that exceeded the movement criteria of 3 mm displacement or 3.0° rotation within a functional run was rejected. Linear trends and low frequency temporal components were removed from the data using a high pass filter with a frequency cut off of 3 cycles per time course.

Each child's functional data sets were co-registered to his / her high-resolution structural MR image acquired during the same scanning session so that any functional activation could be located and interpreted in a high resolution anatomical context (Smith, 2001). In order to average the data across different subjects, all the brain images were spatially normalised to Talairach space (Talairach and Tournoux (1988)), using a linear transform from the anatomical images to the Talairach template (Smith, 2001). The $3.6 \times 3.6 \times 5$ mm^3 fMRI voxels were interpolated to the $1 \times 1 \times 1$ mm^3 resolution of the iso-voxeled structural images. An 8 mm full width at half maximum (FWHM) spatial smoothing Guassian filter was applied to reduce noise in the data (Smith, 2001).

After applying the above exclusion criteria and motion correction, the data for 14 control children and 7 children with FAS / PFAS for Exact Addition, and 15 control children and 9 children with FAS / PFAS for Proximity Judgement was available for further analysis.

3.3 Selection of Regions of Interest

The within-group fMRI analyses performed by Meintjes et al. (2007) were repeated using both Brain Voyager QX and SPM5 and yielded similar results. Seed regions of interest were identified from fMRI activation maps.

The activation maps were obtained from group fixed effect analyses of variance using the general linear model. The time series of each voxel is analysed independently and compared with the different predictors of the GLM, yielding parameter estimates that describe the fit of the model to the data. If a parameter estimate is high relative to its estimated uncertainty, the model fit is significant and there is a believable activation (Smith, 2001). The design matrix of explanatory variables for the number processing data included predictors based on the active and control experimental blocks, convolved by the standard haemodynamic function, and the six motion correction parameters as predictors of no interest. The activations in the two groups of children's data were examined separately for both Exact Addition and Proximity Judgement by comparing activations between the number processing and control tasks. Voxelwise thresholds (Bonferroni corrected for whole-brain multiple comparisons) were set to $p < 0.001$ and $p < 0.3$ for Exact Addition and $p < 0.001$ and $p < 0.1$ for Proximity Judgement, for the control children and children with FASD, respectively. The significance thresholds were chosen according to the different amounts of activation seen in the control and alcohol-exposed groups during the number processing tasks. The cluster size threshold was set to 100 contiguous voxels.

Small regions of interest (of maximum extent $10 \times 10 \times 10$ voxels) were isolated from the most statistically significant area within each cluster in the activation maps and reported. Of the ROIs extracted, those considered important in the number processing and FASD literature were used in further connectivity analyses.

3.4 Connectivity Analyses

3.4.1 Inter-region Correlation and Seed-voxel Connectivity (using concatenated within-task time series)

Inter-region Correlation and Seed-voxel Connectivity (using concatenated within-task time series) analyses were performed in MATLAB (The MathWorks Inc., version 7.3.0.267 (R2006b), Natick, MA, USA) on fMRI data preprocessed in Brain Voyager QX. Statistical analyses were performed in Microsoft Excel (Microsoft Corporation, 2002) and SPM5 for Inter-region Correlation and Seed-voxel Connectivity, respectively.

Average time course information for every ROI for every subject was extracted from fMRI data in Brain Voyager QX and exported as a text file. The MATLAB algorithms for both methods create and use concatenated within-task time series and are repeated for all subjects.

Both techniques involve reading the time series of interest from the text file and statistically adjusting them to remove any confounding effects introduced by global signal and motion. The global signal is calculated by averaging the time course information of all the voxels assumed to be in the brain. The motion parameters, calculated during preprocessing of the data, fully describe any translational and rotational motion that occurred during scanning acquisition. These confounds are regressed out of the time series of interest.

The adjusted time series are split into task specific blocks according to the protocol of the experiment. Every block is shaved of three functional volumes at the start to account for the haemodynamic delay inherent in the fMRI response to a change in experimental condition. Blocks of the same condition are concatenated together to form a single within-task time series. The process is illustrated in Fig.(3.2) using timing information from the number processing tasks.

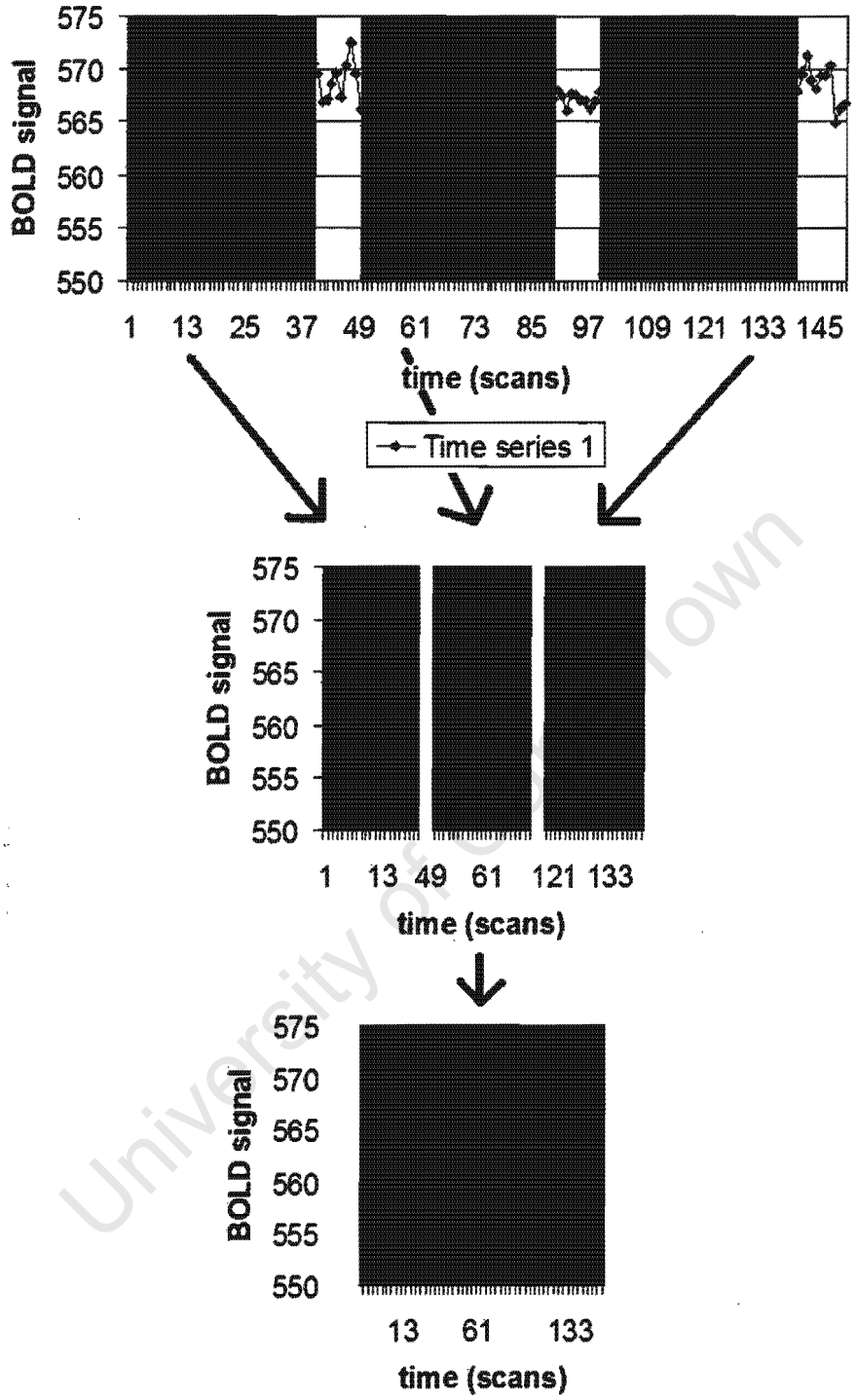

Figure 3.2: Diagram illustrating how a within-task time series is created

Correlation analysis is performed between the within-task time series of a region of interest and a similar within-task time series of a second region of interest (Inter-region Correlation) or between the within-task time series of a region of interest and a similar within-task time series of every voxel in the brain (Seed-voxel Connectivity). One of the numerical outputs of the analysis is a normalised correlation coefficient (z-score), which describes the relationship between the time series of interest. The other numerical output is the slope of a straight line that is fitted to the data, which quantifies the relationship between the time series.

The resultant correlation coefficient z- and slope-values for all subjects were exported for further analysis. The lists of z-score values from Inter-region Correlation analysis were imported into Microsoft Excel. *T*-tests were performed to compare the means of the control and alcohol-exposed within-group correlation values. A significant result ($p < 0.05$, corrected for the number of different inter-region comparisons performed) suggests a statistically significant group difference in connectivity for the particular inter-region functional connection of interest.

The output of the Seed-voxel Connectivity approach using concatenated within-task time series is a three-dimensional matrix of slope values at every voxel for each subject. The matrices were analysed in SPM5 at a group level. Maps showing within-group connectivity at a particular significance threshold can be generated using the contrasts [1 0] and [0 1] where the first place holder refers to the control children's data and the second place holder, the alcohol-exposed children's data. Group comparisons of the connectivity maps using the contrasts [1 -1] and [-1 1], both masked by the contrasts [1 0] and [0 1] (to exclude areas not connected to the ROI), should isolate areas of the brain 'more' connected (i.e. slope values with greater magnitude and / or less variance) in one group than the other. However, no significant differences between groups were apparent, possibly due to the small sample size and high inter-subject variation in the alcohol-exposed group. Therefore, an alternative method was used.

A single, unbiased connectivity map for a particular ROI was generated using the contrast [1 1] with all the subjects' data. Small volumes of interest (of maximum extent $10 \times 10 \times 10$ voxels) were extracted from the most significant part of regions that appeared to be connected to the ROI at $p < 0.001$. The average slope values for each volume of interest were interrogated in MATLAB using *t*-tests to determine whether the connection to the seed region was significant within each group (at $p(Bonf) < 0.05$ for the control group and $p(Bonf) < 0.05$

for the alcohol-exposed group) and whether it differed between the groups (at p(Bonf) < 0.05).

3.4.2 Seed-voxel Connectivity (using all volumes in a general linear model)

Seed-voxel Connectivity (using all volumes in a general linear model) was performed in MATLAB and SPM5 using fMRI data preprocessed in SPM5. A MATLAB algorithm based on simple linear regression was implemented to generate a design matrix of multiple regressors for every subject and every region of interest. The steps of the algorithm are as follows:

Task regressors are created for each condition in the experimental design. For example, regressors were built for the Exact Addition or Proximity Judgement task blocks, the control task blocks and the periods of rest. The regressors are convolved with a haemodynamic response function, modelled by two gamma functions in SPM5, which describe the delay and temporal smoothing inherent in fMRI data.

Connectivity regressors are built for each condition from the task regressors and the seed region's time course. The time series of every voxel in the ROI is extracted from the preprocessed fMRI data and the average calculated. The average time series is multiplied by a global scaling factor, amplified by a factor of 10 and the mean subtracted. The normalised and zero-centred data is regressed of any confounding contributions from motion, global signal or low frequency effects.

The cleaned seed region time course is multiplied by each of the task regressors, resulting in a connectivity regressor for each condition. The contribution of the task regressors to the connectivity terms is removed by regression, ensuring that the connectivity regressors are orthogonalised with respect to the block-design task regressors. The contributions of motion, global signal and low frequency effects are also removed from the connectivity terms. This ensures that the columns of the final design matrix remain linearly independent. It has been confirmed that the matrix is of full rank which implies there is no exact collinearity and the columns are linearly independent.

An example of a design matrix for the number processing data is illustrated in Fig.(3.3) and consists of the following column regressors:

1 – 3: Haemodynamically convolved block-design task regressors for TASK, CONTROL, REST

4 – 6: Connectivity regressors during conditions TASK, CONTROL, REST

7 – 12: Motion parameters

13: Global time series

The design matrices were entered into individual statistical analyses in SPM5, as multiple regressors in the general linear model. The model was fitted to the subject's fMRI data and parameters estimated using a restricted maximum likelihood (ReML) algorithm. A ReML algorithm assumes the same error correlation structure at each voxel and attempts to make the probability of the observed data as large as possible (Van Belle et al., 2004). A statistical parametric map illustrates the three-dimensional arrangement of parameter estimates across the brain at a particular significance threshold.

A contrast of [0 0 0 1 0 0 0 0 0 0 0 0 0], isolating the fourth parameter estimate, was chosen to extract the connectivity between the seed region and every voxel during the number processing task condition.

The contrast maps from all the subjects were entered into a group analysis in SPM5. Areas showing significant within-group connectivity to the seed region (using the contrasts [1 0] and [0 1]) were noted and compared with the results of the Seed-voxel Connectivity approach that uses concatenated within-task time series. Group differences in connectivity were analysed using the contrasts [1 -1] and [-1 1], masked by the contrasts [1 0] and [0 1], thereby excluding areas not showing connectivity to the seed region.

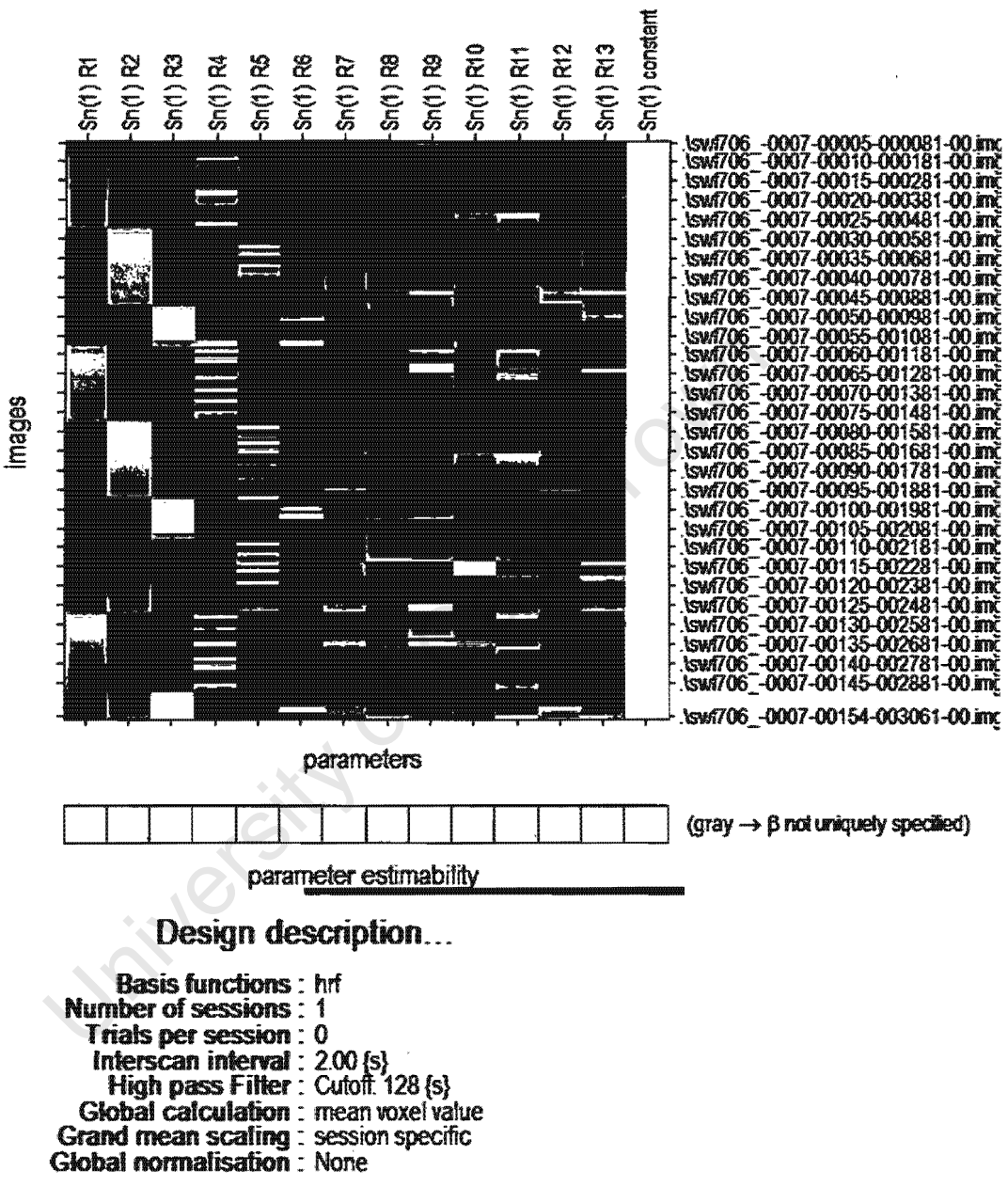

Figure 3.3: Diagram illustrating a design matrix created using the Seed-voxel Connectivity regression model

3.4.3 Psychophysiological Interactions

Like the Seed-voxel Connectivity approach using all volumes in a general linear model, Psychophysiological Interaction analysis was implemented in MATLAB and SPM5 using fMRI data preprocessed in SPM5. A MATLAB algorithm based on PPI theory (Friston et al., 1997) was run to create a design matrix of task regressors, PPI regressors, the seed region's time series and confounds for every subject and every ROI. This is achieved with the following steps:

Haemodynamically convolved task regressors are created for the active and control tasks in the experimental design. Rest periods are specifically not modelled in PPI analysis. Therefore, for the number processing data, two task regressors were created; one for the Exact Addition or Proximity Judgement task and the other for the letter matching control task.

Condition specific PPI regressors are built from the interaction between the task regressors and the seed region's time course. The normalised, zero-centred and cleaned average time series of the seed ROI is multiplied, in a point-wise fashion, by each of the task regressors, creating a PPI regressor for each condition (Boksman et al., 2005). The PPI regressors are orthogonalised with regard to the task regressors, motion, global signal and seed region's time series by regression to avoid any unwanted correlation between the source area's activity and the interaction terms (Friston et al., 1997). An example of the design matrix for the number processing data is illustrated in Fig.(3.4) and includes columns for the different regressors, given by

1 – 2: Haemodynamically convolved block-design task regressors for TASK, CONTROL

3: Seed region time series during the entire run (baseline connectivity)

4: Interaction between the seed region time series and the TASK condition

5: Interaction between the seed region time series and the CONTROL condition

6 – 11: Motion parameters

12: Global time series

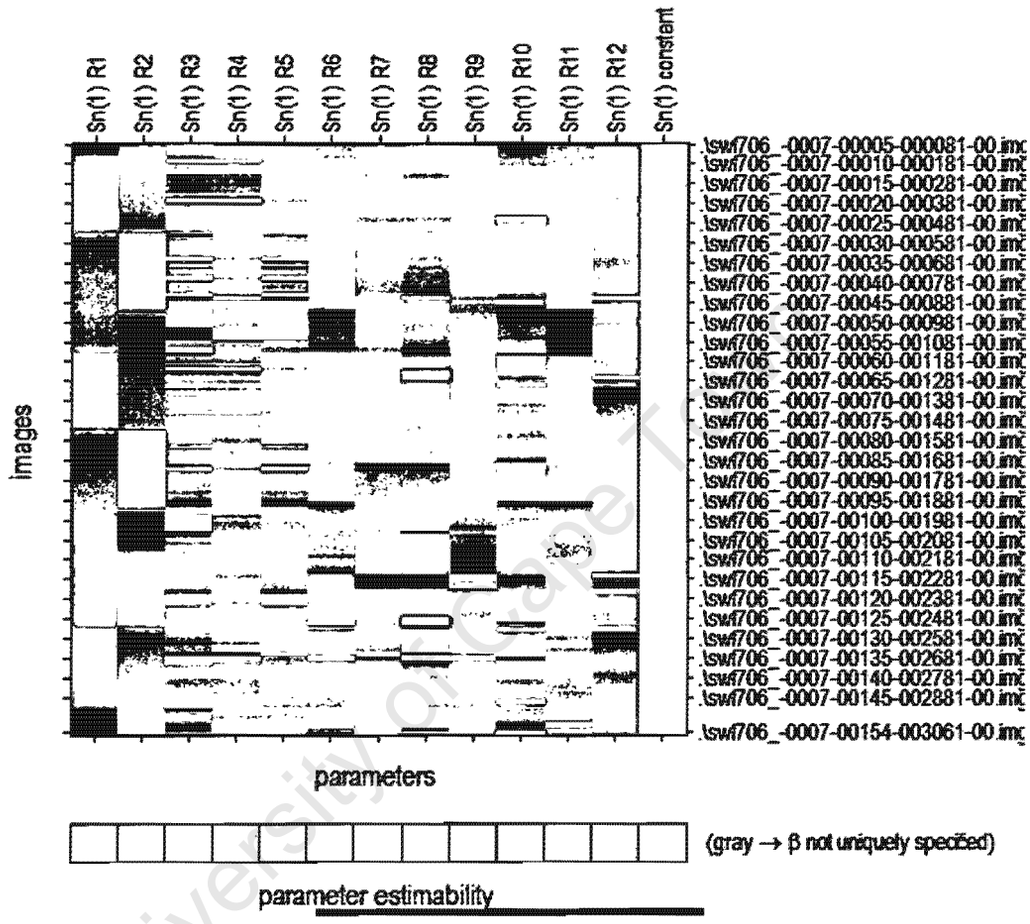

Figure 3.4: Diagram illustrating the design matrix of the PPI regression model

Statistical analyses in SPM5 at the individual level involve fitting the general linear model with multiple regressors described by the design matrix to each voxel's time series and estimating a parameter to quantify the fit of the data.

Different contrasts were implemented to examine different connectivity phenomena in the data. A contrast of [0 0 1 0 0 0 0 0 0 0 0 0], isolating the third parameter estimate (the seed region time series during the entire run), was used to indicate the baseline level of connectivity between the seed region and each voxel. The fourth parameter estimate (the Seed × TASK psychophysiological interaction), isolated with contrast [0 0 0 1 0 0 0 0 0 0 0 0], was chosen to find voxels that show significant psychophysiological interaction (increase / decrease in connectivity) with the seed region during the task relative to baseline. The individual contrast maps could then be entered into a group analysis in SPM5.

Unlike the Seed-voxel Connectivity method, REST was not included as a condition in the PPI method. It was treated as an implicit baseline by the baseline connectivity regressor (i.e. the seed region's time series during the entire run).

It was found that the above method of PPI analysis generated results that were equivalent to those of Seed-voxel Connectivity (using all volumes in a general linear model) using appropriate contrasts. The regression analyses are very similar, except that the Seed-voxel Connectivity method explicitly models the 'rest' condition and does not regress out the seed time series from the connectivity regressors. By applying the contrast [0 0 0 2 -1 -1 0 0 0 0 0 0] (where the weighting factors 2, -1, -1 refer to the connectivity regressors during the TASK, CONTROL and REST conditions, respectively) in the Seed-voxel Connectivity analysis, any regions that show significant covariance with the activity of the seed region of interest over the time course of the task but not during the baseline, can be considered as functionally connected to the seed region for the purpose of performing the task (Boksman et al., 2005) and therefore, equivalent to the PPI output.

Therefore, the Seed-voxel Connectivity method (using all volumes in a general linear model), with the appropriate contrast of [0 0 0 2 -1 -1 0 0 0 0 0 0], was used to create individual PPI maps which were entered into a group analysis in SPM5.

3.4.4 Granger Causality Mapping

Granger causality mapping was implemented in Brain Voyager QX.

The names of the seed regions of interest, experimental protocol timing information and link to each individual's functional data were entered into the analysis. The algorithm creates a set of instantaneous and directed influence Granger causality maps for each specified condition in the protocol file (e.g. for the number processing task and control task) for every specified reference region of interest. The maps are scaled three-dimensional representations of the F-values calculated in the Granger causality analysis (Roebroeck et al., 2005). The instantaneous map shows instantaneous correlation between the reference and voxel ($F_{x,y}$) and the directed influence map illustrates directed influence to and from the reference over the brain ($F_{x\rightarrow y} - F_{y\rightarrow x}$ and $F_{y\rightarrow x} - F_{x\rightarrow y}$).

Granger causality mapping implemented in Brain Voyager works at an individual level and has no group analysis option. Individual maps were exported in Analyze format and imported into SPM5, which requires normally distributed data to perform group analyses. The inherently positive values of the instantaneous maps and abnormal statistical distribution of the directed influence maps made any traditional group analysis impossible.

The difficulty with analysing individual Granger causality maps at a group level is a common one. Abler and colleagues (2006) performed Granger causality mapping for twelve subjects using custom software written in MATLAB and manually compared the individual results in table form. It was not a group comparison, as such.

As neither Brain Voyager QX nor SPM5 could be used to perform group analyses on the individual Granger causality maps, this analysis was halted and no results were achieved.

4 Results

4.1 Selection of Regions of Interest

Exact Addition

Tables (4.1) and (4.2) list the regions of interest (including region name, mean Talairach coordinates, *t*-statistics, and size (maximum 1000 voxels)) extracted from all the clusters showing increased brain activation at the selected significance and cluster thresholds during the Exact Addition task compared to the control task for the control children and the FAS / PFAS group, respectively.

Regions of interest chosen for further functional connectivity analysis, based on their importance in the number processing and FASD literature, are indicated by an asterisk. For the Exact Addition data, they include the left anterior HIPS, left posterior HIPS, right anterior HIPS and bilateral precuneus in the parietal lobe, and left precentral sulcus and bilateral posterior medial frontal cortex in the frontal lobe.

Proximity Judgement

The results of fMRI activity analyses on the Proximity Judgement data collected for the control children and the children with FAS / PFAS are tabulated in Tables (4.3) and (4.4), respectively. The regions of interest (including region name, mean Talairach coordinates, *t*-statistics, and size (maximum 1000 voxels)) were isolated from clusters in the activation maps showing increased brain activity at the selected significance and cluster thresholds during the Proximity Judgement task compared to the control task.

Regions of interest chosen for further functional connectivity analysis are indicated by an asterisk. The parietal regions of interest include the right anterior HIPS, left posterior HIPS, bilateral precuneus and left angular gyrus, while the frontal regions include the left precentral sulcus and bilateral posterior medial frontal cortex.

Table 4.1: Extracted regions of interest in the control group showing increased activity during the Exact Addition task compared to the control task[+]

Region		x	y	z	Size	Max *t*
Parietal						
L	horizontal intraparietal sulcus; anterior*	-44	-42	34	230	6.3
L	horizontal intraparietal sulcus; posterior*	-31	-65	38	883	7.4
L	cingulate gyrus; posterior end	-8	-44	18	587	7.2
R, L	precuneus*	-6	-61	31	998	9.6
Frontal						
R	dorsolateral prefrontal cortex	29	47	19	222	6.2
L	dorsolateral prefrontal cortex	-23	44	19	938	8.7
L	dorsolateral prefrontal cortex	-38	27	19	650	6.8
L	dorsolateral prefrontal cortex	-36	37	7	996	9.2
R, L	medial frontal cortex; posterior	-2	20	36	1000	9.9
L	superior frontal gyrus	-6	15	53	928	8.6
L	precentral sulcus*	-45	11	30	912	8.2
L	superior frontal sulcus	-28	8	49	842	8.0
R, L	middle section of cingulate gyrus	0	0	33	262	6.6
Occipital						
R	superior occipital lobe	15	-95	14	445	7.1
Insula						
R	anterior insula	29	19	1	688	7.8
L	anterior insula	-30	19	-2	855	7.5
Basal ganglia						
R	head of caudate nucleus	15	8	10	205	6.3
L	head of caudate nucleus	-15	3	11	590	7.3

[+] $p(Bonf) < 0.001$; $t(min) = 5.67$; cluster threshold 100 voxels

* Regions of interest chosen for further functional connectivity analysis

Table 4.2: Extracted regions of interest in the alcohol-exposed group showing increased activity during the Exact Addition task compared to the control task[+]

Region		x	y	z	Size	Max *t*
Parietal						
R	horizontal intraparietal sulcus; anterior*	30	-48	37	509	5.7
L	horizontal intraparietal sulcus; anterior	-33	-52	37	497	5.7
L	angular gyrus / posterior end of superior temporal sulcus	-31	-70	21	185	5.1
L	posterior cingulate gyrus	-5	-32	20	266	5.2
R	cingulate gyrus	15	-33	35	414	5.4
L	precuneus	-10	-70	26	882	5.8
Frontal						
R	dorsolateral prefrontal cortex	34	51	10	607	5.8
R	dorsolateral prefrontal cortex	35	44	27	351	5.1
L	dorsolateral prefrontal cortex	-27	45	20	806	5.9
L	dorsolateral prefrontal cortex	-29	44	34	317	5.2
R, L	medial frontal cortex; posterior*	0	20	34	993	6.8
L	precentral sulcus	-36	13	30	900	6.9
Occipital						
R, L	cuneus	-2	-81	18	653	5.8
R	cuneus	8	-77	28	862	6.0
R	cuneus / calcarine sulcus	8	-77	12	836	6.6
L	cuneus / calcarine sulcus	-14	-66	9	795	6.3
R	lingual gyrus	9	-72	5	980	6.7
Temporal						
L	parahippocampal gyrus	-24	-8	-24	586	6.3
Insula						
R	anterior insula	29	22	7	899	7.3
R	claustrum / central insula	31	2	1	899	6.7
L	anterior insula spilling into claustrum / central insula	-28	22	7	993	7.1
L	claustrum / central insula	-32	8	4	885	7.5
Other						
R	anterior cerebellum	20	-32	-35	412	5.6
L	anterior cerebellum	-22	-35	-36	363	5.8
R, L	superior cerebellar cortex	-11	-47	-15	653	6.6
R, L	pons / midbrain / thalamus	0	-20	-13	845	8.4

[+] p(Bonf) < 0.3; *t*(min) = 4.56; cluster threshold 100 voxels

* Regions of interest chosen for further functional connectivity analysis

Table 4.3: Extracted regions of interest in the control group showing increased activity during the Proximity Judgement task compared to the control task[+]

Region		x	y	z	Size	Max *t*
Parietal						
R	horizontal intraparietal sulcus; anterior*	41	-43	44	522	7.7
L	horizontal intraparietal sulcus; posterior*	-28	-68	37	958	7.6
R, L	precuneus	-2	-65	35	996	8.4
R	precuneus	33	-80	33	883	8.2
Insula						
R	anterior insula	30	20	4	260	6.6
L	anterior insula	-28	20	3	770	7.5
Frontal						
R	dorsolateral prefrontal cortex	40	45	20	727	7.3
L	dorsolateral prefrontal cortex	-21	51	11	292	6.5
L	dorsolateral prefrontal cortex	-36	41	7	622	7.6
R, L	medial frontal cortex; posterior*	1	22	42	940	8.1
L	precentral sulcus and middle frontal gyrus*	-43	14	31	977	8.4
R	superior frontal sulcus	22	13	44	325	6.3
L	superior frontal sulcus	-27	12	48	783	7.8
R	superior frontal sulcus	21	23	38	802	6.9
Occipital						
R, L	cuneus	-4	-59	17	634	7.1

[+] $p(Bonf) < 0.001$; $t(min) = 5.69$; cluster threshold 100 voxels

* Regions of interest chosen for further functional connectivity analysis

Table 4.4: Extracted regions of interest in the alcohol-exposed group showing increased activity during the Proximity Judgement task compared to the control task[+]

Region		x	y	z	Size	Max *t*
Parietal						
R	angular gyrus	37	-59	31	943	6.6
L	angular gyrus*	-38	-62	32	996	8.2
R, L	precuneus *	-3	-56	30	1000	8.5
R, L	posterior part of cingulate gyrus	2	-35	35	781	6.1
Frontal						
R	dorsolateral prefrontal cortex	25	55	11	872	6.9
L	dorsolateral prefrontal cortex	-24	55	10	816	7.6
L	dorsolateral prefrontal cortex	-44	41	9	580	6.1
L	middle frontal gyrus	-35	20	43	471	5.9
R	medial frontal cortex; anterior	14	48	10	193	5.4
L	medial frontal cortex; posterior	-11	26	36	291	6.3

[+] $p(Bonf) < 0.1$; $t(min) = 4.78$; cluster threshold 100 voxels

* Regions of interest chosen for further functional connectivity analysis

4.2 Connectivity Analyses

4.2.1 Inter-region Correlation

Inter-region Correlation was performed between the regions of interest chosen for their prevalence in the number processing literature. For the Exact Addition data, pair-wise comparisons were computed for all combinations of the left anterior HIPS, left posterior HIPS, right anterior HIPS, bilateral precuneus, left precentral sulcus and bilateral posterior medial frontal cortex. Similarly, for the Proximity Judgement data, the right anterior HIPS, left posterior HIPS, bilateral precuneus, left angular gyrus, left precentral sulcus and bilateral posterior medial frontal cortex were compared with one another. The *t*-tests performed on the mean z-score data in Microsoft Excel yielded no significant differences in functional connectivity between the control and alcohol-exposed groups for any of the inter-region combinations for either Exact Addition or Proximity Judgement.

4.2.2 Seed-voxel Connectivity (using concatenated within-task time series)

Exact Addition

Significant connections (quantified by the slope value) to the seed region of interest during the Exact Addition task, for both the control group (at $p < 0.05$, corrected) and the alcohol-exposed group (at $p < 0.05$, corrected), are reported in Tables (4.5) and (4.6), for the parietal and frontal seed regions, respectively. Any significant differences in connectivity between the groups (at $p < 0.05$, corrected) are indicated by an asterisk.

In the control children's data, the parietal seed regions show the following connectivity: the left anterior HIPS shows parietal connectivity to the right anterior HIPS and left precuneus and frontal connectivity to the left precentral gyrus. The left posterior HIPS shows parietal connections to the right posterior HIPS and bilateral precuneus and frontal connections to the left superior frontal sulcus and right middle frontal gyrus. The right anterior HIPS seed region shows functional connectivity to the left anterior HIPS, parietally, and right middle frontal gyrus and left precentral sulcus, frontally. The bilateral precuneus seed region shows parietal connectivity to a bilateral posterior cingulate gyrus area and bilateral angular gyrus.

The frontal seed regions show the following connectivity in the control children's data: the left precentral sulcus shows frontal connections to the right middle frontal gyrus, bilateral pMFC and left anterior insula and parietal connections to the bilateral anterior HIPS and left angular gyrus. This is illustrated in the statistical parametric map in Fig.(4.1), although the connectivity results reported in Table (4.6) were obtained using MATLAB, based on volumes of interest identified from a combined control / alcohol-exposed connectivity map in SPM5. The pMFC shows frontal connections to the left precentral gyrus and bilaterally to anterior insula, superior frontal gyrus and DLPFC.

In comparison, connectivity in the alcohol-exposed group of children is less extensive at the chosen significance threshold. The left anterior HIPS seed region shows frontal connectivity to the left medial frontal gyrus, while the left posterior HIPS shows parietal connectivity to the bilateral precuneus. The right anterior HIPS shows connectivity to the left anterior HIPS. The bilateral precuneus seed region shows connectivity to the left angular gyrus. The left

precentral sulcus seed region shows no significant connectivity. The pMFC seed region shows connectivity to the left precentral gyrus and bilateral connectivity to the superior frontal cortex and DLPFC.

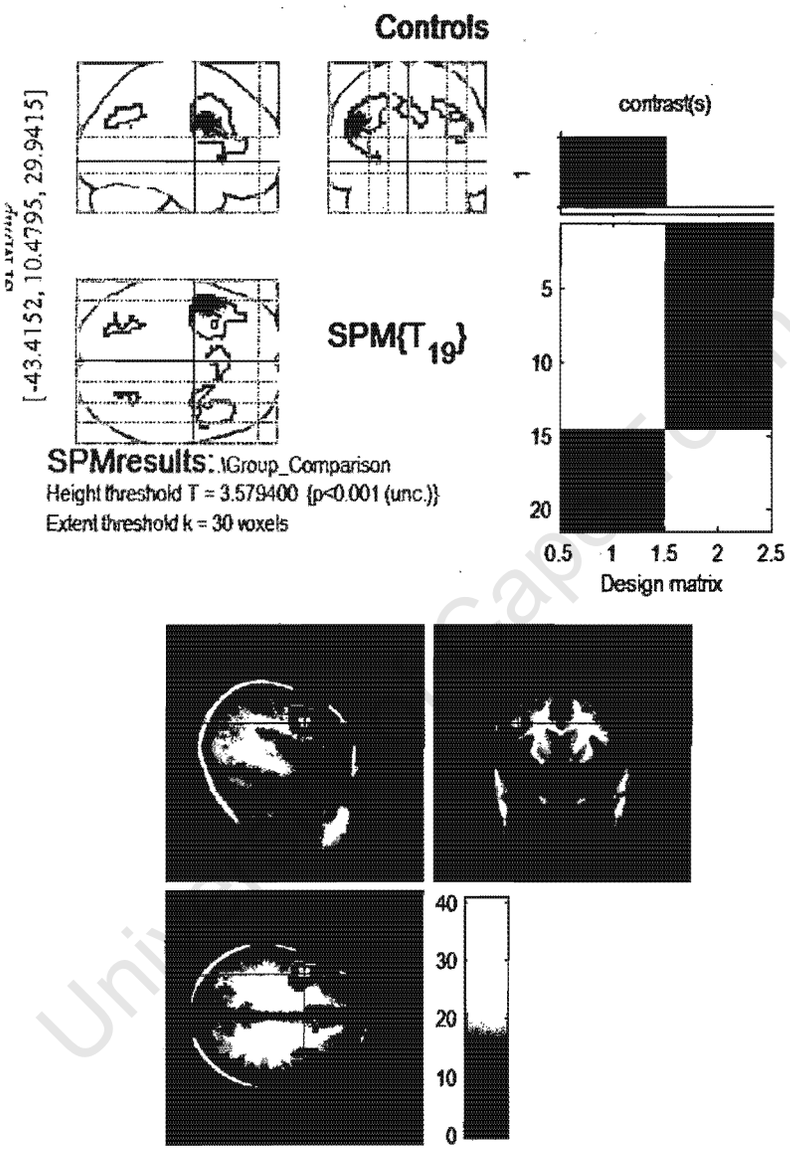

Figure 4.1: Illustration of fronto-parietal connectivity seen in the Seed-voxel Connectivity statistical parametric map (using concatenated within-task time series) for the left precentral sulcus seed region [-45 11 30] for the control group during the Exact Addition task ($p < 0.001$; $t(\text{min}) = 3.58$; cluster threshold 30 voxels)

Table 4.5: Results of Seed-voxel Connectivity analysis (using concatenated within-task time series) for Exact Addition using parietal seed regions[+]

Seed region of interest					Volume of interest						Controls[+]		Exposed[+]	
Name		Coordinates			Name		Coordinates				Mean slope	Standard deviation	Mean slope	Standard deviation
Parietal														
L	HIPS; anterior	-44	-42	34	R	HIPS; anterior	48	-37	40		0.202	0.138		
					L	precuneus	-12	-46	43		0.170	0.102		
					L	precentral gyrus	-39	-4	43		0.158	0.121		
					L	medial frontal gyrus	-18	32	31				0.225	0.072
L	HIPS; posterior	-31	-65	38	R	HIPS; posterior	33	-58	43		0.362	0.207		
					R, L	precuneus	-3	-64	34		0.327	0.266	0.329	0.157
					L	superior frontal sulcus	-30	11	52		0.335	0.126		
					R	middle frontal gyrus	39	26	31		0.267	0.125		
R, L	precuneus	-6	-61	31	L	angular gyrus	-33	-67	34		0.193	0.159	0.252	0.100
					R	angular gyrus	33	-67	34		0.217	0.149		
					R, L	cingulate gyrus; posterior	0	-43	19		0.494	0.247		
R	HIPS; anterior	30	-48	37	L	HIPS; anterior	-30	-49	37		0.374	0.176	0.316	0.122
					R	middle frontal gyrus	33	17	31		0.272	0.131		
					L	precentral sulcus	-42	11	28		0.230	0.188		

[+] Reported at p(Bonf) < 0.05, corrected for multiple comparisons

Table 4.6: Results of Seed-voxel Connectivity analysis (using concatenated within-task time series) for Exact Addition using frontal seed regions[+]

Seed region of interest					Volume of interest						Controls[+]		Exposed[+]	
Name		Coordinates			Name		Coordinates				Mean slope	Standard deviation	Mean slope	Standard deviation
Frontal														
L	precentral sulcus	-45	11	30	R	middle frontal gyrus	42	23	25		0.374	0.161		
					R, L	medial frontal cortex; posterior	0	20	40		0.344	0.278		
					L	anterior insula	-30	23	4		0.231	0.192		
					L	angular gyrus	-27	-67	31		0.191	0.100		
					L	HIPS; anterior	-27	-49	43		0.175	0.146		
					R	HIPS; anterior	30	-52	43		0.209	0.144		
R, L	medial frontal cortex; posterior	0	20	34	R	insula; anterior	36	11	1		0.251	0.109		
					L	insula; anterior	-36	11	1		0.251	0.199		
					L	precentral gyrus	-48	5	31		0.194	0.166	0.220	0.080
					R	dorsolateral prefrontal cortex	27	44	22		0.269	0.189		
					L	dorsolateral prefrontal cortex	-27	44	22		0.261	0.204	0.241	0.093
					R	superior frontal gyrus	27	38	31		0.212	0.145	0.374	0.186
					L	superior frontal gyrus	-24	38	28		0.174	0.142	0.305	0.142

[+] Reported at p(Bonf) < 0.05, corrected for multiple comparisons

Proximity Judgement

Tables (4.7) and (4.8) list significant connections (quantified by the slope value) to the parietal and frontal seed regions of interest, respectively, during the Proximity Judgement task for both the control and alcohol-exposed groups (at $p < 0.05$, corrected). Any significant differences in connectivity between the groups (at $p < 0.05$, corrected) are indicated by an asterisk.

In the control children's data, the right anterior HIPS seed region shows parietal connections to the left anterior HIPS and bilateral posterior HIPS with frontal connections to the right middle frontal gyrus. The left posterior HIPS shows parietal connectivity to the right posterior HIPS, left anterior HIPS and bilateral precuneus, and frontal connectivity to the left superior frontal sulcus. The bilateral precuneus seed region shows bilateral connectivity to the angular gyrus and posterior cingulate gyrus, and frontal connectivity to the right middle frontal gyrus and left precentral gyrus. Connectivity to the bilateral precuneus seed region in the control children is illustrated in the SPM in Fig.(4.2). However, the results reported in Table (4.7) were obtained using MATLAB, based on volumes of interest identified from a combined control / alcohol-exposed connectivity map in SPM5. The left AG shows parietal connections to the right angular gyrus and bilateral precuneus, and frontal connections to the left middle frontal gyrus.

The frontal seed regions show the following connectivity patterns in the control children's data: the left precentral sulcus shows frontal connectivity to the right precentral sulcus and left anterior insula, and parietal connections to the left angular gyrus and bilateral precuneus. The pMFC shows frontal connectivity to the bilateral anterior insula, bilateral anterior cingulate cortex and right dorsolateral prefrontal cortex.

Slightly different connectivity patterns appear in the alcohol-exposed children's data at the chosen significance threshold. The parietal seed regions show the following connectivity: the right anterior HIPS shows parietal connections to the left anterior HIPS and bilateral posterior HIPS. The left posterior HIPS shows parietal connectivity to the right posterior HIPS, left anterior HIPS and bilateral precuneus. The bilateral precuneus seed region shows bilateral connections to the bilateral angular gyrus. The left angular gyrus shows parietal connections to the right angular gyrus and bilateral precuneus. The frontal seed regions show

the following connectivity in the alcohol-exposed children's data: the left precentral sulcus seed region shows frontal connectivity to the right precentral sulcus. The bilateral pMFC seed region shows frontal connectivity to the bilateral anterior cingulate cortex and diffuse areas in both right and left middle frontal gyri. One of the connections between the pMFC and the left middle frontal gyrus is significantly different between the groups.

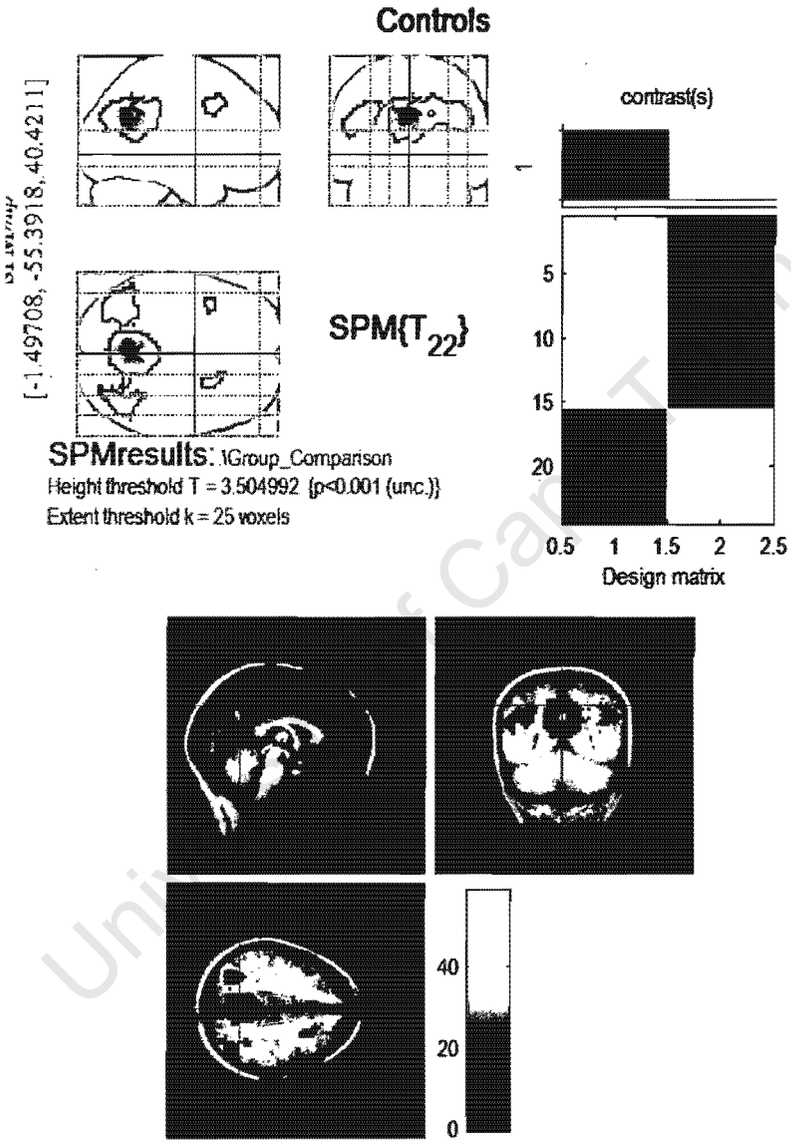

Figure 4.2: Illustration of fronto-parietal connectivity seen in the Seed-voxel Connectivity statistical parametric map (using concatenated within-task time series) for the bilateral precuneus seed region [-3 -56 30] for the control group during the Proximity Judgement task ($p < 0.001$; $t(\text{min}) = 3.50$; cluster threshold 25 voxels)

Table 4.7: Results of Seed-voxel Connectivity analysis (using concatenated within-task time series) for Proximity Judgement using parietal seed regions[+]

Seed region of interest					Volume of interest						Controls[+]		Exposed[+]	
Name		Coordinates			Name		Coordinates				Mean slope	Standard deviation	Mean slope	Standard deviation
Parietal														
R	HIPS; anterior	41	-43	44	R	HIPS; posterior	27	-67	37		0.257	0.181	0.348	0.189
					L	HIPS; anterior	-42	-43	43		0.306	0.152	0.328	0.194
					L	HIPS; posterior	-27	-67	37		0.229	0.210	0.276	0.141
					R	middle frontal gyrus	27	5	49		0.284	0.182		
L	HIPS; posterior	-28	-68	37	L	HIPS; anterior	-39	-46	43		0.205	0.153	0.276	0.154
					R	HIPS; posterior	30	-70	37		0.432	0.229	0.525	0.166
					R, L	precuneus	0	-61	34		0.408	0.232	0.380	0.170
					L	superior frontal sulcus	-30	8	52		0.259	0.131		
R, L	precuneus	-3	-56	30	L	angular gyrus	-48	-58	31		0.306	0.230	0.389	0.162
					R	angular gyrus	45	-61	31		0.378	0.175	0.396	0.089
					R, L	cingulate gyrus; posterior	0	-34	31		0.265	0.203		
					R	middle frontal gyrus	27	11	46		0.150	0.122		
					L	precentral gyrus	-39	14	37		0.167	0.130		
L	angular gyrus	-38	-62	32	R	angular gyrus	39	-69	34		0.337	0.192	0.410	0.090
					R, L	precuneus	0	-61	37		0.460	0.241	0.410	0.198
					L	middle frontal gyrus	-39	17	28		0.212	0.157		

[+] Reported at p(Bonf) < 0.05, corrected for multiple comparisons

Table 4.8: Results of Seed-voxel Connectivity analysis (using concatenated within-task time series) for Proximity Judgement using frontal seed regions[+]

Seed region of interest					Volume of interest				Controls[+]		Exposed[+]	
Name		Coordinates			Name		Coordinates		Mean slope	Standard deviation	Mean slope	Standard deviation
Frontal												
L	precentral sulcus	-43	14	31	R	precentral sulcus	45	14	31	0.293	0.229	0.398	0.254
					L	angular gyrus	-33	-67	31	0.225	0.164		
					R, L	precuneus	0	-61	31	0.273	0.250		
					L	insula; anterior	-27	20	4	0.243	0.130		
R, L	medial frontal cortex; posterior	1	22	42	R	insula; anterior	27	20	4	0.185	0.147		
					L	insula; anterior	-30	20	-2	0.310	0.194		
					R, L	anterior cingulate cortex	-3	38	22	0.410	0.216	0.350	0.190
					R	dorsolateral prefrontal cortex	27	44	25	0.331	0.274		
					R	middle frontal gyrus	33	29	34			0.444	0.218
					L	middle frontal gyrus*	-33	29	34			0.423	0.147
					L	middle frontal gyrus	-45	8	37			0.267	0.142

[+] Reported at p(Bonf) < 0.05, corrected for multiple comparisons

* Significant difference in connectivity between the control and alcohol-exposed groups at p(Bonf) < 0.05

4.2.3 Seed-voxel Connectivity (using all volumes in a general linear model)

Fig.(4.3) and (4.4) show examples of statistical parametric maps generated using both Seed-voxel Connectivity approaches (i.e. using all volumes in a general linear model compared to using concatenated within-task time series) for the seed regions left precentral sulcus in Exact Addition and bilateral precuneus in Proximity Judgement, respectively.

The results are very similar. This qualitative assessment, although not rigorous, confirms the similarity between the two techniques, which are implemented using algorithms based on the same theory. Apparent differences in the functional connectivity maps may be due to thresholding effects on the different content (i.e. parameter estimates compared to slope values) of the maps.

Seed-voxel Connectivity analysis (using all volumes in a general linear model) did not yield any differences in connectivity between the groups, for the seed regions of interest. This shows either a general lack of differences in functional connectivity between the groups of children during the Exact Addition and Proximity Judgement tasks, or failure of the method to perform significant group analysis with the small sample size of the alcohol-exposed group (seven and nine in Exact Addition and Proximity Judgement, respectively).

Owing to the known similarity of the theory and apparent similarity of the results between the two Seed-voxel Connectivity approaches, this method (using all volumes in a general linear model) was not pursued further.

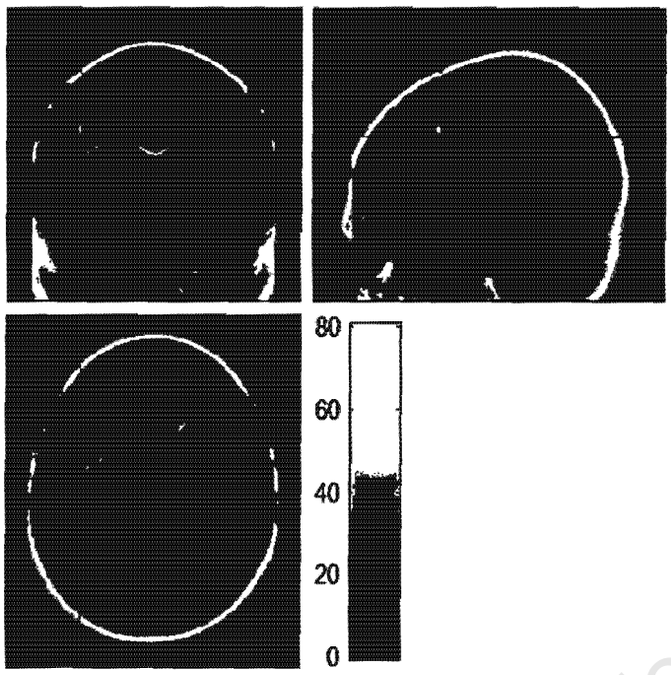

(a)

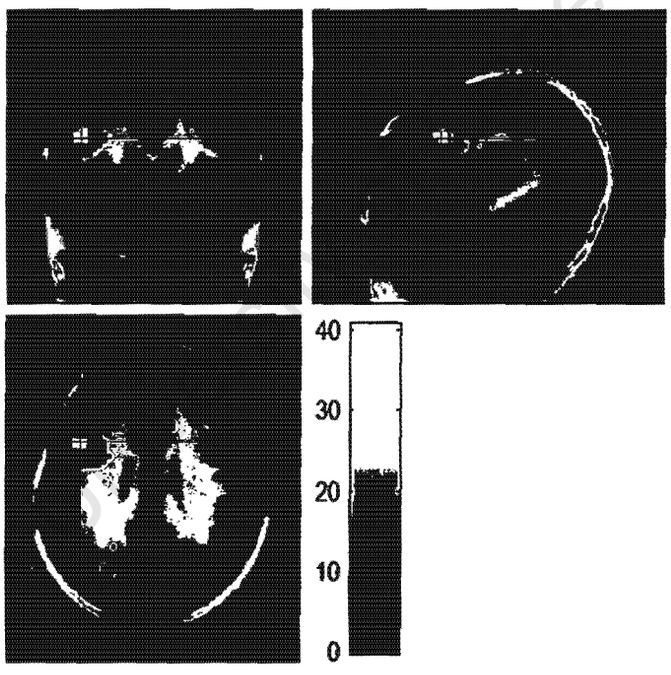

(b)

Figure 4.3: Diagram showing similar functional connectivity results for the (a) Seed-voxel Connectivity (using all volumes in a general linear model) and (b) Seed-voxel Connectivity (using concatenated within-task time series) methods using the left precentral sulcus seed region for the control group during Exact Addition

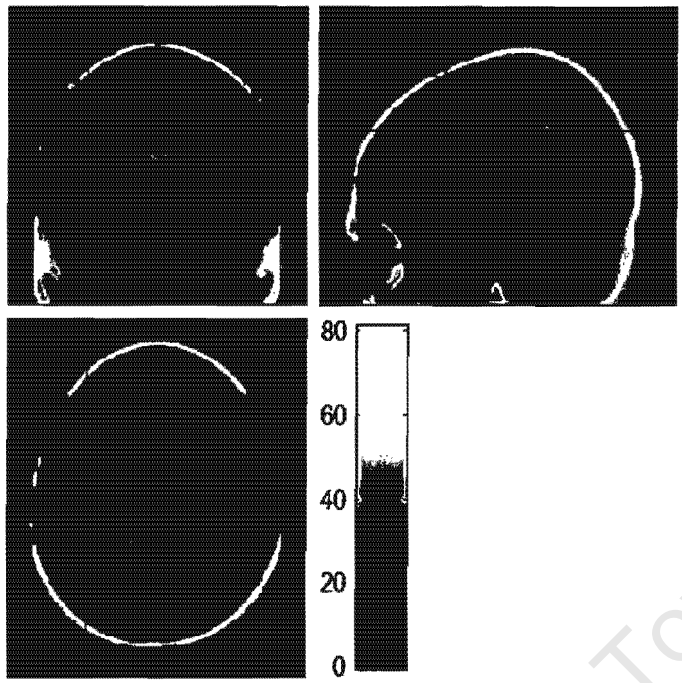

(a)

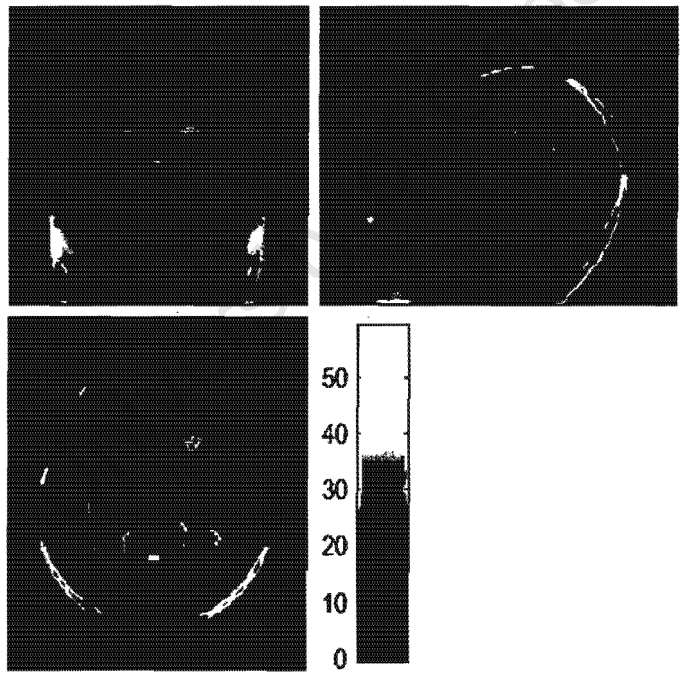

(b)

Figure 4.4: Illustration of similar functional connectivity results for the Seed-voxel Connectivity approaches using (a) all volumes in a general linear model and (b) concatenated within-task time series, to the bilateral precuneus seed region for the control group during Proximity Judgement.

4.2.4 Psychophysiological Interactions

Tables (4.9) and (4.10) list the volumes of interest that show psychophysiological interactions with the chosen seed regions of interest at an uncorrected $p < 0.01$ during the Exact Addition and Proximity Judgement tasks, respectively. The volumes of interest that show significant PPI connectivity to seed regions of interest at $p < 0.05$ (FDR) are indicated by an asterisk.

The bilateral pMFC seed region shows a significant PPI connection to the right posterior cingulate in the control children during the Exact Addition task, illustrated in Fig (4.5). The right anterior HIPS seed region shows a significant PPI connection to the left posterior cingulate gyrus in the control children during the Proximity Judgement task, illustrated in Fig.(4.6).

No significant PPI connectivity with the chosen seed regions was found in the alcohol-exposed children at $p < 0.05$ (FDR). Similarly, no significant PPI group differences were found.

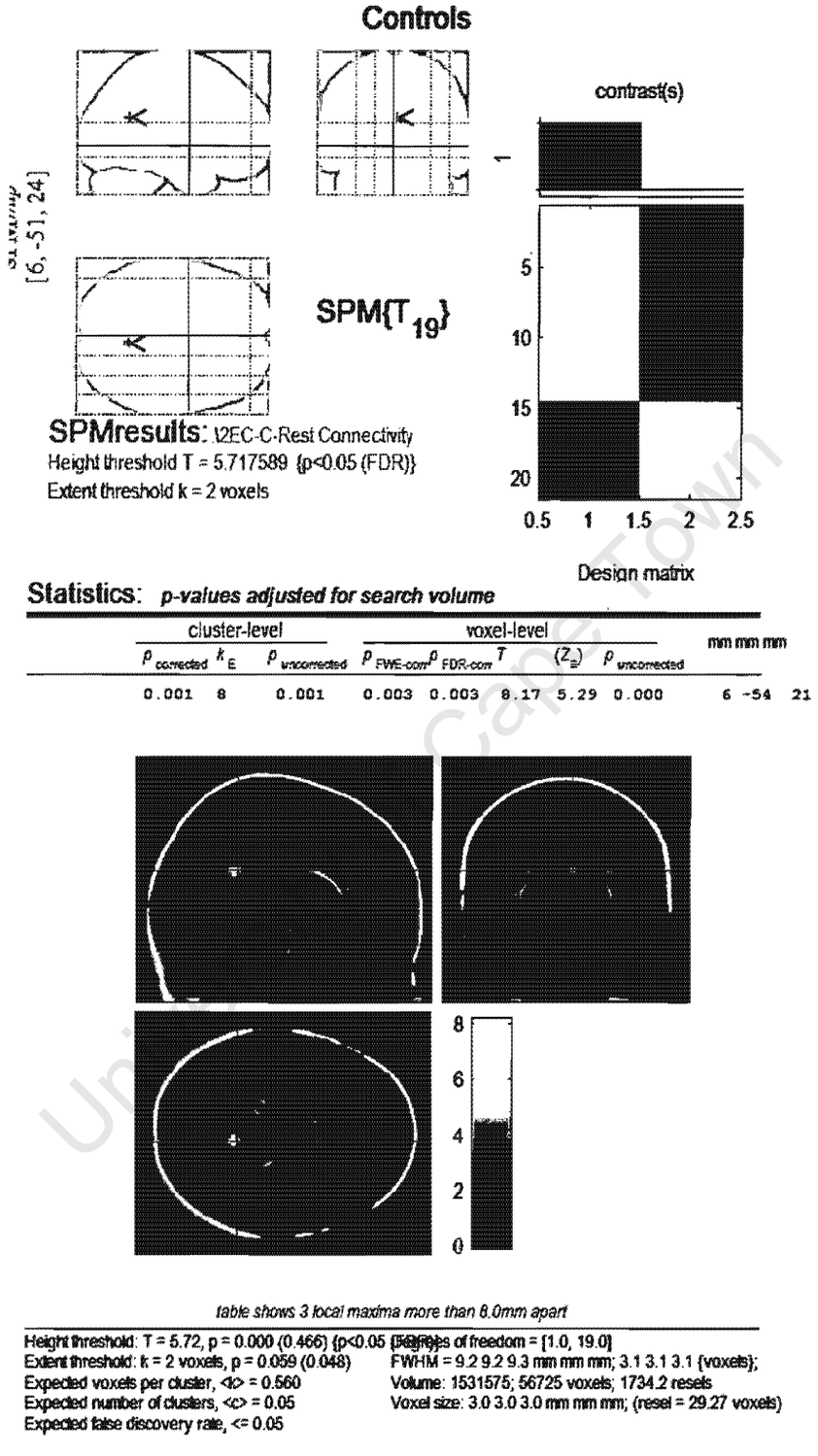

Figure 4.5: Illustration of a volume of interest in the right posterior cingulate [6 -54 21] showing significant PPI connectivity to the bilateral pMFC [0 30 42] seed region in the non-exposed control children during the Exact Addition task at $p < 0.05$ (FDR); $t(\min) = 5.72$.

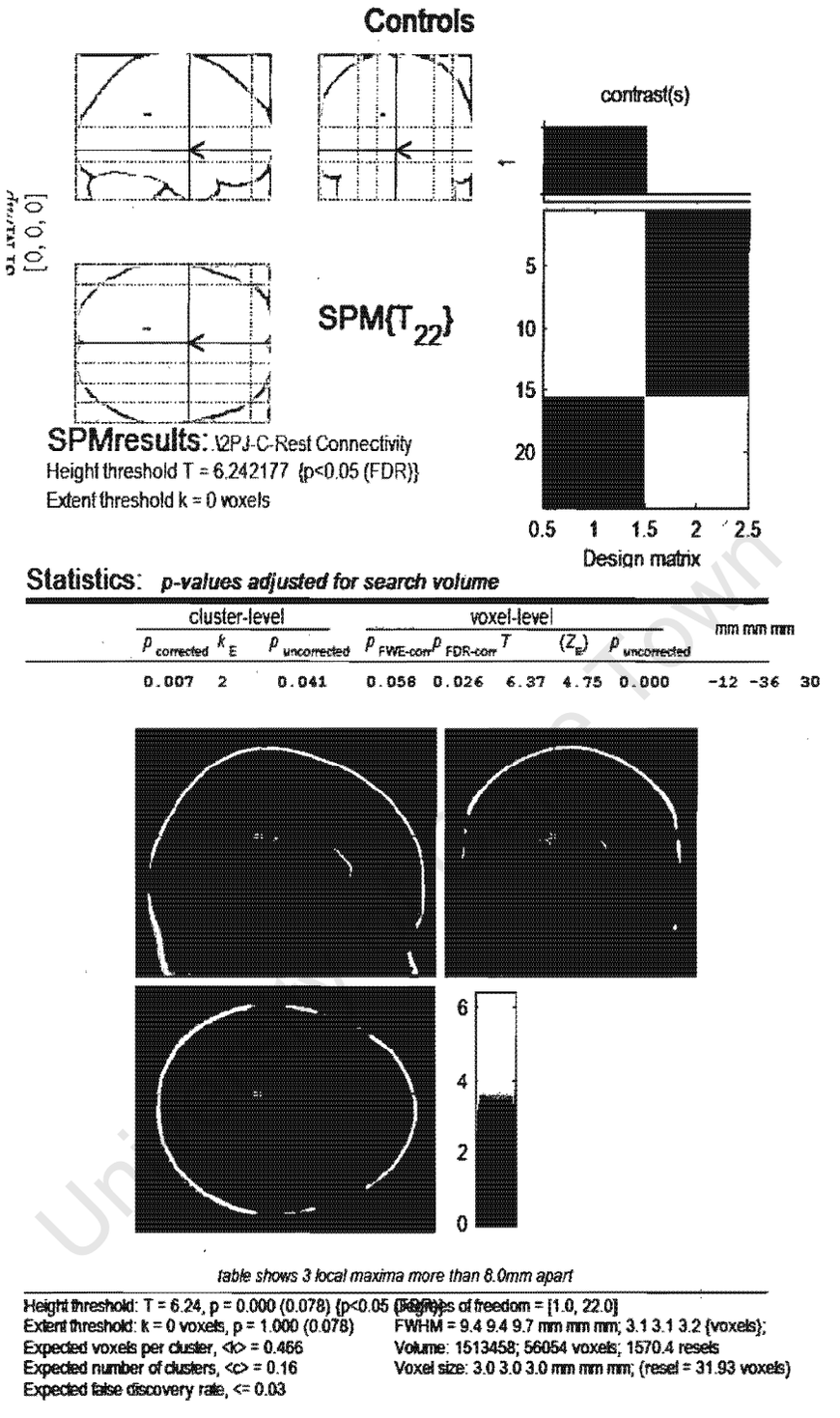

Figure 4.6: Illustration of a volume of interest in the left posterior cingulate gyrus [-12 -36 30] showing significant PPI connectivity to the right anterior HIPS [45 -42 48] seed region in the non-exposed control children during the Proximity Judgement task at $p < 0.05$ (FDR); $t(\text{min}) = 6.24$

Table 4.9: Results showing PPI connectivity for the Exact Addition task[+]

Seed Region					Volume of interest					Controls[+]	Exposed[+]
Name		Coordinates			Name		Coordinates			*t*-statistic	*t*-statistic
L	precentral sulcus	-45	12	33	R	middle frontal gyrus	21	30	42	5.11	–
					R	precuneus	24	-45	48	4.17	–
					L	medial frontal gyrus	-15	-15	51	–	6.94
					L	precuneus	-6	-54	42	–	4.25
R, L	medial frontal cortex; posterior	0	30	42	R	posterior cingulate*	6	-54	21	8.17	–
					L	middle temporal gyrus	-39	-63	27	5.07	–
					R	middle occipital gyrus	33	-81	6	4.47	–
R	horizontal intraparietal sulcus; anterior	33	-54	45	R, L	precuneus	0	-48	54	–	4.54
L	horizontal intraparietal sulcus; posterior	-30	-69	48	R	caudate nucleus; body	12	15	9	4.39	–
					L	caudate nucleus; body	-3	12	9	4.03	–
R, L	precuneus	-3	-69	42	R	inferior parietal lobule	39	-36	36	4.93	–
					L	superior frontal gyrus	-3	-6	66	–	3.48
					R	superior frontal gyrus	6	-6	72	–	3.45

[+] Reported at $p < 0.01$ uncorrected; $t(\text{min}) = 2.51$; cluster threshold 100 voxels

* Significant PPI connectivity at $p < 0.05$ (FDR); $t(\text{min}) = 5.72$; cluster threshold 2 voxels

Table 4.10: Results showing PPI connectivity for the Proximity Judgement task[+]

Seed Region					Volume of interest					Controls[+]	Exposed[+]
Name		Coordinates			Name		Coordinates			*t*-statistic	*t*-statistic
L	precentral sulcus and middle frontal gyrus	-48	15	33	L	precuneus	-9	-48	36	5.96	–
R, L	medial frontal cortex; posterior	0	24	48	L	precuneus	-15	-60	30	–	5.86
					R	precuneus	9	-66	27	–	3.87
R	horizontal intraparietal sulcus; anterior	45	-42	48	R	inferior parietal lobule	45	-57	36	6.24	–
					L	cingulate gyrus; posterior*	-12	-36	30	6.37	–
L	horizontal intraparietal sulcus; posterior	-27	-69	45	L	precuneus	-12	-51	30	–	5.36
					R	posterior cingulate	9	-48	24	–	4.53
R, L	precuneus	0	-63	42	L	inferior parietal lobule	-33	-39	45	4.26	–
					L	middle frontal gyrus	-39	15	30	–	4.17
					L	precentral gyrus	-51	3	27	–	3.97
L	angular gyrus	-36	-66	39	–	–	–	–	–	–	–

[+] Reported at $p < 0.01$ uncorrected; $t(\text{min}) = 2.51$; cluster threshold 100 voxels

* Significant PPI connectivity at $p < 0.05$ (FDR); $t(\text{min}) = 5.72$; cluster threshold 2 voxels

5 Discussion

5.1 Selection of Regions of Interest

The regions of interest extracted from the fMRI activation maps for further connectivity analysis were chosen for their prominence in number processing literature, as well as their importance in the findings of the fMRI study of number processing in children with FASD performed by Meintjes and colleagues (2007).

In the fMRI analysis of the control children's data, the activation of the anterior HIPS appears to be right lateralised during the Proximity Judgement task and left lateralised during the Exact Addition task. This is consistent with results reported by Stanescu-Cosson et al. (2000). The anterior HIPS, in both hemispheres, have been shown to be involved in non-verbal representation of quantity (Dehaene et al., 2003; 2004). In order to investigate the functional connectivity to these regions and possible differences in connectivity between the groups of children, seed regions in the left and right anterior HIPS were extracted from the control and alcohol-exposed Exact Addition activation maps, respectively, and a seed region in the right anterior HIPS was extracted from the control Proximity Judgement activation map.

The left posterior HIPS, which is significantly activated during both number processing tasks in the control children and shows significantly less activitation in the alcohol-exposed children during both tasks (Meintjes et al., 2007), has been implicated in visual short-term memory storage (Todd and Marois, 2004). Any functional links between this area of the posterior parietal cortex and frontal / prefrontal areas, responsible for maintaining this storage, are of interest.

The bilateral precuneus and adjacent posterior cingulate cortex (forming a medial parietal region) have been found to be active during arithmetic fact retrieval (Gruber et al., 2001) and semantically cued word retrieval (Fletcher et al., 1996). The bilateral precuneus is significantly activated during both number processing tasks in the control group. However, it is the significantly greater activation of the bilateral precuneus spilling into the posterior

cingulate gyrus in the alcohol-exposed group compared to non-exposed controls during the Proximity Judgement task (Meintjes et al., 2007) that led to this region being chosen as a seed region of interest for functional connectivity analysis.

The angular gyrus (AG) was not significantly activated in the control children during either task but was significantly activated by the alcohol-exposed children during both tasks, on the left in Exact Addition and bilaterally in Proximity Judgement. The left AG is known to be involved in language-mediated processes, including verbal number manipulation (Simon et al., 2002; Dehaene et al., 2003), and the apparent absence of activation in control children at the chosen significance threshold and presence of activation in children with FASD warranted further connectivity analysis.

The consistent activation of the left precentral sulcus (PCS) in the control children's data during both number processing tasks is in agreement with Zago and colleagues (2001), who suggest that the region is involved in the developmental acquisition of number. In comparison, the absence of significant activation (at the selected thresholds) of the left PCS in the alcohol-exposed children during both number processing tasks and significantly less activation of the left PCS during Proximity Judgement compared to the control children (Meintjes et al., 2007), may be indicative of abnormal functional connectivity to the region and therefore, worth analysing further.

The bilateral posterior medial frontal cortex (pMFC) showed significant activation in the non-exposed controls during both number processing tasks and significantly less activation in the alcohol-exposed children during Proximity Judgement but not during Exact Addition (Meintjes et al., 2007), possibly indicating different degrees of error monitoring during performance of the different tasks (Ridderinkof et al., 2004). The pMFC was chosen as a seed region for further connectivity analysis to investigate, among others, the close functional relationship between the pMFC and prefrontal cortex (PFC) alluded to by Ridderinkhof and colleagues (2004).

5.2 Connectivity Analyses

Inter-region Correlation

Pair-wise comparisons of inter-region correlation yielded no significant differences between the groups. The lack of results indicates an apparent absence of significant connectivity differences between the groups in the functional connections tested for the Exact Addition and Proximity Judgement number processing tasks. It emphasises that a pair-wise comparison method is limited when little is known about the expected connectivity and better suited to the case where a hypothesis, based on *a priori* model, is available for testing. An exploratory mapping technique such as Seed-voxel Connectivity may be more appropriate when trying to assess functional connectivity to more than a few regions of interest or in cases where a model for testing is absent.

Seed-voxel Connectivity

Functional integration of a network of parietal and frontal areas, particularly including the dorsolateral prefrontal cortex (DLPFC), is predicted to be responsible for number processing in adults (Chochon et al., 1999; Stanescu-Cosson et al., 2000). However, significant connections from the parietal seed regions to the DLPFC were not found in the control children during either Exact Addition or Proximity Judgement tasks. This result, although seemingly contradictory, tends to agree with the findings of Scherf et al. (2006), who determined that children only weakly recruit the DLPFC and parietal areas involved in working memory in adults, seeming to favour a compensatory network, which includes the caudate nucleus and anterior insula, until functional specialisation has occurred during adolescence.

Various significant frontal functional connections to the precentral and middle frontal gyri were found during both number processing tasks. In their meta-analysis of human fronto-parietal networks for language, space and number, Simon et al. (2004) repeatedly found activation of the left precentral gyrus and left middle frontal gyrus during calculation tasks, with the bilateral middle frontal gyrus also active during attention tasks.

The left posterior HIPS, reportedly involved in visual short-term memory storage (Todd and Marois, 2004) showed frontal connectivity to the left superior frontal sulcus in both Exact Addition and Proximity Judgement tasks. Todd and Marois (2004) suggest that the working memory function of the frontal / prefrontal cortex helps in the consolidation and maintenance of the visual short-term memory stored in the posterior parietal cortex. The left superior frontal sulcus, in particular, has been shown to be active during an arithmetic computation task (Zago et al., 2001) and specialised for sustained activity during spatial working memory (Courtney et al., 1998). Klingberg and colleagues (2002) have suggested that functional interactions between the intraparietal sulcus and superior frontal sulcus are involved in visuo-spatial working memory in adults and, to a lesser degree, in children.

Exact Addition

In the Exact Addition task, the control children's Seed-voxel Connectivity results seem to confirm the pattern of fronto-parietal connectivity expected in number processing tasks (e.g. Chochon et al., 1999; Stanescu-Cosson et al., 2000). The parietal seed regions, in general, showed connectivity within the parietal lobe, believed to be responsible for number representation and processing, and connections to frontal lobe areas, believed to play a non-numeric supportive role (Menon et al., 2000).

When either left or right anterior HIPS was chosen as the seed region, significant interconnections between them were found, possibly illustrating dual involvement in the quantitative representation of number (Dehaene et al., 2003). In Dehaene's model, number is represented initially bilaterally in the HIPS although in some studies activations tend to be stronger in the left for calculation (e.g. Stanescu-Cosson et al., 2000).

The left anterior HIPS showed frontal connectivity to the left precentral gyrus. A similar fronto-parietal connection was proposed to exist by Simon et al. (2004) after noting a number of arithmetic studies that show simultaneous activation of the left HIPS and the left precentral gyrus, particularly during calculation (e.g. Chochon et al., 1999; Zago et al., 2001). Monkey studies have shown strong functional connections between the ventral intraparietal area (VIP) and premotor area F4 (Rizzolatti et al., 1998). Therefore, Simon et al. (2004) propose that the precentral gyrus in the human is homologous to the F4 premotor area in the

monkey and therefore, functionally connected to the HIPS for the purpose of performing calculations.

The right anterior HIPS seed region showed a frontal connection to the left precentral sulcus, which has been shown to be involved in the developmental acquisition of number, related to finger counting (Zago et al., 2001). In addition, the right anterior HIPS and left posterior HIPS seed regions showed connectivity to areas in the right middle frontal gyrus, which have been shown to be active during tasks requiring attention (Simon et al., 2004).

Although the left anterior and posterior HIPS seed regions showed connectivity to areas in the precuneus in the control children's data, the bilateral precuneus seed region showed connectivity to the more posterior and inferior bilateral angular gyrus and bilateral posterior cingulate gyrus. The functional connection to the bilateral posterior cingulate gyrus can be understood in terms of the findings of Gruber and colleagues (2001), who found the medial parietal region, encompassing the bilateral precuneus and adjacent posterior cingulate cortex, to be important in arithmetic fact retrieval during calculation tasks. The retrieval of facts stored in verbal memory is believed to be the function of the angular gyrus (Dehaene et al., 2003) and the connection with the bilateral precuneus may indicate the presence of a fact retrieval network.

The left PCS showed a pattern of fronto-parietal connectivity in the control children's data during the Exact Addition task with frontal connections to the contralateral right middle frontal gyrus, bilateral pMFC and left anterior insula and parietal connections to the bilateral anterior HIPS and left angular gyrus. This seems to show that the left PCS is functionally linked to areas involved in both quantity manipulation and support, confirming a fundamental and intricate involvement in number processing (Zago et al., 2001).

The bilateral pMFC, believed to be involved in the supportive function of error monitoring (Ridderinkhof et al., 2004), showed only frontal connectivity. It showed functional connections to the left precentral gyrus, found to be active during calculation tasks (Chochon et al., 1999; Zago et al., 2001; Simon et al., 2004) and bilaterally to the superior frontal gyri, found to be activated in a range of tasks including calculation and visuo-spatial working memory (Zago et al., 2001; Simon et al., 2004). In addition, the pMFC showed bilateral connections to the anterior insula, which are believed to be associated with the retrieval of

names of familiar objects, including digits (Pesenti et al., 2000), and the middle dorsolateral prefrontal cortex (DLPFC), believed to be involved in response selection and execution (Badre & Wagner, 2004). The close functional association between the pMFC and prefrontal cortex (PFC), suggested by Ridderinkhof et al. (2004), is supported by the extensive functional connectivity seen.

The alcohol-exposed children showed less extensive connectivity during the Exact Addition task at the significance threshold chosen, as indicated by the fewer connections reported. For example, the left posterior HIPS showed parietal connectivity to the bilateral precuneus but no frontal connectivity at the chosen threshold. Similarly, the bilateral pMFC seed region showed significant connectivity to the left DLPFC, bilateral superior frontal gyri and left precentral gyrus but not to the right DLPFC or bilateral anterior insula. The left precentral sulcus seed region showed no significant frontal or parietal connectivity. The only connection that was significant in the alcohol-exposed children, but not seen in the control children, was between the left anterior HIPS and left medial frontal gyrus.

Although the result of less extensive functional connectivity in the alcohol-exposed children's data seemingly suggests different functional connectivity compared to the controls, no significant differences between the groups were found in the Exact Addition analysis. The small number of subjects in the alcohol-exposed group (seven in the Exact Addition task) and inter-subject variability presumably greatly reduced the power to detect group differences.

Proximity Judgement

As for Exact Addition, the control children's data for the Proximity Judgement task showed an expected pattern of fronto-parietal connectivity (e.g. Chochon et al., 1999; Stanescu-Cosson et al., 2000). The parietal seed regions showed more extensive connectivity (quantified by an increased number of regions significantly connected to the seed region) within the parietal lobe than during the Exact Addition task. For example, the right anterior HIPS seed region showed extensive parietal connectivity including contralateral functional connectivity to the left HIPS region, encompassing both anterior and posterior HIPS, and ipsilateral functional connectivity extending to the right posterior HIPS. Similarly, the left posterior HIPS showed parietal connectivity to the left anterior and right posterior HIPS.

This presents a possible link between the quantitative representation of number (function of the anterior HIPS (Dehaene et al., 2003)) and visual short-term memory storage (function of the posterior HIPS (Todd and Marois, 2004)) during Proximity Judgement processing that was not seen during Exact Addition processing.

For the control children's data, as in Exact Addition, the right anterior HIPS seed region showed frontal connectivity to the right middle frontal gyrus during Proximity Judgement, which has been shown to be active during tasks requiring attention (Simon et al., 2004).

The bilateral precuneus seed region, which did not show any frontal connections in Exact Addition, exhibited symmetrical fronto-parietal connectivity in the control children's Proximity Judgement data. It showed the same parietal connections to the bilateral angular gyrus, which is believed to be involved in verbal processing of number (Dehane et al., 2003) and posterior cingulate cortex, which is believed to be involved in arithmetic fact retrieval in conjunction with the precuneus (Gruber et al., 2001). However, the bilateral precuneus seed region also showed frontal connections to the right middle frontal gyrus, shown to be active during tasks requiring attention (Simon et al., 2004) and left precentral sulcus, believed to be involved in the mediation of numerical knowledge (Zago et al., 2001).

The left angular gyrus seed region, chosen for its presence in the alcohol-exposed children's activation data, shows fronto-parietal connectivity in the control children's data. It showed parietal connections to the contralateral right angular gyrus, which has been shown to be coactivated with the left angular gyrus during an exact calculation task, especially when task complexity was increased (Menon et al., 2000) and bilateral precuneus, which is believed to be involved in arithmetic fact retrieval (Gruber et al., 2001). The left angular gyrus showed frontal connections to the left middle frontal gyrus, found to be activated during calculation and attention tasks (Simon et al., 2004). The absence of significant connectivity to the HIPS regions may indicate independence of the angular gyrus from the quantity manipulation function of the HIPS and if so, may tentatively agree with the Dehaene and colleagues (2003) model of distinct neural circuits in the parietal cortex responsible for different number processing functions.

The left precentral sulcus showed less extensive fronto-parietal connectivity during Proximity Judgement than Exact Addition in the control children's data. Particularly, the

absences of significant parietal connectivity to the bilateral anterior HIPS and significant frontal connectivity to the pMFC are noteworthy, possibly indicating different degrees of involvement of the left precentral sulcus in the neural networks responsible for Proximity Judgement and Exact Addition processing. The results may suggest the possibility that circuits involving number knowledge (and therefore functional connectivity with the left precentral sulcus) are less important in Proximity Judgement, which can be performed based on an intuitive sense for relative quantities (Pica et al., 2004; Dehaene et al., 2004).

In the control children's data, the bilateral pMFC seed region showed similar connectivity to the bilateral anterior insula and right DLPFC seen in the Exact Addition data but no significant connectivity to the left DLPFC. The functional connectivity between the bilateral pMFC and anterior cingulate cortex emphasises a common involvement in response error monitoring (Ridderinkhof et al., 2004).

By contrast, in the alcohol-exposed children's data, the bilateral pMFC seed region showed extensive functional connectivity to the bilateral middle frontal gyrus for the Proximity Judgement task, not seen in the control children's connectivity results. One of the connections to the left middle frontal gyrus was significantly different between the groups. The left middle frontal gyrus has been shown to be activated during calculation tasks and tasks requiring attention (Simon et al., 2004) while the right middle frontal gyrus has been shown to be activated during tasks only requiring attention (Simon et al., 2004). The significant functional connectivity between the bilateral pMFC and bilateral middle frontal gyrus seen in the alcohol-exposed children may indicate a requirement for additional attention networks for task completion compared to non-exposed controls.

In the functional connectivity analysis of the alcohol-exposed children's Proximity Judgement data, the parietal seed regions showed extensive intra-parietal connectivity but no significant frontal connectivity at the statistical threshold. Similarly, the frontal seed regions showed frontal connectivity but no significant parietal connectivity. This seems to imply less extensive fronto-parietal connectivity in alcohol-exposed children compared to controls. Only one significant group difference was found in the Proximity Judgement data and it was between the frontal areas bilateral pMFC and left middle frontal gyrus. The small sample size (nine alcohol-exposed children in the Proximity Judgement analysis) and inter-subject variability is assumed to have affected the statistical power of the analyses.

Psychophysiological Interactions

The significant PPI result for the Exact Addition data indicates that the interaction of the activity in the bilateral pMFC seed region and Exact Addition task relative to baseline was highly correlated with the activity seen in the right posterior cingulate. This is a functional connection not seen in the Seed-voxel Connectivity results (using concatenated within-task time series), but which implies a fronto-parietal functional connection between the bilateral pMFC, believed to be responsible for error monitoring (Ridderinkhof et al., 2004) and posterior cingulate, believed to be involved in the arithmetic fact retrieval (Gruber et al., 2001), both necessary functions for the correct completion of a calculation task.

Similarly, the interaction of the Proximity Judgement task context and activity in the right anterior HIPS seed region seems to have contributed to the activity seen in the left posterior cingulate gyrus. Although extensive intraparietal Inter-region Correlation was found during the Proximity Judgement task, parietal connectivity from the right anterior HIPS seed region to the left posterior cingulate gyrus was not isolated. The PPI connection infers a functional link between the right anterior HIPS, believed to be involved in the quantitative representation of number (Dehaene et al., 2003), and left posterior cingulate gyrus, which forms part of the medial parietal region assumed to be involved in the retrieval of arithmetic facts (Gruber et al., 2001).

6 Conclusion

The objective of this study was to examine the functional brain connectivity of control children and children with foetal alcohol spectrum disorder (FASD) during two number processing tasks. A primary aim was to determine normal functional connectivity involved in the performance of Exact Addition and Proximity Judgement tasks using the control children's fMRI data. A secondary aim was to investigate the functional connectivity seen in the alcohol-exposed children's fMRI data and compare it with the control children's functional connectivity results.

Functional MRI data, previously collected by Meintjes and colleagues (2007) in an fMRI activation analysis of control children and children with FASD during number processing, was available for analysis. Different functional connectivity methods were studied and implemented in Brain Voyager QX, MATLAB and SPM5 software packages.

Regions of interest were isolated for their functional activation during the number processing tasks, prevalence in the number processing literature and importance in the fMRI activation analysis findings of Meintjes et al. (2007). Pair-wise comparisons of Inter-region Correlation yielded no significant differences in functional connectivity between the groups of children for the regions chosen. The exploratory functional connectivity methods proved more useful in the investigation of functional connectivity to the seed regions of interest.

Seed-voxel Connectivity analysis of the control children's data showed a pattern of fronto-parietal functional connectivity similar to that predicted in the number processing literature for adults (e.g. Chochon et al., 1999; Stanescu-Cosson et al., 2000). Of particular interest is the lack of expected fronto-parietal connectivity to the DLPFC. However, this finding may be explained by an observation that children do not seem to activate a network of parietal and DLPFC areas in working memory tasks to the same degree as adults (Scherf et al., 2006)

Psychophysiological Interaction analysis emphasised the contribution of areas in the posterior cingulate, believed to be involved in arithmetic fact retrieval (Gruber et al., 2001), in the context of number processing.

The alcohol-exposed children showed less extensive functional connectivity, particularly fronto-parietal, than the control children in both number processing tasks at a corrected significance threshold, but few significant group differences. The small sample size of alcohol-exposed subjects (seven and nine in the Exact Addition and Proximity Judgement tasks, respectively) is presumed to have affected the power of the statistical analysis.

This study has contributed information about the functional connectivity seen in control and alcohol-exposed children during Exact Addition and Proximity Judgement number processing tasks. The less extensive fronto-parietal functional connectivity seen in the alcohol-exposed children compared to the non-exposed controls may explain some of the functional activation differences reported (Meintjes et al., 2007) and behavioural and cognitive deficits observed in alcohol-exposed children. However, the results are inconclusive and further studies with more alcohol-exposed subjects are necessary.

References

Abler, B., Roebroeck, A., Goebel, R., Höse, A., Schönfeldt-Lecuona, C., Hole, G., Walter, H. (2006). Investigating directed influences between activated brain areas in a motor-response task using fMRI. Magnetic Resonance Imaging, 24, 181–185.

Aertsen, A., Preissl, H. (1991). Dynamics of activity and connectivity in physiological neuronal networks. In: Ed. Schuster, H.G. Non Linear Dynamics and Neuronal Networks. pp. 281–302. VCH: New York, NY.

Archibald, S.L., Fennema-Notestine, C., Gamst, A., Riley, E.P., Mattson, S.N., Jernigan, T.L. (2001). Brain dysmorphology in individuals with severe prenatal alcohol exposure. Developmental Medicine & Child Neurology, 43, 148–154.

Arfanakis, K., Cordes, D., Haughton, V.M., Moritz, C.H., Quigley, M.A., Meyerand, M.E. (2000). Combining independent component analysis and correlation analysis to probe interregional connectivity in fMRI task activation datasets. Magnetic Resonance Imaging, 18, 921–930.

Badre, D., Wagner, A.D. (2004). Selection, integration, and conflict monitoring: assessing the nature and generality of prefrontal cognitive control mechanisms. Neuron, 41, 473–487.

Boksman, K., Theberge, J., Williamson, P., Drost, D.J., Malla, A., Densmore, M., Takhar, J., Pavlosky, W., Menon, R.S., Neufeld, R.W.J. (2005). A 4.0-T fMRI study of brain connectivity during word fluency in first-episode schizophrenia. Schizophrenia Research, 75, 247–263.

Büchel, C., Friston, K. (2000). Assessing interactions among neuronal systems using functional neuroimaging. Neural Networks, 13, 871–882.

Büchel, C., Friston, K. (1997). Modulation of connectivity in visual pathways by attention: cortical interactions evaluated with structural equation modelling and fMRI. Cerebral Cortex, 7, 768–778.

Burden, M.J., Jacobson, S.W., Jacobson, J.L. (2005a). The relation of prenatal alcohol exposure to cognitive processing speed and efficiency in childhood. Alcoholism: Clinical and Experimental Research, 29, 1473–1483.

Burden, M.J., Jacobson, S.W., Sokol, R.J., Jacobson, J.L. (2005b). Effects of prenatal alcohol exposure on attention and working memory at 7.5 years of age. Alcoholism: Clinical and Experimental Research, 29, 443–452.

Bushberg, J.T., Seibert, J.A., Leidholdt Jr, E.M., Boone, J.M. (2002). The essential physics of medical imaging. (2nd ed.). Lippincott Williams and Wilkins: Philadelphia, PA.

Buxton, R.B. (2002). Introduction to functional magnetic resonance imaging: principles and techniques. Cambridge University Press: Cambridge.

Caclin, A., Fonlupt, P. (2006). Effect of initial fMRI data modelling on the connectivity reported between brain areas. NeuroImage, 33, 515–521.

Carmichael Olson, H., Feldman, J.J., Streissguth, A.P., Sampson, P.D., Bookstein, F.L. (1998). Neuropsychological deficits in adolescents with fetal alcohol syndrome: clinical findings. Alcoholism: Clinical and Experimental Research, 22, 1998–2012.

Chochon, F., Cohen, L., van de Moortele, P.F., Dehaene, S. (1999). Differential contributions of the left and right inferior parietal lobules to number processing. Journal of Cognitive Neuroscience, 11, 617–630.

Clarren, S.K. (1977). Central nervous system malformations in two offspring of alcoholic women. Birth Defects Original Article Series, 13, 151–153.

Clarren, S.K. (1986). Neuropathology in fetal alcohol syndrome. In: Ed. West, J.R. Alcohol and brain development. pp. 158–166. Oxford University Press: New York, NY.

Clarren, S.K., Smith, D.W. (1978). The fetal alcohol syndrome. New England Journal of Medicine, 298, 1063–1067.

Coles, C.D., Platzman, K.A., Lynch, M.E., Freides, D. (2002). Auditory and visual sustained attention in adolescents prenatally exposed to alcohol. Alcoholism: Clinical and Experimental Research, 26, 263–271.

Coles, C.D., Platzman, K.A., Raskind-Hood, C.L., Brown, R.T., Falek, A., Smith, I.E. (1997). A comparison of children affected by prenatal alcohol exposure and attention deficit, hyperactivity disorder. Alcoholism: Clinical and Experimental Research, 21, 150–161.

Cordes, D., Haughton, V.M., Arfanakis, K., Wendt, G.J., Turski, P.A., Moritz, C.H., Quigley, M.A., Meyerand, M.E. (2000). Mapping functionally related regions of brain with functional connectivity MR imaging. American Journal of Neuroradiology, 21, 1636–1644.

Courtney, S. M., Petit, L., Maisog, J. M., Ungerleider, L. G., Haxby, J. V. (1998). An area specialized for spatial working memory in human frontal cortex. Science 279, 1347–1351.

Croxford, J., Viljoen, D. (1999). Alcohol consumption by pregnant women in the Western Cape. South African Medical Journal, 89, 962–965.

Das, P., Kemp, A.H., Liddell, B.J., Brown, K.J., Olivieri, G., Peduto, A., Gordon, E., Williams, L.M. (2005). Pathways for fear perception: Modulation of amygdala activity by thalamo-cortical systems. NeuroImage, 26, 141–148.

Dehaene, S., (1992). Varieties of numerical abilities. Cognition, 44, 1–42.

Dehaene, S. (1997). The Number Sense: how the mind creates mathematics. Oxford University Press: Oxford.

Dehaene, S., Cohen, L. (1995). Towards an anatomical and functional model of number processing. Mathematical Cognition, 1, 83–120.

Dehaene, S., Cohen, L. (1997). Cerebral pathways for calculation: Double dissociation between rote verbal and quantitative knowledge of arithmetic. Cortex, 33, 219–250.

Dehaene, S., Molko, N., Cohen, L., Wilson, A.J. (2004). Arithmetic and the brain. Current Opinion in Neurobiology, 14, 218–224.

Dehaene, S., Piazza, M., Pinel, P., Cohen, L. (2003). Three parietal circuits for number processing. Cognitive Neuropsychology, 20, 487–506.

Dehaene, S., Spelke, E., Pinel, P., Stanescu, R., Tsivkin, S. (1999). Sources of mathematical thinking: behavioral and brain-imaging evidence. Science, 284, 970–974.

Delazer, M., Domahs, F., Lochy, A., Karner, E., Benke, T., Poewe, W. (2004). Number processing and basal ganglia dysfunction: a single case study. Neuropsychologia, 42, 1050–1062.

Eger, E., Sterzer, P., Russ, M.O., Giraud, A-L., Kleinschmidt, A. (2003). A supramodal number representation in human intraparietal cortex. Neuron, 37, 719–725.

Feigenson, L., Dehaene, S., Spelke, E. (2004). Core systems of number. Trends in Cognitive Neuroscience, 8, 307–314.

Fletcher, P.C., Shallice, T., Frith, C.D., Frackowiak, R.S.J., Dolan, R.J. (1996). Brain activity during memory retrieval: the influence of imagery and semantic cueing. Brain, 119, 1587–1596.

Friston, K.J. (1998). Imaging neuroscience: Principles or maps? Proceedings of the National Academy of Sciences U.S.A., 95, 796–802.

Friston, K.J., Buechel, C., Fink, G.R., Morris, J., Rolls, E., Dolan, R.J. (1997). Psychophysiological and modulatory interactions in neuroimaging. NeuroImage, 6, 218–229.

Friston, K.J., Frith, C.D., Frackowiak, R.S.J. (1993a). Time dependent changes in effective connectivity measured with PET. Human Brain Mapping, 1, 69–79.

Friston, K.J., Frith, C.D., Liddle, P.F., Frackowiak, R.S. (1993b). Functional connectivity: the principal-component analysis of large (PET) data sets. Journal of Cerebral Blood Flow Metabolism, 1, 5–14.

Friston, K.J., Holmes, A.P., Poline, J-B., Grasby, P.J., Williams, S.C.R., Frackowiak, R.S.J., Turner, R. (1995). Analysis of fMRI time series revisited. NeuroImage, 2, 45–53.

Gerstmann, J. (1940). Syndrome of finger agnosia disorientation for right and left agraphia and acalculia. Archives of Neurology and Psychiatry, 44, 398–408.

Geweke, J. (1982). Measurement of linear dependence and feedback between multiple time series. Journal of the American Statistical Association, 77, 304–313.

Gjedde, A. (2001). Brain energy metabolism and the physiological basis of the haemodynamic response. In: Eds. Jezzard, P., Matthews, P.M., Smith, S.M. Functional MRI: an introduction to methods. pp. 37 – 65. Oxford University Press: Oxford.

Goebel, L.R., Roebroeck, A., Kim, D., Formisano, E. (2003). Investigating directed cortical interactions in time-resolved fMRI data using vector autoregressive modeling and Granger causality mapping. Magnetic Resonance Imaging, 21, 1251–1261.

Goldschmidt, L., Richardson, G.A., Stoffer, D.S., Geva, D., Day, N.L. (1996). Prenatal alcohol exposure and academic achievement at age six: a nonlinear fit. Alcoholism: Clinical and Experimental Research, 20, 763–770.

Gonzalez-Lima, F., McIntosh, A.R. (1995). Analysis of neural network interactions related to associative learning using structural equation modeling. Mathematics and Computers in Simulation, 40, 115–140.

Granger, C.W.J. (1969) Investigating causal relations by econometric models and cross-spectral methods. Econometrica, 37, 424–438.

Gruber, O., Indefrey, P., Steinmetz, H., Kleinschmidt, A. (2001). Dissociating neural correlates of cognitive components in mental calculation. Cerebral Cortex, 11, 350–359.

Harrison, L., Penny, W.D., Friston, K.J. (2003). Multivariate autoregressive modeling of fMRI time series. NeuroImage, 19, 1477–1491.

Horwitz, B. (2003). The elusive concept of brain connectivity. NeuroImage, 19, 466–470.

Howell, K.K., Lynch, M.E., Platzman, K.A., Smith, G.H., Coles, C.D. (2006). Prenatal alcohol exposure and ability, academic achievement, and school functioning in adolescence: a longitudinal follow-up. Journal of Pediatric Psychology, 31, 116–126.

Hoyme, H.E., May, P.A., Kalberg, W.O., Kodituwakku, P., Gossage, J.P., Trujillo, P.M., Buckley, D.G., Miller, J.H., Aragon, A.S., Khaole, N., Viljoen, D.L., Jones, K.L., Robinson, L.K. (2005). A practical clinical approach to diagnosis of fetal alcohol spectrum disorders: clarification of the 1996 Institute of Medicine criteria. Pediatrics, 115, 39–47.

Jacobson, J.L., Meintjes, E.M., Jacobson, S.W., Gatenby, J.C., Molteno, C.D., Cannistraci, C.J., Dehaene, S., Hoyme, H.E., Robinson, L.K., Gore, J.C. (2006). Arithmetic and Executive Function in Fetal Alcohol Syndrome: Preliminary fMRI Findings. Alcoholism: Clinical and Experimental Research, 30, 176A–176A Suppl.

Jacobson, S.W., Jacobson, J.L., Sokol, R.J. (1994). Effects of fetal alcohol exposure on infant reaction time. Alcoholism: Clinical and Experimental Research, 18, 1125–1132.

Jacobson, S.W., Jacobson, J.L., Sokol, R.J., Chiodo, L.M., Corobana, R. (2004). Maternal age, alcohol abuse history, and quality of parenting as moderators of the effects of prenatal alcohol exposure on 7.5-year intellectual function. Alcoholism: Clinical and Experimental Research, 28, 1732–1745.

Jacobson, S.W., Jacobson, J.L., Sokol, R.J., Ager, J.W. (1993). Prenatal alcohol exposure and infant information processing ability. Child Development, 64, 1706–1721.

Jacobson, S.W., Stanton, M.E., Molteno, C.D., Burden, M.J., Fuller, D.S., Hoyme, H.E., Robinson, L.K., Khaole, N., Jacobson, J.L. (2008). Impaired eyeblink conditioning in children with fetal alcohol syndrome. Alcoholism: Clinical and Experimental Research, 32, 365–372.

Jones, K.L., Smith, D.W. (1973). Recognition of the fetal alcohol syndrome in early infancy. Lancet, 2, 999–1001.

Kaemingk, K.L., Mulvaney, S., Halverson, P.T. (2003). Learning following prenatal alcohol exposure: performance on verbal and visual multitrial tasks. Archives of Clinical Neuropsychology, 18, 33–47.

Kaminski, M., Ding, M, Trucculo, W.A., Bressler, S.L. (2001). Evaluating causal relations in neural systems: Granger causality, directed transfer function and statistical assessment of significance. Biological Cybernetics, 85, 145–157.

Klingberg, T., Forssberg, H., Westerberg, H. (2002). Increased brain activity in frontal and parietal cortex underlies the development of visuospatial working memory capacity during childhood. Journal of Cognitive Neuroscience, 14, 1–10.

Kodituwakku, P.W., Handmaker, N.S., Cutler, S.K., Weathersby, E.K., Handmaker, S.D. (1995). Specific impairments in self-regulation in children exposed to alcohol prenatally. Alcoholism: Clinical and Experimental Research, 19, 1558–1564.

Kopera-Frye, K., Dehaene, S., Streissguth, A.P. (1996). Impairments of number processing induced by prenatal alcohol exposure. Neuropsychologia, 34, 1187–1196.

Lawler, K.A., Cowey, A. (1987). On the role of posterior parietal and prefrontal cortex in visuo-spatial perception and attention. Experimental Brain Research, 65, 695–698.

Malisza, K.L., Allman, A-A., Shiloff, D., Jakobson, L., Longstaffe, S., Chudley, A.E. (2005). Evaluation of spatial working memory function in children and adults with fetal alcohol spectrum disorders: a functional magnetic resonance imaging study. Pediatric Research, 58, 1150–1157.

Marrelec, G., Krainik, A., Duffau, H., Pelegrini-Issac, M., Lehericy, S., Doyon, J., Benali, H. (2006). Partial correlation for functional brain interactivity investigation in functional MRI. NeuroImage, 32, 228–237.

Matthews, P.M. (2001). An introduction to functional magnetic resonance imaging of the brain. In: Eds. Jezzard, P., Matthews, P.M., Smith, S.M. Functional MRI: an introduction to methods. pp. 3–34. Oxford University Press: Oxford.

Mattson, S.N. (Contributing Author) (2000). Prenatal alcohol exposure: effects on brain structure and function. In: Tenth special report to the U.S. congress on alcohol and health. pp. 285–299. National Institute of Alcohol Abuse and Alcoholism.

Mattson, S.N., Riley, E.P. (1996). Brain anomalies in fetal alcohol syndrome. In: Ed. Abel, E.A. Fetal alcohol syndrome: from mechanism to prevention. pp. 51–68. CRC Press: Boca Raton, FL.

Mattson, S.N., Riley, E.P. (1998). A review of the neurobehavioural deficits in children with fetal alcohol syndrome or prenatal exposure to alcohol. Alcoholism: Clinical and Experimental Research, 22, 279–294.

Mattson, S.N., Riley, E.P., Delis, D.C., Stern, C., Jones, K.L. (1996). Verbal learning and memory in children with fetal alcohol syndrome. Alcoholism: Clinical and Experimental Research, 20, 810–816.

Mattson, S.N., Riley, E.P., Gramling, L., Delis, D.C., Jones, K.L. (1997). Heavy prenatal alcohol exposure with or without physical features of fetal alcohol syndrome leads to IQ deficits. Journal of Pediatrics, 131, 718–721.

May, P.A., Brooke, L., Gossage, J.P., Croxford, J., Adnams, C., Jones, K.L., Robinson, L., Viljoen, D. (2000). Epidemiology of fetal alcohol syndrome in a South African community in the Western Cape Province. American Journal of Public Health, 90, 1905–1912.

Meintjes, E.M., Jacobson, S.W., Jacobson, J.L., Gatenby, J.C., Molteno, C.D., Warton, C., Cannistraci, C.J., Dehaene, S., Gore, J.C. (2007). fMRI study of number processing in children with fetal alcohol spectrum disorder (FASD). Proceedings of 13th Annual Meeting of the Organisation for Human Brain Mapping (HBM), Chicago, IL, USA, 10–17 June 2007.

Menon, V., Rivera, S.M., White, C.D., Glover, G.H., Reiss, A.L. (2000). Dissociating prefrontal and parietal cortex activation during arithmetic processing. NeuroImage, 12, 357–365.

Naccache, L., Dehaene, S. (2001). The priming method: imaging unconscious repetition priming reveals an abstract representation of number in the parietal lobes. Cerebral Cortex, 11, 966–974.

Nieder, A., Freedman, D.J., Miller, E.K. (2002). Representation of the quantity of visual items in the primate prefrontal cortex. Science, 297, 1708–1711.

Nieder, A., Miller, E.K. (2003). Coding of cognitive magnitude: compressed scaling of numerical information in the primate prefrontal cortex. Neuron, 37, 149–157.

Ogawa, S., Menon, R.S., Tank, D.W., Kim, S.G., Merkle, H., Ellermann, J.M., Ugurbil, K. (1993). Functional brain mapping by blood oxygenation level-dependent contrast magnetic resonance imaging. Biophysical Journal, 64, 803–812.

O'Hare, E.D., Kan, E., Yoshii, J., Mattson, S.N., Riley, E.P., Thompson, P.M., Toga, A.W., Sowell, E.R. (2005). Mapping cerebellar vermal morphology and cognitive correlates in prenatal alcohol exposure. Neuroreport, 16, 1285–1290.

Pesenti, M., Thioux, M., Seron, X., De Volder, A. (2000). Neuroanatomical substrates of Arabic number processing, numerical comparison, and simple addition: a PET study. Journal of Cognitive Neuroscience, 12, 461–479.

Piazza, M., Giacomini, E., Le Bihan, D., Dehaene, S. (2003). Single-trial classification of parallel pre-attentive and serial attentive processes using functional magnetic resonance imaging. Proceedings of the Royal Society of London B, 270, 1237–1245.

Pica, P., Lemer, C., Izard, V., Dehaene, S. (2004). Exact and approximate arithmetic in an Amazonian indigene group. Science, 306, 499–503.

Pinel, P., Dehaene, S., Riviere, D., Le Bihan, D. (2001). Modulation of parietal activation by semantic distance in a number comparison task. NeuroImage, 14, 1013–1026.
Prohovnik, I., Hakansson, K.H., Risberg, J. (1980). Observations on the functional significance of regional cerebral blood flow in "resting" normal subjects. Neuropsychologia, 18, 203–217.

Raichle, M.E., MacLeod, A.M., Snyder, A.Z., Powers, W.J., Gusnard, D.A., Shulman, G.L. (2001). A default mode of brain function. Proceedings of the National Academy of Sciences U.S.A., 98, 676–682.

Raichle, M.E., Snyder, A.Z. (2007). A default mode of brain function: A brief history of an evolving idea. NeuroImage, 37, 1083–1090.

Ramnani, N., Behrens, T.E.J., Penny, W., Matthews, P.M. (2004). New approaches for exploring anatomical and functional connectivity in the human brain. Biological Psychiatry, 56, 613–619.

Rasmussen, C. (2005). Executive functioning and working memory in fetal alcohol spectrum disorder. Alcoholism: Clinical and Experimental Research, 29, 1359–1367.

Ridderinkhof, K.R., Ullsperger, M., Crone, E.A., Nieuwenhuis, S. (2004). The role of the medial frontal cortex in cognitive control. Science, 306, 443–447.

Riley, E.P., McGee, C.L., Sowell, E.R. (2004). Teratogenic effects of alcohol: a decade of brain imaging. Am. J. Med. Genet. C. Semin. Med. Genet., 127, 35–41.

Riikonen, R., Salonen, I., Partanen, K., Verho, S. (1999). Brain perfusion SPECT and MRI in foetal alcohol syndrome. Developmental Medicine & Child Neurology, 41, 652–659.

Rizzolatti, G., Luppino, G., Matelli, M. (1998). The organization of the cortical motor system: new concepts. Electroencephalogr. Clin. Neurophysiol., 106, 283–296.

Roebroeck, A., Formisano, E., Goebel R. (2005). Mapping directed influence over the brain using Granger causality and fMRI. NeuroImage, 25, 230–242.

Roebuck, T.M., Simmons, R.W., Mattson, S.N., Riley, E.P. (1998a). Prenatal exposure to alcohol affects the ability to maintain postural balance. Alcoholism: Clinical and Experimental Research, 22, 252–258.

Roebuck, T.M., Simmons, R.W., Richardson, C., Mattson, S.N., Riley, E.P. (1998b). Neuromuscular responses to disturbance of balance in children with prenatal exposure to alcohol. Alcoholism: Clinical and Experimental Research, 22, 1992–1997.

Rogers, B.P., Anderson, A.W., Gatenby, J.C., Cannistraci, C.J., Gore, J.C. (2007). Effect of task pacing on activation of the horizontal intra-parietal sulcus during number comparison. Proceedings of 13th Annual Meeting of the Organisation for Human Brain Mapping (HBM), Chicago, IL, USA, 10–17 June 2007.

Scherf, K.S., Sweeney, J.A., Luna, B. (2006). Brain basis of developmental change in visuospatial working memory. Journal of Cognitive Neuroscience, 18, 1045–1058.

Simon, O., Kherif, F., Flandin, G., Poline, J.B., Riviere, D., Mangin, J.F., Le Bihan, D., Dehaene, S. (2004). Automatized clustering and functional geometry of human parietofrontal networks for language, space, and number. NeuroImage, 23, 1192–1202.

Simon, O., Mangin, J.F., Cohen, L., Le Bihan, D., Dehaene, S. (2002). Topographical layout of hand, eye, calculation, and language-related areas in the human parietal lobe. Neuron, 33, 475–487.

Smith, S.M. (2001). Overview of fMRI analysis. In: Eds. Jezzard, P., Matthews, P.M., Smith, S.M. Functional MRI: an introduction to methods. pp. 215–227. Oxford University Press: Oxford.

Sowell., E.R., Lu, L.H., O'Hare, E.D., McCourt, S.T., Mattson, S.N., O'Connor, M.J., Bookheimer, S.Y. (2007). Functional magnetic resonance imaging of verbal learning in children with heavy prenatal alcohol exposure. Neuroreport, 18, 635–639.

Sowell, E.R., Mattson, S.N., Kan, E., Thompson, P.M., Riley, E.P., Toga, A.W. (2008). Abnormal cortical thickness and brain–behavior correlation patterns in individuals with heavy prenatal alcohol exposure. Cerebral Cortex, 18, 136–144.

Sowell, E.R., Mattson, S.N., Thompson, P.M., Jernigan, T.L., Riley, E.P., Toga, A.W. (2001a). Mapping callosal morphology and cognitive correlates: effects of heavy prenatal alcohol exposure. Neurology, 57, 235–244.

Sowell, E.R., Thompson, P.M., Mattson, S.N., Tessner, K.D., Jernigan, T.L., Riley, E.P., Toga, A.W. (2001b). Voxel-based morphometric analyses of the brain in children and adolescents prenatally exposed to alcohol. Neuroreport, 12, 515–523.

Sowell, E.R., Thompson, P.M., Mattson, S.N., Tessner, K.D., Jernigan, T.L., Riley, E.P., Toga, A.W. (2002a). Regional brain shape abnormalities persist into adolescence after heavy prenatal alcohol exposure. Cerebral Cortex, 12, 856–865.

Sowell, E.R., Thompson P.M., Peterson, B.S., Mattson, S.N., Welcome, S.E., Henkenius, A.L., Riley, E.P., Jernigan, T.L., Toga, A.W. (2002b). Mapping cortical gray matter asymmetry patterns in adolescents with heavy prenatal alcohol exposure. NeuroImage 17, 1807–1819.

Stanescu-Cosson, R., Pinel, P., van de Moortele, P.F., Le Bihan, D., Cohen, L., Deheane, S. (2000). Understanding dissociations in dyscalculia: a brain imaging study of the impact of number size on the cerebral networks for exact and approximate calculation. Brain, 123, 2240–2255.

Stedman, T.L. (2000). Stedman's medical dictionary. (27th ed.). Lippincott Williams & Wilkins: Baltimore, MA.

Stratton, K., Howe, C., Battaglia, F. (1996). Fetal alcohol syndrome: diagnosis, epidemiology, prevention, and treatment. National Academy of Sciences: Washington, DC.

Streissguth, A.P., Aase, J.M., Clarren, S.K., Randels, S.P., LaDue, R.A., Smith, D.F. (1991). Fetal Alcohol Syndrome in adolescents and adults. Journal of the American Medical Association, 265, 1961–1967.

Streissguth, A.P., Barr, H.M., Carmichael Olson, H., Sampson, P.D., Bookstein, F.L., Burgess, D.M. (1994). Drinking during pregnancy decreases word attack and arithmetic scores on standardized tests: adolescent data from a population-based prospective study. Alcoholism: Clinical and Experimental Research, 18, 248–254.

Streissguth, A.P., Barr, H.M., Sampson, P.D. (1990). Moderate prenatal alcohol exposure: effects on child IQ and learning problems at age 7 1/2 years. Alcoholism: Clinical and Experimental Research, 14, 662–669.

Streissguth, A.P., Bookstein, F.L., Sampson, P.D., Barr, H.M. (1989). Neurobehavioral effects of prenatal alcohol: part III. PLS analyses of neuropyschologic tests. Neurotoxicology and Teratology, 11, 493–507.

Talairach, J., Tournoux, P. (1988). Co-planar stereotaxic atlas of the human brain: 3-dimensional proportional system: an approach to cerebral imaging. Georg-hieme Verlag: Stuttgart, New York, NY.

Todd, J.J., Marois, R. (2004). Capacity limit of visual short-term memory in human posterior parietal cortex. Nature, 428, 751–754.

Van Belle, G., Fisher, L.D., Heagerty, P.J., Lumley, T. (2004). Biostatistics: a methodology for the health sciences. (2nd ed.). John Wiley & Sons, Inc.: New Jersey.

Zago, L., Pesenti, M., Mellet, E., Crivello, F., Mazoyer, B., Tzourio-Mazoyer, N. (2001). Neural correlates of simple and complex mental calculation. NeuroImage, 13, 314–327.